The Rotation Capacity of Plastic Hinges in Reinforced Concrete Beams : A Theoretical Study

Plem, Erik

1981

LUND INSTITUTE OF TECHNOLOGY · LUND · SWEDEN
DEPARTMENT OF STRUCTURAL MECHANICS
REPORT NO. R 81 - 1

ERIK PLEM

THE ROTATION CAPACITY OF PLASTIC HINGES IN REINFORCED CONCRETE BEAMS – A THEORETICAL STUDY

THE ROTATION CAPACITY OF PLASTIC HINGES IN REINFORCED CONCRETE BEAMS - A THEORETICAL STUDY

Erik Plem

Translated by
L J Gruber, BSc(Eng), MICE, MIStructE

This translation relates to Research Grant No 770598-9 from the National Swedish Council for Building Research to the Department of Structural Mechanics and Concrete Construction, Lund Institute of Technology, Lund.

CONTENTS

SYMBOLS

A_c	effective area of cross section
A_s	cross sectional area of tension reinforcement
A_{sc}	cross sectional area of compression reinforcement
A_{sv}	cross sectional area of a bar in a stirrup
E_c	initial modulus of elasticity of concrete for short-term loading
E_s	modulus of elasticity of reinforcing steel
EI	bending stiffness
F_c	resultant force due to concrete stresses in the compression zone
F_s	force in the tension reinforcement
F_{sc}	force in the compression reinforcement
M	bending moment
M_c	reference moment
M_i	bending moment at subdivision point No i
M_m	span moment
M_r	moment which initiates cracking
M_u	ultimate moment
M_y	yield moment
N_c	reference force
Q	point load
Q_u	ultimate load
Q_y	yield force
V_n	shear force at subdivision point No n
V_y	shear force at subdivision point No n at incipient plastic flow at the plastic hinge
V_o	shear force at subdivision point No o
W_e	external work
W_i	total consumed deformation energy
a	moment shift
a_i	maximum elastic deflection at subdivision point No i

a_n	maximum elastic deflection at subdivision point No n
a_n	fictitious length of plastic hinge
a_y	length of yield region
a_{80}	length of plastic hinge over which the moment is greater than 0.8 M_u
b	width of beam
c	distance of compression reinforcement from compression face
d	effective depth of cross section
e_c	non-dimensional initial modulus of elasticity of concrete
e_s	non-dimensional modulus of elasticity of reinforcing steel
f_{cc}	compressive strength of concrete
f_{cck}	characteristic value of the compressive strength of concrete
f_{ct}	tensile strength of concrete
f_{sc}	compressive strength of compression reinforcement
f_{st}	tensile strength of tension reinforcement
f_{stk}	characteristic value of the tensile strength of the reinforcement
f_{stu}	maximum tensile strength of the reinforcement
f_{sv}	tensile strength of stirrup reinforcement
l	span
l_o	length of rotation span
q	distributed ultimate load
q_y	distributed yield load
r	radius of curvature
r_i	radius of curvature at subdivision point No i
s	spacing of stirrups
x	depth of compression zone
x_m	depth of fictitious compression zone
y_c	ordinate of the position of F_c
y_i	ordinate of the centroid of strip No i
y_s	ordinate of the centroid of tensile reinforcement
y_{sc}	ordinate of the centroid of compression reinforcement

ΔA_c cross sectional area of a strip in the compression zone

ΔQ increment in Q

Δw increment in deformation energy per unit length of beam

$\Delta \varepsilon_i$ increment in mean strain in strip No i

$\Delta \varepsilon_s$ increment in strain in tensile reinforcement

$\Delta \varepsilon_{sc}$ increment in strain in compression reinforcement

$\Delta \psi$ Δw in non-dimensional form

$\Delta \psi_c$ contribution of concrete to $\Delta \psi$

$\Delta \psi_s$ contribution of tensile reinforcement to $\Delta \psi$

$\Delta \psi_{sc}$ contribution of compression reinforcement to $\Delta \psi$

α E_s/E_c

α $\Delta A_c/A_c$

α a in non-dimensional form

α_y a_y in non-dimensional form

β coefficient which determines the shape of the moment curve

γ non-dimensional distance of compression reinforcement from compression face

γ_c partial coefficient for concrete in compression

γ_r partial coefficient for rotation capacity

γ_s partial coefficient for reinforcement in tension

δ non-dimensional bending stiffness

ε strain

ε_c strain in concrete

ε_{cu} ultimate compressive strain in concrete

ε_{cuk} characteristic value of the ultimate compressive strain in concrete

ε_i mean strain in concrete strip No i

ε_o limit strain (strain at maximum stress)

ε_s strain in tension reinforcement

ε_{sc} strain in compression reinforcement

ε_{su} ultimate strain in reinforcing steel

ε_{suk} characteristic value of the ultimate strain in reinforcing steel

ε_1 lower strain hardening limit of reinforcing steel

ε_2 strain at limit of proportionality for reinforcing steel

η f_{stu}/f_{st}

η_i non-dimensional ordinate of strip No i

η_s y_s in non-dimensional form

η_{sc} y_{sc} in non-dimensional form

θ rotation

θ_{calc} calculated rotation capacity

θ_{obs} observed rotation capacity

θ_r rotation requirement of a plastic hinge

θ_u rotation capacity of a plastic hinge

θ_{uv} rotation capacity calculated with shear force taken into consideration

κ_i non-dimensional deflection at subdivision point No i

κ_n non-dimensional deflection at subdivision point No n

λ slenderness of rotation span

μ bending moment in non-dimensional form

μ_i non-dimensional bending moment at subdivision point No i

μ_u ultimate moment in non-dimensional form

μ_y yield moment in non-dimensional form

μ_1 moment variation in tension zone

μ_2 moment variation in compression zone

ν f_{sc}/f_{st}

ξ depth of compression zone in non-dimensional form

ξ_m fictitious depth of compression zone in non-dimensional form

ξ_o non-dimensional depth of compression zone under elastic conditions

ρ non-dimensional radius of curvature

σ stress

σ_c stress in concrete at compression face

σ_{ci} mean stress in strip No i

σ_s stress in tension reinforcement

σ_{sc} stress in compression reinforcement

φ creep factor for concrete

ϕ_e external work in non-dimensional form

ϕ_i internal work of deformation in non-dimensional form

ψ deformation energy per unit length of beam in non-dimensional form

ψ_c contribution of concrete to ψ

ψ_{sc} contribution of compression reinforcement to ψ

ψ_t contribution of compression zone to ψ

ψ_1 deformation energy in tension zone per unit length of beams

ψ_2 deformation energy in compression zone per unit length of beam

ω effective reinforcement ratio for tension reinforcement

ω_b effective reinforcement ratio for balanced reinforcement

ω_c effective reinforcement ratio for compression reinforcement

ω_{cr} critical value of ω with respect to rotation capacity

ω_{fic} fictitious value of ω

ω_v effective reinforcement ratio for stirrups

ω_o $e_s\omega/\omega_c$

Abbreviations

CEB Comité Euro-international du Beton

CW cold worked

HR hot rolled

PH plastic hinge

1 INTRODUCTION

1.1 The limit state method of design

The loadbearing capacity of a statically indeterminate structure such as a continous beam or a frame can be determined by means of the limit state method, based on the theory of plasticity, as follows.

If the construction material is assumed to possess ideal elasto-plastic properties, with a stress-strain diagram according to FIG. 1.1a, it will react in a purely elastic manner to external loads so long as the maximum stress in the worst stressed section of the structure is less then the yield stress σ_y of the material. Over this loading range the moment-curvature relation of the section is represented by the straight line OA in the figure. If, as the external load is increased, the yield stress σ_y is reached, plastic flow begins under the influence of the yield moment M_y. As the load is further increased, plastic flow spreads out within the section until, at a certain load level, the section is completely plastic. Sections situated adjacent to that subjected to the highest stress are at the same time in a state of partial plastic flow. During the increase in moment while plastic flow spreads over the most heavily stressed section, i.e. while the moment increased from M_y to the ultimate moment M_u, the moment-curvature diagram of the section conforms to the portion AB in FIG. 1.1a. As the external load is further raised, the moment in the section under consideration is constant and equal to M_u while the curvature increases. During this stage of loading the moment-curvature diagram is represented by the straight line BC in the figure. Failure of the material is assumed to occur when the curvature reaches the value $(1/r)_u$ determined by attainment of the ultimate strain ε_u of the material.

For purposes of simplification it is assumed in the following introductory argument that the properties of the material and the sectional shape of the beam element are such that an arbitrarily chosen section in the structure has an ideal elasto-plastic moment-curvature diagram, i.e. that the length of the portion AB of the curve is negligible. The diagram then becomes bilinear.

The loads acting on the structure are assumed to be fixed in position in relation to this and to increase continuously and proportionately from zero until the value of the limiting load is reached. At a certain load level the most heavily stressed section of the structure will become completely plastic, i.e. the moment in this section now reaches the maximum value, $M_y=M_u$, which this section is capable of sustaining.

An initial plastic hinge will thus have been formed in the structure. During further increase in load the moment is constant and of known magnitude at this plastic hinge, and the degree of static indeterminacy has therefore decreased by one unit while load further increases from this load level. During the further increase in load, after some time another plastic hinge will be formed at some other point in the structure at a higher load level. The moment is now of known magnitude at this section also, and the degree of static indeterminacy has decreased by another unit while load further rises.

As load is gradually increased, the degree of static indeterminacy thus decreases as new plastic hinges are formed, and the structure will therefore, at a certain load level, change into a statically determinate structure for further increase in load. When, on further increase in load, one more plastic hinge is formed, the structure finally changes into a mechanism and collapse ensues.

The load which acts on the statically determinate structure immediately before the last plastic hinge is formed is thus a measure of the loadbearing capacity of the structure, its limiting or ultimate load.

As the load increases between two load levels at which two consecutive plastic hinges are formed, there takes place, simultaneously with the increase in load, a plastic rotation at the already formed plastic hinges. In order therefore that it should be possible for the load to be increased right up to the limiting load determined by behaviour of the structure as a mechanism, it is essential that the necessary plastic rotation can take place at the plastic hinges without material failure at these points.

The process described above can be illustrated by means of a worked example.

Let us study a beam of the configuration and loading shown in FIG. 1.1b. It is assumed that this beam has ideal elasto-plastic properties at every section in conformity with the moment-curvature diagram shown in the figure. The ultimate moment M_u of the beam is then assumed to be the same for both positive and negative bending moments, and the symbol M_u therefore refers to the absolute value of the moment.

The structure is statically indeterminate in the first degree, and the formation of an initial plastic hinge therefore makes the structure statically determinate for further increase in load. When a second plastic hinge is formed the structure changes into a mechanism in response to attainment of the collapse load.

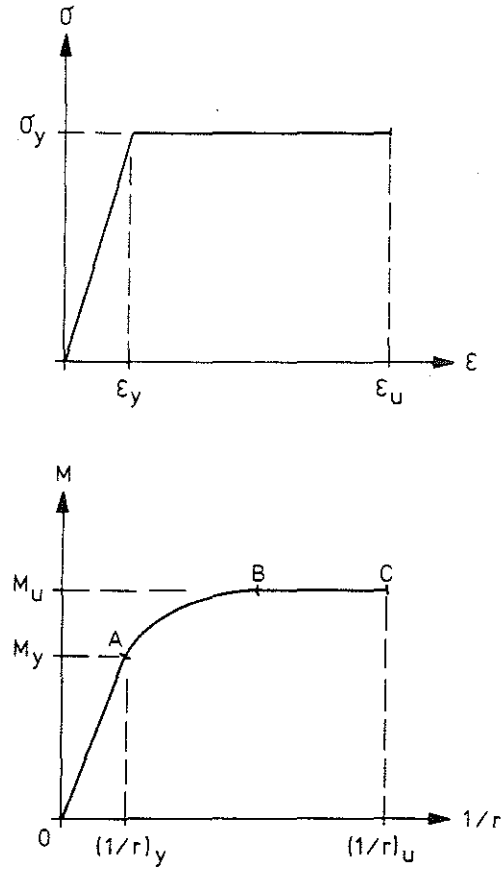

FIG 1.1a Stress-strain curve for ideal elasto-plastic material. Schematic moment-curvature curve for the cross section of an ideal elasto-plastic material.

Let us note what happens inside the structure as conditions gradually become plastic due to increase in the load Q from zero.

For small values of Q the structure behaves in a completely elastic manner. The moment distribution can be calculated by the elastic theory and has the shape shown in the figure, with the greatest moment at the section of fixity. As load is gradually increased, Q assumes a value Q_y at which a plastic hinge PH is formed at the section of fixity. The magnitude of Q_y is determined by the condition

$$\frac{3}{16} Q_y l = M_u$$

which gives

$$Q_y = \frac{16 M_u}{3l} \qquad (1.1.1)$$

During gradual increase in load up to Q_y there is no rotation at the rigidly restrained section. When load is increased beyond Q_y a plastic rotation θ takes place at the plastic hinge formed. The increase in load $\Delta Q = Q - Q_y$ is not accompanied by a corresponding increase in fixing moment, since the moment at the section of fixity has already attained its maximum value. With the assumed shape of the moment-curvature diagram, the rotation at the plastic hinge can therefore be calculated by the elastic theory as for a beam simply supported at both ends. We thus have

$$\theta = \frac{1}{16} \frac{\Delta Q l^2}{EI} \qquad (1.1.2)$$

When the load Q is greater than Q_y, the span moment under the point load is

$$M_m = \frac{1}{4} Ql - \frac{1}{2} M_u \qquad (1.1.3)$$

At this load level the structure is statically determinate for further increase in load since the support moment has assumed the known value M_u, and the span moment can therefore be calculated according to the equilibrium equation (1.1.3.).

The ultimate load Q_u of the structure is reached when a plastic hinge is also formed at the midpoint of the span, i.e. when M_m attains the value M_u. When this occurs a mechanism is formed and collapse therefore ensues. This limit state is determined by Equation (1.1.3) with $Q = Q_u$ and $M_m = M_u$

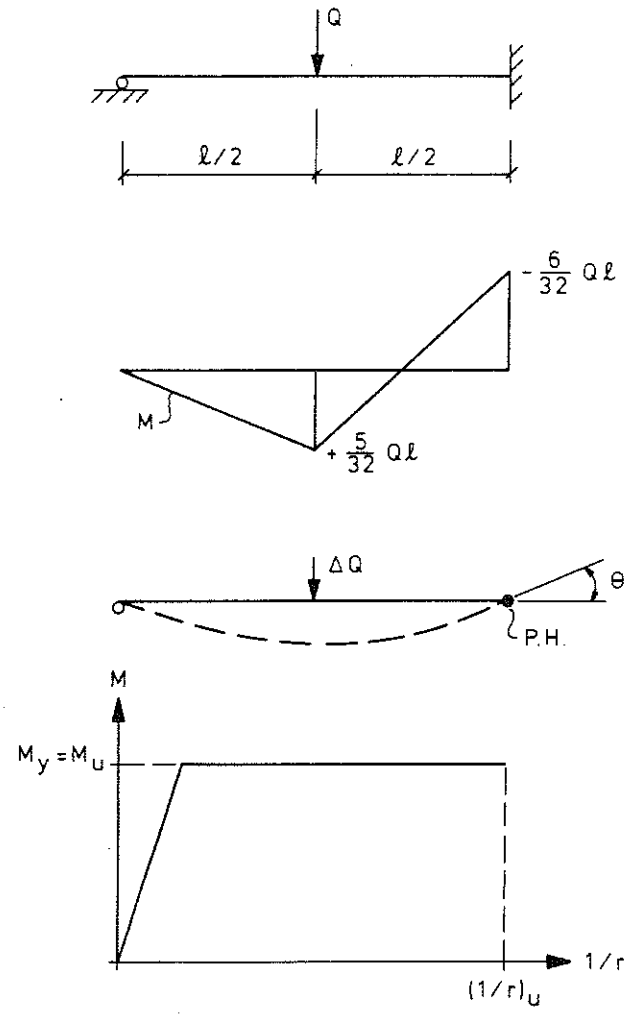

FIG 1.1b Beam fixed at one end with point load Q and associated moment distribution according to the elastic theory. Plastic rotation θ at the plastic hinge PH due to the point load ΔQ. Moment-curvature curve for the beam section.

$$M_u = \frac{1}{4} Q_u - \frac{1}{2} M_u$$

which gives

$$Q_u = \frac{6M_u}{l} \qquad (1.1.4)$$

After the first plastic hinge has been formed at the section of fixity, the load can therefore be further increased by

$$\Delta Q = Q_u - Q_y = \frac{6M_u}{l} - \frac{16M_u}{3l} = \frac{2M_u}{3l} = \frac{Q_y}{8} \qquad (1.1.5)$$

before the structure collapses.

During increase in the load from Q_y to Q_u there takes place a plastic rotation about the plastic hinge at the section of fixity, which can be calculated using Equations (1.1.2) and (1.1.5).

$$\theta_r = \frac{1}{16} \frac{2M_u}{3l} \frac{l^2}{EI} = \frac{1}{24} \frac{M_u l}{EI} \qquad (1.1.6)$$

The plastic rotation calculated from (1.1.6) is that required in order that a beam mechanism may be formed at the ultimate load Q_u. If material failure occurs owing to excessive material strain in the first plastic hinge before the load Q reaches the value Q_u, the actual ultimate load is less than Q_u and the ultimate load determined by the limit state method is therefore too high. We can thus say that the plastic hinge has a rotation requirement θ_r which, in the case studied, is calculated from Equation (1.1.6). This rotation requirement must be compared with the ability of the plastic hinge to rotate in a plastic manner without consequent material failure, i.e. without attainment of the ultimate curvature $(1/r)_u$ in FIG. 1.1b. This ability is denoted the rotation capacity θ_u of the plastic hinge.

One condition for the limit state method described above to be capable of use for determination of the ultimate load of a structure is that the rotation requirement should be no greater then the rotation capacity. The condition

$$\theta_r \leq \theta_u \qquad (1.1.7)$$

must therefore be satisfied for all plastic hinges in the statically determinate structure which are needed to sustain the increase in load immediately prior to formation of the mechanism due to the limiting load.

For steel structures the condition (1.1.7) is generally satisfied. Apart from extreme exeptional cases, there is therefore no need as a rule to pay much attention to the rotation capacity of plastic hinges. The situation is diffenent in reinforced concrete structures where it has been found in experiments that the rotation capacity of plastic hinges in structures loaded to failure may be insufficient to permit the redistribution of moments which a design according to the plastic theory assumes. It is therefore essential that it should be possible to calculate, at the design stage, the rotation requirement and rotation capacity for those plastic hinges which are assumed in design according to the limit state method.

It is evident from the above worked example that it is in pronciple easy to calculate the rotation requirement of a plastic hinge. The rotation requirement will therefore be dealt with only in a summary manner in this report, and attention will instead be concentrated on an analysis of the rotation capacity of plastic hinges in reinforced concrete structures.

1.2 Rotation requirement

The rotation requirement of plastic hinges in statically indeterminate beam structures of reinforced concrete, acted upon by different external loads and imposed deformations, has been studied by Alemo (1976) and others. It appears that the rotation requirement of a plastic hinge can be given the general form

$$\theta_r = \kappa_o \frac{M_u l}{EI} \qquad (1.2.1)$$

i.e. the same form as in the above worked example - see Equation (1.1.6).

If any imposed deformations which may be present are ignored, then κ_o is a coefficient which is a function only of the configuration of the structure and the type and placing of the load. See also Plem (1973).

M_u is the ultimate moment of the plastic hinge under consideration, and can be written

$$M_u = A_s f_{st} d(1 - \frac{\omega}{2}) \qquad (1.2.2)$$

where

A_s = cross sectional area of reinforcement at the plastic hinge
f_{st} = tensile strength of tension reinforcement
d = effective depth of the section containing the plastic hinge
ω = effective reinforcement ratio

A plastic hinge is often discontinous, for instance when it forms over an intermediate support in a continous beam. In such cases it is easiest to study rotation requirement and rotation capacity separately for each side. The expression (1.2.1) refers to the rotation requirement on one side of the plastic hinge, and l is the length of the beam on the side being considered.

EI is the mean beam stiffness calculated for the concrete in Stage II, i.e. when it is cracked and elastic. The stiffness may be obtained from a diagram constructed by Larsen & Vigerust (1966) in the form

$$EI = A_{sm} E_s d^2 \xi \qquad (1.2.3)$$

where

A_{sm} = a mean value over the length of the beam of the cross sectional area of the reinforcement, adapted in view of the moment distribution
E_s = modulus of elasticity of the reinforcing steel
ξ = a function of $\alpha\rho$ where $\alpha = E_s/E_c$, i.e. the ratio of the modulus of elasticity of steel to that of concrete, and ρ is the geometrical reinforcement ratio

If A_{sm} is assumed to be proportional to A_s and Equations (1.2.2) and (1.2.3) are substituted into Equation (1.2.1), we have

$$\theta_r = \frac{\kappa_1}{\xi} \frac{f_{st}}{E_s} \frac{l}{d} \left(1 - \frac{\omega}{2}\right) \qquad (1.2.4)$$

According to the above equation, for a given reinforcement the rotation requirement is directly proportional to the slenderness l/d of the beam. If the ratio $(1-\omega/2)/\xi$ is studied for variable normal reinforcement ratios, it is found that the rotation requirement θ_r decreases for increasing values of ω.

As will be seen from the example in Section 1.1, it is in principle easy to calculate the rotation requirement of a plastic hinge. The calculation can be carried out with the aid of information in the usual manuals or by means of

the energy equation. However, for structures of a high degree of static indeterminacy, such as multistorey frames, calculation can be laborious. For such structures, Baker (1956) developed a systematic calculation method which, when formulated in matrix notation, is suitable for computer programs.

Other factors, not studied in detail here, may affect the magnitude of the rotation requirement. Brief comments on these are as follows.

Displacements of supports can, depending on the directions of the displacements, increase or decrease the rotation requirement.

Creep of the concrete is generally dealt with in calculations by reducing the modulus of elasticity of concrete. This increases the parameter $\alpha\rho$, and reduces ξ. According to Equation (1.2.4), creep thus increases the rotation requirement.

Depending on the geometrical design and reinforcement of the structure, shrinkage of the concrete may increase or decrease the rotation requirement.

Cracking of the concrete always reduces the rotation requirement. This is commented on further in Section 1.3.

1.3 Rotation capacity

In principle, the rotation capacity of a plastic hinge in a reinforced concrete beam can be determined from the moment-curvature diagram of the beam section concerned. Such a diagram is shown to the right ot FIG. 1.3a, in which M is the bending moment and 1/r the beam curvature. In the diagram M_y is the moment at yield and M_u the ultimate moment. The figure in the centre illustrates a variation "b" in moment over the beam length l_o between a plastic hinge PH and the nearest point of zero moment. In the following, this section of the beam will be referred to as the rotation span of the plastic hinge. The variation "b" in moment may be considered to correspond to a uniformly distributed load on a beam fixed at PH. On top of this diagram there is another diagram which represents the variation in beam curvature along the rotation span. It has been drawn up with the aid of the moment diagram and the moment-curvature diagram.

A corresponding transformation of the beam curvature diagram by means of another moment curve "a", which may be considered to correspond to the variation in moment in the vicinity of a plastic hinge in the span in a beam subjected to a uniformly distributed load, is shown to the left in the figure.

The rotation between the end cross sections of the portion l_o of the beam is obtained as the integral of the curvature over the length l_o, i.e. as the area below the 1/r curve constructed. Part of this rotation is elastic and reversible, another part is plastic and irreversible. The latter has been shaded in the figure and marked "B". According to the definition, this part is the rotation capacity θ_u of the plastic hinge. Traditionally, the rotation capacity is regarded as though it were concentrated at the plastic hinge but, as will be seen, it is in reality distributed over part of the length of the rotation span. It is also evident from the figure that the magnitude of the rotation capacity is dependent on the magnitude of the area "A" above the M-1/r diagram, and on the shape of the moment curve. Area "B" is larger at moment curve "a" than at moment curve "b", which means that the rotation capacity in the former case is greater than in the latter case.

It will be evident from the above that the rotation capacity of a plastic hinge in a given situation can be obtained by calculation of the area "B" in FIG. 1.3a. However, such an approach is not applied in the following, since in recent year interest has focussed on the study of the behaviour of structures under the action of extreme loads. Impact loads play a dominant part in this connection, and the effect of impact loads on a beam structure cannot be studied without including the deformation energy of the structure in the calculations. Calculation of the rotation capacity θ_u in the following has therefore been based on a study of the variation of energy in the part of the beam adjacent to a plastic hinge. In this way the calculation method devised attains such properties that it can relatively easily be further developed into a calculation method for analysis of statically indeterminate beams subjected to impact loads. Such development has been planned, but has been deferred until later work.

The moment-curvature diagram in FIG. 1.3a assumes a section cracked from the outset. If an initially uncracked section is assumed, the general appearance of the moment-curvature diagram will conform to the line OAFED in FIG. 1.3b. The slope of the line OB represents the bending stiffness of the uncracked section, and the slope of the line OC represents the bending stiffness of the cracked section. The moment M_r is the moment which initiates cracking. If the area AFCBA above the moment curve is transformed and the corresponding curvature contribution is subsequently integrated over the length of the rotation span, the rotation which occurs due to cracking is obtained. This phenomenon has been studied by Rechardt (1968) and others.

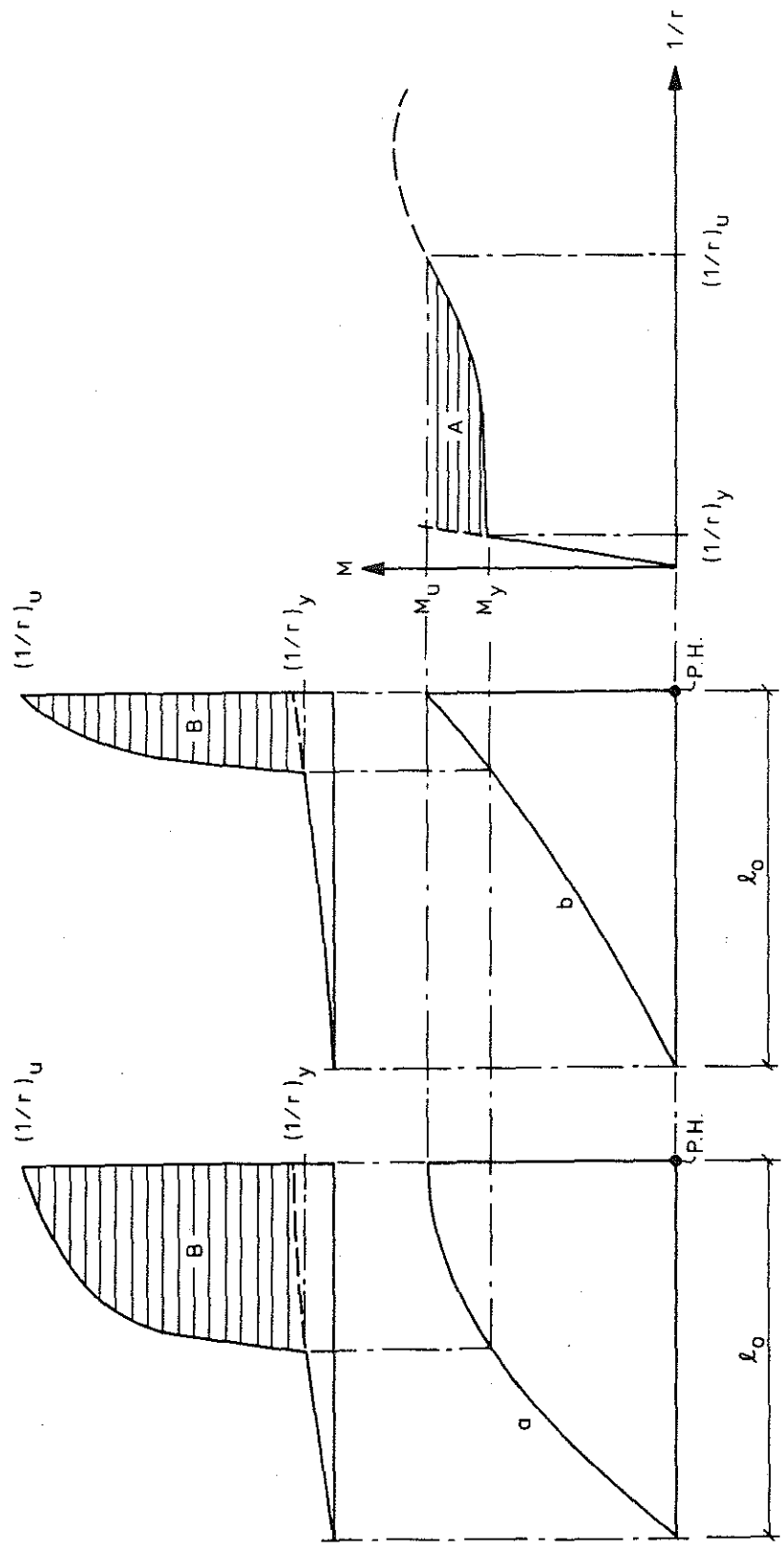

FIG 1.3a Distributions of curvature along the rotation span of length l_0. The distributions have been calculated by transforming the moment-curvature curve of the beam section by means of the moment curves a and b.

The intention here is to regard the rotation capacity as an unambiguously determined quantity associated with the plastic hinge and the part of the beam adjacent to this. The contribution due to cracking of the concrete is therefore not included in the rotation capacity, but is assumed instead to be taken into account as a corresponding reduction of the rotation requirement θ_r when the condition (1.1.7) is checked. For the same reason, no study is made either of the effect on the rotation capacity due to shrinkage of the concrete. The effect of shrinkage cannot be unambiguously associated with the plastic hinge region, but is dependent on the response of the entire structure to the deformation action.

1.4 The scope of the work

The primary object of the work reported here has been to study the way in which different material properties influence the rotation capacity of a plastic hinge. If such a study is to be meaningful, it is essential that the calculations should be based on realistic stress-strain curves for the constituent materials concrete and steel. Such curves are presented in Chapter 2. However, the stipulation regarding realism in describing materials poses computational difficulties of such magnitude that it has been impossible to construct exact formulae for calculation for the rotation capacity. The calculation method which is developed in Chapters 3-6 has therefore been formulated right from the beginning in view of the need to program it for processing in a computer. Such a program has been developed, and it is presented and commented on in an appendix.

Certain limitations in the usefulness of the program must be pointed out. Only rectangular cross sections have been studied. However, T-beams can also be dealt with provided that the entire compression zone is situated in the flange. In such a case the width of the flange must be used as the width of the beam in calculating the effective reinforcement ratio ω. This limitation is of quite a minor nature since most beams in practical use have a rectangular or T section.

The program does not take into account gradual curtailment, if any, of the reinforcing steel over the length of the rotation span. It is probable that this does not play a major role since most of the consumption of energy occurs in a very limited region adjacent to the plastic hinge. It may be expected that in practical beam design the quantity of reinforcement is constant over this region.

The effect of normal force has been ignored.

Results of calculations regarding combinations of typical steels and concrete types, and also the calculated rotation capacity when the parameter values chosen for the typical steels and concrete types have been departed from, are shown in Chapter 7.

The effect on rotation capacity due to creep of concrete within the rotation span is studied in Chapter 8.

The effect of compression reinforcement and the effect of concrete creep in conjunction with compression reinforcement is dealt with in Chapter 9.

In calculations regarding the above phenomena, discussed in Chapters 7-9, the effect of shear force which may be present simultaneously with the bending moment has been ignored. In Chapter 10 the analytical model is modified in such a way that it is possible, at least approximately, to study the effect of shear force. It is found that the effect of shear force is considerable when the rotation span is not slender.

The presence of stirrups around the compression zone of the beam has been found to increase the rotation capacity considerably. This is studied in Chapter 11 where an approximate method which also includes this beneficial effect in the developed analytical model is derived in a semi-empirical manner.

The developed calculation method has been compared with the results of tests carried out at the Department of Structural Engineering, Division of Concrete Structures, Chalmers University of Technology, Gothenburg. It is found that there is reasonable agreement between the experimental and calculated rotation capacities. One partial result of this comparison is utilised in Chapter 10 of this report. It is planned that a complete report will be published elsewhere.

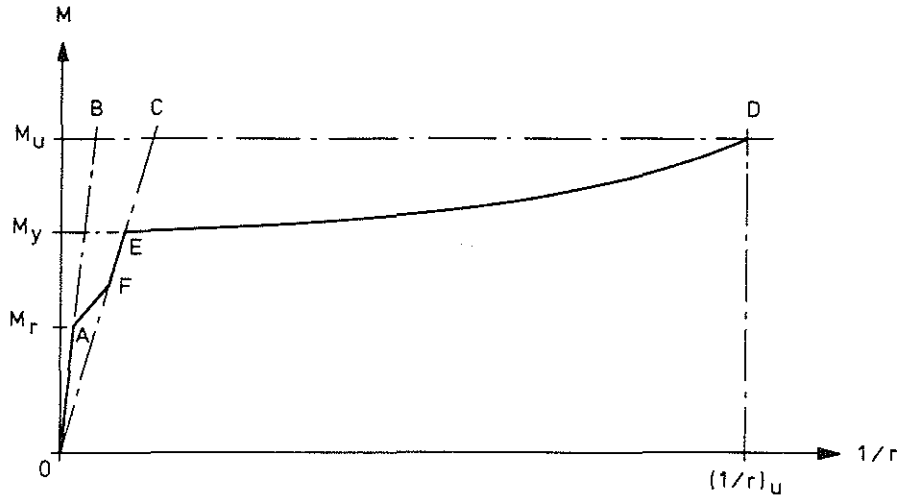

FIG 1.3b Moment-curvature curve for an initially uncracked beam section. The cracking moment of the section is M_r.

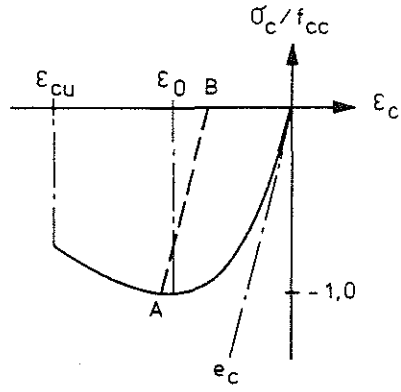

FIG 2.1a Schematic form of the stress-strain diagram for concrete in compression in non-dimensional terms. The line AB represents removal of the load.

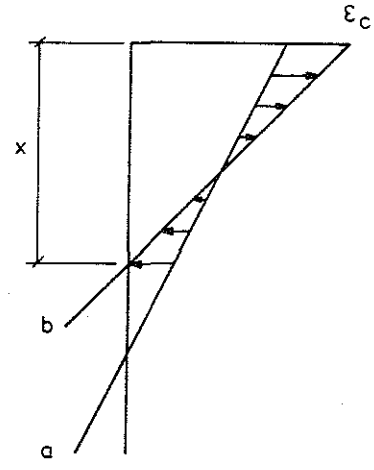

FIG 2.1b Distribution of strain in the compression zone of the concrete for two consecutive situations a and b. In one area the concrete is being subjected to load while in another area it is being unloaded.

2 THE STRESS-STRAIN CURVES FOR STEEL AND CONCRETE

The selected calculation procedure permits the application of realistic stress-strain curves for the steel and concrete. Analytical expressions which give a good approximation of the mechanical properties of these materials when subjected to short-term loads are given below. Concrete and steel are dealt with separately.

2.1 The stress-strain curve for concrete

Concrete in tension is assumed to be cracked. Active concrete is therefore only found in the compression zone of the beam, with the stress-strain curve generally in conformity with FIG. 2.1a. In order that the formulae derived later on may have the greatest possible general application, the stresses are made non-dimensional by dividing them by the compressive strength f_{cc} of the concrete. In this way the modulus of elasticity is also non-dimensional. The expression for the non-dimensional initial modulus of elasticity for short-term loading is

$$e_c = \frac{E_c}{f_{cc}} \qquad (2.1.1)$$

In FIG. 2.1b the compression zone of depth x is examined in a situation just before crushing failure. During the gradual increase in load up to failure, the distribution of strain at a certain instant was represented by line a. A little later the distribution is given by line b. The figure shows that the compression zone is divided into two regions, an upper one where the concrete is being subjected to load and therefore conforms to the basic full-line curve of the stress-strain diagram, and a lower one in which the concrete is still in compression but is being unloaded. For concrete in the latter region the stress-strain relation is described by an unloading curve which is assumed to be a straight line of slope e_c, shown by the dashed line AB in FIG. 2.1a. This is taken into account in the developed computer program.

A large number of analytical expressions are given in the literature to describe the stress-strain curve of concrete in compression. Use is made here of that proposed by Sargin & Handa (1969) which can be written as

$$\frac{\sigma_c}{f_{cc}} = -\frac{\kappa_1\left(\frac{\varepsilon_c}{\varepsilon_o}\right)+(\kappa_2-1)\left(\frac{\varepsilon_c}{\varepsilon_o}\right)^2}{1+(\kappa_1-2)\left(\frac{\varepsilon_c}{\varepsilon_o}\right)+\kappa_2\left(\frac{\varepsilon_c}{\varepsilon_o}\right)^2} \qquad (2.1.2)$$

The coefficient κ_1 contained in this expression is obtained as

$$\kappa_1 = -e_c \varepsilon_o \qquad (2.1.3)$$

where ε_o is the limit strain (with the appropriate sign) corresponding to the maximum compressive stress $\sigma_c/f_{cc} = -1.0$. The shape of the curve between $\varepsilon_c = 0$ and $\varepsilon_c = \varepsilon_o$ is essentially governed by the value of κ_1, while its shape after it has passed its extreme point is mainly determined by the coefficient κ_2. This latter coefficient has no direct physical meaning. In purely practical terms, the value of κ_2 is determined by making σ_c/f_{cc} have the correct value at the ultimate compressive strain ε_{cu}.

In order that the effect of different concrete properties on the rotation capacity may be studied, comparative calculations with two distinct types of concrete, denoted A and B, are performed in Chapter 7.

Concrete of Type A is broadly in conformity with that recommended by the CEB, characterised by $\varepsilon_o = -2.0\,‰$ and $\varepsilon_{cu} = -3.5\,‰$. An appropriate value of the non-dimensional modulus of elasticity e_c has been considered to be 1200. It will be shown later, in Chapter 7, what the effect is on the rotation capacity if a departure is made from the chosen value.

According to Equation (2.1.3) the value of the coefficient $\kappa_1 = 1200 \cdot 0.002 = 2.4$. The coefficient κ_2 is determined in such a way that $\sigma_c/f_{cc} = -0.8$ for $\varepsilon_{cu} = -3.5\,‰$. This condition yields $\kappa_2 = 0.363$. With the selected coefficients, the stress-strain curve for concrete of Type A is that shown in FIG. 2.1c.

Compared with experimentally determined values of ε_o and ε_{cu}, it would appear that the values recommended by the CEB have been chosen with a comfortable margin of safety. In actual fact, the magnitudes of ε_o and ε_{cu} do not make much difference, when these parameters are to be applied for the calculation of the ultimate moment. In this connection it is ε_{cu} which is of the greatest significance, since it determines the boundary ω_b between an over-reinforced and normally reinforced section, where ω_b detones the effective reinforcement ratio corresponding to balanced reinforcement. For the calculation of the rotation capacity, however, it is found that it is important for ε_{cu} not to be limited too stringently unless absolutely necessary. For this reason it has been decided to include in the study of the rotation capacity a concrete which has mechanical properties more in keeping

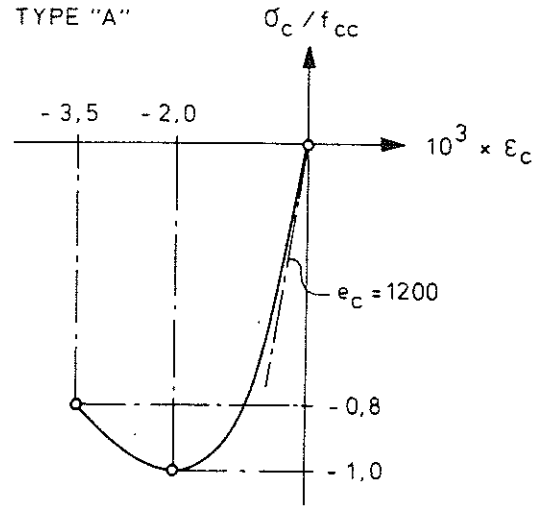

FIG 2.1c Non-dimensional stress-strain diagram for concrete type A in compression

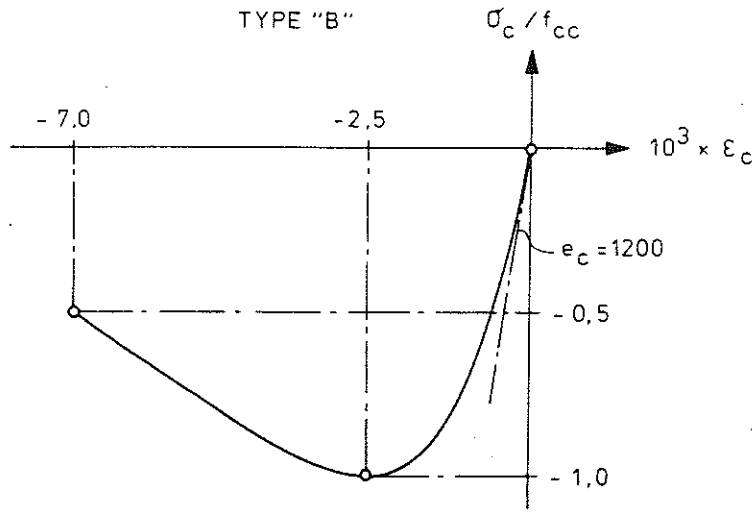

FIG 2.1d Non-dimensional stress-strain diagram for concrete type B in compression

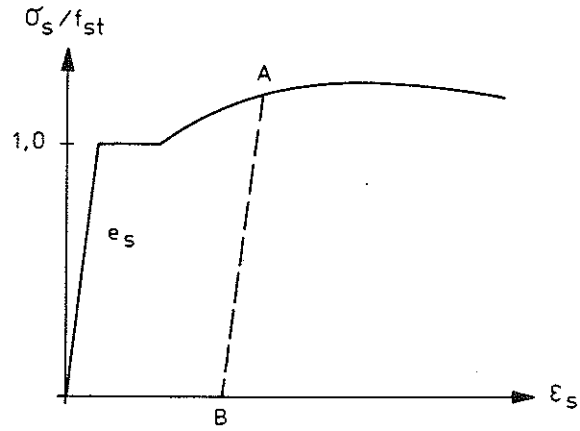

FIG 2.2a Schematic form of the stress-strain diagram for tension reinforcement in non-dimensional terms. The line AB is an unloading line. The diagram relates to steel with a pronounced yield point.

with actual conditions. Such a concrete will in the following be referred to as concrete of Type B.

On the basis of tests carried out by Mattock (1965) and Corley (1966), the characteristic compressive strains ε_o = -2.5 ‰ and ε_{cu} = -7.0 ‰ are chosen for concrete of Type B. For this concrete also, the modulus of elasticity is put e_c = 1200, which makes κ_1 = 1200·0.0025 = 3.0. The coefficient κ_2 is given such a value that σ_c/f_{cc} = -0.5 for ε_{cu} = -7.0 ‰ , which gives κ_2 = 0.342. Concrete of Type B thus determined by the selected parameters has stress-compressive strain curve shown in FIG. 2.1d.

The effect of creep in the concrete is discussed separately in Chapter 8.

2.2 The stress-strain curve for reinforcing steel

The stress-strain curve for reinforcement in tension is shown schematically in FIG. 2.2a. It is assumed that the stress-strain curve for reinforcement in compression is of the same type.

In the case of steel also it is found convenient to use non-dimensional stresses, which are obtained by division by the tensile strength f_{st} of the steel defined as the yield stress of hot-rolled steel and the 0.2% proof stress of cold-worked steel. Owing to this, the modulus of elasticity of the steel is also non-dimensional. The non-dimensional modulus of elasticity is

$$e_s = \frac{E_s}{f_{st}} \qquad (2.2.1)$$

Compressive reinforcement may be subjected to unloading during the gradually increasing stressing of the section up to failure. A situation may be arise where the depth of the compression zone decreases as the strain in the tensile reinforcement increases. The tensile reinforcement may also be subjected to unloading as the section proceeds towards failure. This may occur if there is a steep drop in concrete stresses as the compressive strain in the concrete increases. In this case, once the maximum value has been passed, the bending moment drops rapidly as the curvature increases. In view of these phenomena, the basic curve of the stress-strain diagram must be supplemented by unloading curves schematically represented by the straight line AB of slope e_s in FIG. 2.2a. This has been taken into account in the program.

The stress-strain curve for a hot-rolled steel (denoted in the following HR steel) may be approximated by straight lines and a second degree parabola, in principle as shown in FIG. 2.2b. The exact form is determined by the following parameters:

e_s, the non-dimensional modulus of elasticity of the steel, defined by Equation (2.2.1),

ε_2, an indirect parameter which is defined from the equation $\varepsilon_2 = 1/e_s$ and can therefore be interpreted as the strain corresponding to the limit of proportionality of the steel,

ε_1, the strain corresponding to the boundary between the yield region and the strain hardening region of the steel.

ε_o, the limit strain which occurs at the maximum tensile strength f_{stu},

ε_{su}, the ultimate strain,

η, the ratio of f_{stu} to f_{st}.

For the sake of simplicity, the diagram is assumed to be horizontal between ε_o and ε_{su}. As a rule, this has no effect on the rotation capacity since f_{stu} is hardly ever reached.

With the parameters defined above, the stress-strain relation for HR steel may be expressed as

$$\frac{\sigma_s}{f_{st}} = \begin{cases} \varepsilon_s e_s & 0 \le \varepsilon_s < \varepsilon_2 \\ 1{,}0 & \varepsilon_2 \le \varepsilon_s < \varepsilon_1 \\ \eta-(\eta-1)\left(\dfrac{\varepsilon_o-\varepsilon_s}{\varepsilon_o-\varepsilon_1}\right)^2 & \varepsilon_1 \le \varepsilon_s < \varepsilon_o \\ \eta & \varepsilon_o \le \varepsilon_s \le \varepsilon_{su} \end{cases} \qquad (2.2.2)$$

When values of the parameters which represent a typical HR steel are to be chosen, the difficulty arises that these parameters vary over quite a large range, not only between grades of steel but also, due to statistical scatter, for one and the same grade of steel. By studying the stress-strain

curves for Swedish HR steels, and taking into consideration the scatter in these, the following parameter values have been chosen to define a representative HR steel.

$e_s = 350$
$n = 1.4$
$\varepsilon_1 = 0.015$
$\varepsilon_o = 0.080$
$\varepsilon_{su} = 0.100$

Obviously, for instance for deformed bars Ks 40, the value of ε_{su} is considerably higher than the ultimate strain selected above, but this has no appreciable influence on the rotation capacity since, after all, ε_{su} is never reached before the section fails.

As far as the non-dimensional modulus of elasticity e_s is concerned, since E_s is practically constant and equal to 200 GPa for different grades of steel, e_s varies as a function of f_{st}. FIG. 2.2c shows the relationship between the nominal yield stresses or 0.2% proof stresses of common Swedish reinforcing steels. It is seen in the figure that, as a convenient mean value, $e_s = 350$ may be chosen for both hot rolled and cold worked steel.

Within reasonable limits, deviations from the selected value have only a marginal effect on the calculated rotation capacity. This is demonstrated in Chapter 7.

With the selected parameters, the stress-strain curve for the typical HR steel is that shown in FIG. 2.2b.

The stress-strain curve for a cold worked reinforcing steel (denoted in the following CW steel) can be approximated by a straight line and part of an ellipse, in principle according to FIG. 2.2d and e. The exact shape is determined by the parameters e_s, n, ε_2, ε_1, ε_o and ε_{su}, the definitions of which are the same as in the case of the HR steel. Of the above parameters ε_2 and ε_1 need not be given explicity since they are uniquely determined by the chosen curve geometry and the other parameters.

The stress-strain curve for the CW steel is calculated as follows. See also FIG. 2.2e.

$$\varepsilon_1 = 0{,}002 + \frac{1}{e_s} \qquad (2.2.3)$$

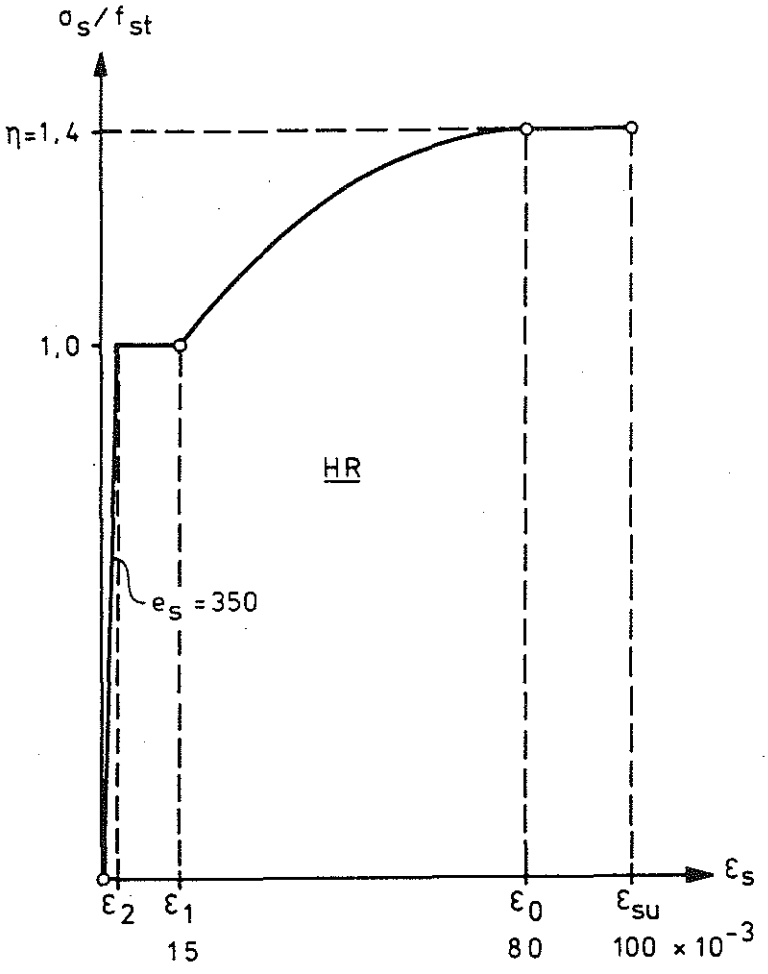

FIG 2.2b Non-dimensional stress-strain diagram for a representative HR steel.

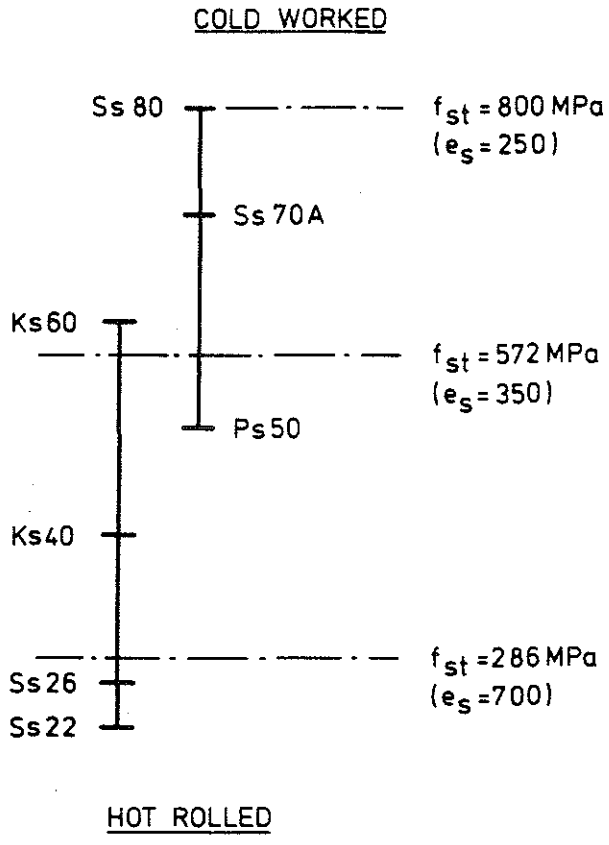

FIG 2.2c The relationships between the nominal yield stresses and 0.2% proof stresses of common Swedish reinforcing steels.

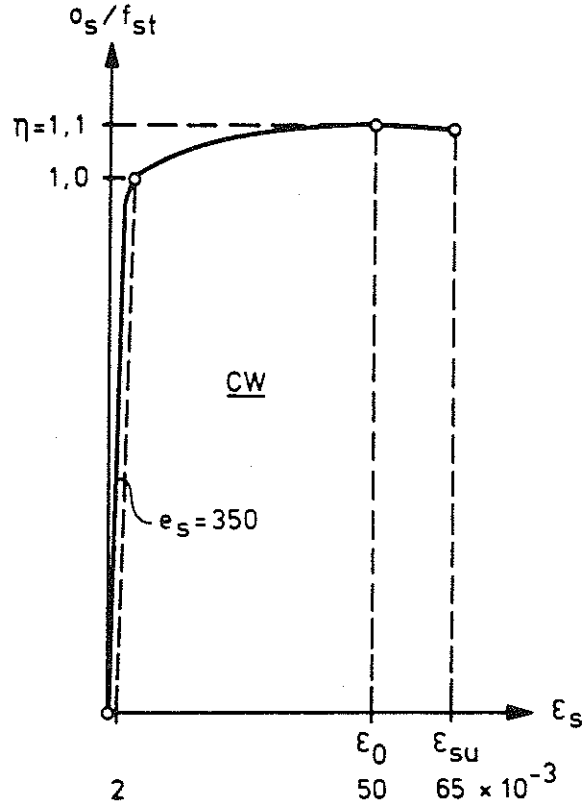

FIG 2.2d Non-dimensional stress-strain diagram for a representative CW steel.

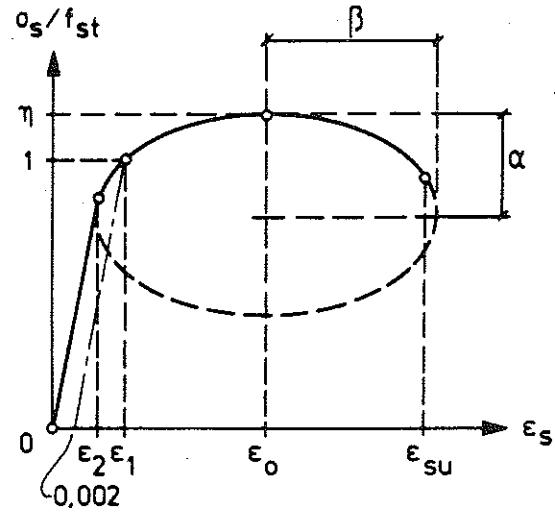

FIG 2.2e Stress-strain diagram of a CW steel approximated by a straight line and part of an ellipse.

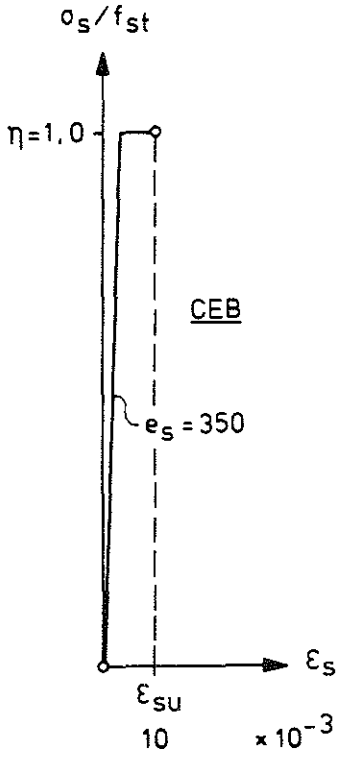

FIG 2.2f The stress-strain diagram recommended by the CEB for reinforcing steel.

The horizontal semi-axis of the ellipse has the length

$$\beta = \frac{1}{g_1}\left(g_2 + \sqrt{g_2^2 - g_1 g_3}\right) \qquad (2.2.4)$$

where

$$g_1 = e_s^2(\varepsilon_o-\varepsilon_1)^2-4(e_s\varepsilon_o-\eta)(\eta-1) \qquad (2.2.5)$$

$$g_2 = (e_s\varepsilon_o-\eta)(\eta-1)((e_s\varepsilon_o-\eta)-(\eta-1)) \qquad (2.2.6)$$

$$g_3 = (e_s\varepsilon_o-\eta)^2(\eta-1)^2 \qquad (2.2.7)$$

The length of the vertical semi-axis of the ellipse is

$$\alpha = \frac{\beta(\varepsilon_o-\varepsilon_1)}{\sqrt{(\eta-1)(2\beta-(\eta-1))}} \qquad (2.2.8)$$

The strain at the limit of proportionality is calculated from the expression

$$\varepsilon_2 = \frac{\varepsilon_o + \frac{\alpha^2}{\beta^2}(\eta-\beta)e_s}{1 + \frac{\alpha^2}{\beta^2}e_s^2} \qquad (2.2.9)$$

The expression for the stress-strain curve is therefore

$$\frac{\sigma_s}{f_{st}} = \begin{cases} e_s\varepsilon_s & 0 \le \varepsilon_s < \varepsilon_2 \\ \eta-\beta\left(1-\sqrt{1-\left(\frac{\varepsilon_o-\varepsilon_s}{\alpha}\right)^2}\right) & \varepsilon_2 \le \varepsilon_s \le \varepsilon_{su} \end{cases} \qquad (2.2.10)$$

In the following, the steel described by the parameters

$e_s = 350$
$\eta = 1.1$
$\varepsilon_o = 0.050$
$\varepsilon_{su} = 0.065$

is considered to be a typical CW steel.

With the selected parameters, the stress-strain curve for the typical CW steel is that shown in FIG. 2.2d.

For both the HR and CW steels, the selected curves are representative mean curves. A study is made in Chapter 7 of the rotation capacities which are obtained using the above stress-strain curves, and the changes which occur in the rotation capacity when these selected curves are varied in different ways.

As a supplement to the stress-strain curves for HR and CW steels, the stress-strain curve at present recommended by the CEB for reinforcing steel is also included here. The shape of this curve is given in FIG. 2.2f. It is characterised by the parameters

$e_s = 350$
$n = 1.0$
$\varepsilon_1 = \varepsilon_o = \varepsilon_{su} = 0.010$

the value assigned to e_s being the same as that applied for the steel types specified by the more complete stress-strain curves in FIG. 2.2b and d.

The reason why the CEB has selected this stress-strain curve for reinforcing steel appears to be that, computationally, it yields practically the same ultimate moment as the two more realistic curves studied here. However, as will be seen from Chapter 7, such a simplified stress-strain diagram cannot be used as the basis for calculation of the rotation capacity.

3 THE DEPTH OF THE COMPRESSION ZONE

Using Bernoulli's hypothesis and a condition of equilibrium, the relation between beam curvature and depth of compression zone is calculated in this Chapter.

3.1 Calculation geometry

Using the symbols F_s for force in the tension reinforcement, F_{sc} for force in the compression reinforcement and F_c for the resultant of the concrete stresses in the compression zone of the beam, resolution of forces yields the equilibrium condition.

$$F_c + F_{sc} + F_s = 0 \qquad (3.1.1)$$

The positions and positive directions of these forces are shown in FIG. 3.1a.

In the view of the numerical caluclation procedure, the compression zone is divided into strips of equal depth parallel to the neutral axis. In principle, this division can be effected in two distinct ways. One is characterised by the fact that the depth of the compression zone which is applicable at a certain instant is divided into a constant number of strips. This means that the depth of a strip varies in step with the depth of the compression zone. When this method of subdivision is applied, a strip will successively represent different parts of the concrete in the compression zone during the loading process.

The second method of subdivision is characterised by the fact that a fictitious compression zone depth is introduced and that this is kept constant during application of the load. The fictitious depth x_m is made so large that it will at all times accommodate the real compression zone applicable at that instant. When this method is applied, all the strips are not active and the number of active strips changes during application of the load. In return, there is the advantage that the depth of a strip remains constant, and that each strip always represents the same concrete area. This latter aspect is significant when the previous history of the concrete must be taken into account, for instance when a strip is relieved of load.

The latter alternative is chosen here. It is illustrated in FIG. 3.1b. The strips are numbered from 1 to n, and the ordinate y_i to the centroid of strip No i is calculated according to the figure from the expression

$$y_i = -\frac{x_m}{n}\left(i - \frac{1}{2}\right) \qquad (3.1.2)$$

where n is the number of strips.

If we introduce the non-dimensional ordinate

$$\eta_i = \frac{y_i}{d} \qquad (3.1.3)$$

where d is the effective depth of the section, and the non-dimensional depth of the compression zone

$$\xi_m = \frac{x_m}{d} \qquad (3.1.4)$$

Equation (3.2.1) can be written as

$$\eta_i = \frac{1}{n}\,\xi_m\left(\frac{1}{2} - i\right) \qquad (3.1.5)$$

If $\Delta A_c = x_m b/n$ denotes the area of a strip, and $A_c = bd$ the effective area of section, the non-dimensional part area α can be calculated from the expression

$$\alpha = \frac{\Delta A_c}{A_c} = \frac{1}{n}\,\xi_m \qquad (3.1.6)$$

which, substituted into Equation (3.1.5), yields

$$\eta_i = \alpha\left(\frac{1}{2} - i\right) \qquad (3.1.7)$$

According to FIG. 3.1b, the ordinate to the centroid of the tension reinforcement is

$$y_s = d - x_m$$

or, in non-dimensional form,

$$\eta_s = 1 - \xi_m \qquad (3.1.8)$$

According to the figure, the ordinate to the centroid of the compression reinforcement is

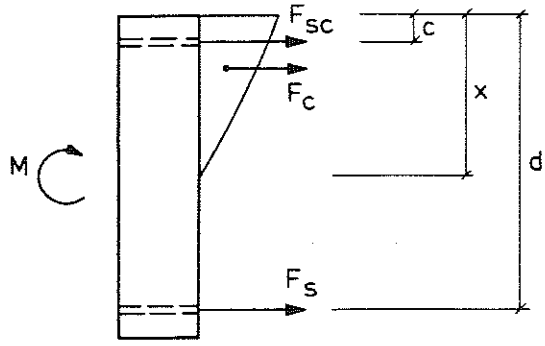

FIG 3.1a External moment M and internal forces F_{sc}, F_c and F_s to be used in establishing the equilibrium equation of the cross section. The figure shows the positive directions of forces and moments.

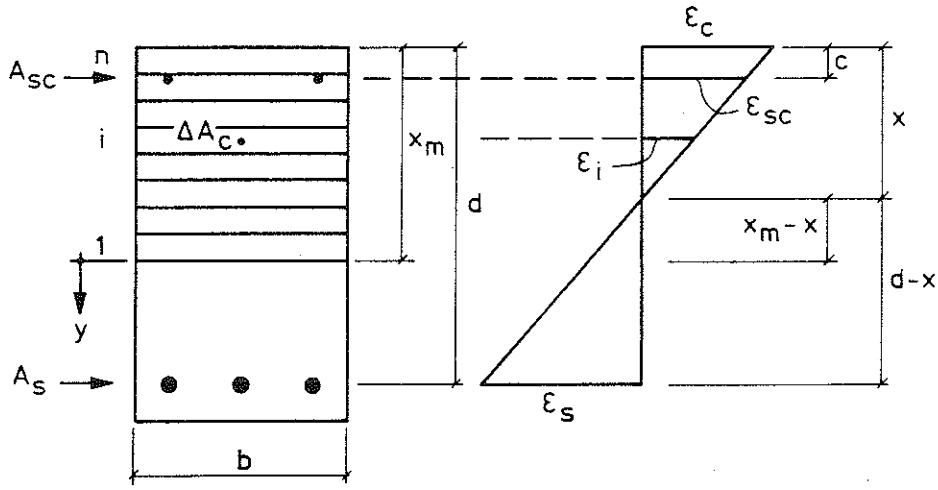

FIG 3.1b Geometry of cross section and distribution of strain over the depth of the section.

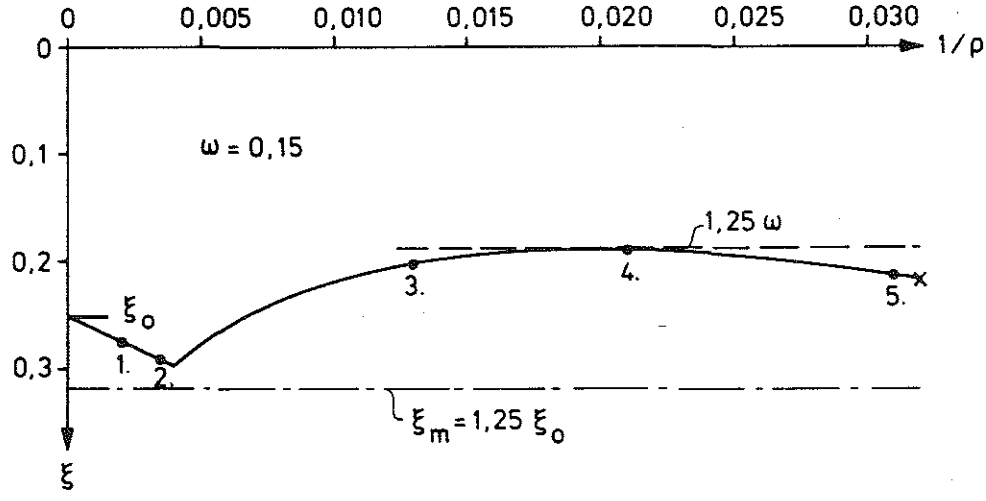

FIG 3.3a Variation in the depth ξ of the compression zone for increasing stress in the cross section. The numbered points refer to the stress distributions shown in FIG 3.3b.

$$y_{sc} = -x_m + c$$

where c is the distance between the compression reinforcement and the most heavily stressed edge. Using the notation

$$\gamma = \frac{c}{d} \qquad (3.1.9)$$

we obtain the non-dimensional ordinate of the compression reinforcement

$$\eta_{sc} = \frac{y_{sc}}{d} = \gamma - \xi_m \qquad (3.1.10)$$

The relevant strains are calculated as follows. According to Bernoulli's hypothesis and FIG. 3.1b, we obtain for the curvature of the beam the expression

$$\frac{1}{r} = \frac{\varepsilon_s}{d - x}$$

where r is the radius of curvature, ε_s the strain in the tension reinforcement, and x the depth of the compression zone at that instant. If this is multiplied by the effective depth d of the beam, we have

$$\frac{1}{\rho} = \frac{d}{r} = \frac{\varepsilon_s}{1 - \xi} \qquad (3.1.11)$$

where ρ is the non-dimensional radius of curvature and ξ denotes the non-dimensional depth of the compression zone at the instant under consideration. The expression (3.1.11) gives the depth of the compression zone

$$\xi = 1 - \rho\varepsilon_s \qquad (3.1.12)$$

as a function of the values of the radius of curvature and strain in the tension reinforcement which are applicable at each particular instant.

Further, from FIG. 3.1b we derive the relation

$$-\frac{\varepsilon_c}{x} = \frac{\varepsilon_s}{d - x} \qquad (3.1.13)$$

or

$$\varepsilon_c = -\frac{x}{d - x}\varepsilon_s = \xi\frac{\varepsilon_s}{1 - \xi}$$

which, after substitution into it of Equations (3.1.11) and (3.1.12) yields

$$\varepsilon_c = -(1 - \rho\varepsilon_s)\frac{1}{\rho} = \varepsilon_s - \frac{1}{\rho} \qquad (3.1.14)$$

In the above, ε_c is the maximum compressive strain in the concrete corresponding to the given parameter values $1/\rho$ and ε_s. The value of ε_c is compared with the ultimate compressive strain ε_{cu} in the concrete to see if crushing failure occurs in the concrete.

According to FIG. 3.1b, the strain ε_{sc} in the compression reinforcement is obtained from the expression

$$\frac{\varepsilon_{sc}}{\varepsilon_c} = \frac{x-c}{x} = \frac{\xi-\gamma}{\xi}$$

or, with ξ according to Equation (3.1.12) and ε_c according to Equation (3.1.14),

$$\varepsilon_{sc} = \frac{1-\rho\varepsilon_s-\gamma}{1-\rho\varepsilon_s}\left(\varepsilon_s - \frac{1}{\rho}\right) = \varepsilon_s - \frac{1}{\rho}(1-\gamma) \qquad (3.1.15)$$

The mean strain for concrete strip No i is obtained from the expression

$$\frac{\varepsilon_i}{\varepsilon_c} = \frac{-y_i-(x_m-x)}{x} = \frac{-\eta_i-\xi_m+\xi}{\xi}$$

which, using Equations (3.1.12) and (3.1.14), is re-written to read

$$\varepsilon_i = \frac{-\eta_i-\xi_m+1-\rho\varepsilon_s}{1-\rho\varepsilon_s}\left(\varepsilon_s - \frac{1}{\rho}\right) = \varepsilon_s - \frac{1}{\rho}(1-\xi_m-\eta_i)$$

or, with η_i according to Equation (3.1.7),

$$\varepsilon_i = \varepsilon_s - \frac{1}{\rho}\left(1-\xi_m+\alpha\left(i-\frac{1}{2}\right)\right) \qquad (3.1.16)$$

All the relevant strains have now been expressed in terms of the parameters $1/\rho$ and ε_s.

3.2 Depth of the compression zone under elastic conditions

The position of the neutral axis is calculated in the following from Equation (3.1.1). The case characterised by purely elastic conditions is studied first. The following relationships are obtained from FIG. 3.1b.

$$\frac{\varepsilon_c}{\varepsilon_s} = -\frac{\xi}{1-\xi} \qquad (3.2.1)$$

and

$$\frac{\varepsilon_{sc}}{\varepsilon_s} = -\frac{\xi-\gamma}{1-\xi} \qquad (3.2.2)$$

From Equation (3.2.1), Hooke's law and Equations (2.1.1) and (2.2.1) we obtain

$$\frac{\sigma_c}{E_c}\frac{E_s}{\sigma_s} = \frac{\sigma_c}{f_{cc}}\frac{f_{st}}{\sigma_s}\frac{e_s}{e_c} = -\frac{\xi}{1-\xi}$$

from which

$$\frac{\sigma_c}{f_{cc}} = -\frac{e_c}{e_s}\frac{\xi}{1-\xi}\frac{\sigma_s}{f_{st}} \qquad (3.2.3)$$

From Equation (3.2.2) we similary obtain

$$\frac{\sigma_{sc}}{E_s}\frac{E_s}{\sigma_s} = \frac{\sigma_{sc}}{f_{sc}}\frac{f_{st}}{\sigma_s}\frac{f_{sc}}{f_{st}} = -\frac{\xi-\gamma}{1-\xi}$$

If we introduce the symbol

$$\nu = \frac{f_{sc}}{f_{st}} \qquad (3.2.4)$$

we obtain the expression

$$\frac{\sigma_{sc}}{f_{sc}} = -\frac{1}{\nu}\frac{\xi-\gamma}{1-\xi}\frac{\sigma_s}{f_{st}} \qquad (3.2.5)$$

The equilibrium condition (3.1.1) is now written as

$$\frac{1}{2}\sigma_c x b + A_{sc}\sigma_{sc} + A_s\sigma_s = 0$$

which, after multiplication by 2 and division by the reference force

$$N_c = bdf_{cc} = A_c f_{cc} \qquad (3.2.6)$$

yields the equation

$$\frac{\sigma_c}{f_{cc}}\frac{x}{d} + 2\frac{A_{sc}}{A_c}\frac{f_{sc}}{f_{cc}}\frac{\sigma_{sc}}{f_{sc}} + 2\frac{A_s}{A_c}\frac{f_{st}}{f_{cc}}\frac{\sigma_s}{f_{st}} = 0$$

If the effective reinforcement ratios

$$\omega = \frac{A_s}{A_c}\frac{f_{st}}{f_{cc}} \qquad (3.2.7)$$

$$\omega_c = \frac{A_{sc}}{A_c}\frac{f_{sc}}{f_{cc}} \qquad (3.2.8)$$

are substituted in this, we have the expression

$$\frac{\sigma_c}{f_{cc}} \xi + 2\omega_c \frac{\sigma_{sc}}{f_{sc}} + 2\omega \frac{\sigma_s}{f_{st}} = 0 \qquad (3.2.9)$$

The expressions (3.2.3) and (3.2.5) and the new quantity

$$\omega_o = \frac{e_s}{e_c} \omega \qquad (3.2.10)$$

are substituted into (3.2.9), which yields a second degree equation for determination of the depth ξ of the compression zone. The equation

$$\xi^2 + 2\omega_o (1 + \frac{1}{\nu} \frac{\omega_c}{\omega}) \xi = 2\omega_o (1 + \frac{\gamma}{\nu} \frac{\omega_c}{\omega})$$

has the solution

$$\xi = \omega_o \{-(1 + \frac{1}{\nu} \frac{\omega_c}{\omega}) + \sqrt{(1 + \frac{1}{\nu} \frac{\omega_c}{\omega})^2 + \frac{2}{\omega_o} (1 + \frac{\gamma}{\nu} \frac{\omega_c}{\omega})}\} \qquad (3.2.11)$$

3.3 Depth of the compression zone under elasto-plastic conditions

Under elasto-plastic conditions, the depth of the compression zone cannot be determined explicitly. The depth is instead calculated by means of an iterative process as follows. For this case, the equilibrium condition (3.1.1) is written in the form

$$\sum_1^n \Delta A_c \sigma_{ci} + A_{sc} \sigma_{sc} + A_s \sigma_s = 0$$

where the summation extends over the n strips into which the fictitious compression zone is divided. If this is divided by the reference force N_c according to Equation (3.2.6), we have

$$\sum_1^n \frac{\Delta A_c}{A_c} \frac{\sigma_{ci}}{f_{cc}} + \frac{A_{sc}}{A_c} \frac{f_{sc}}{f_{cc}} \frac{\sigma_{sc}}{f_{sc}} + \frac{A_s}{A_c} \frac{f_{st}}{f_{cc}} \frac{\sigma_s}{f_{st}} = 0$$

or, making use of Equations (3.2.7), (3.2.8) and (3.1.6),

$$\alpha \sum_1^n \frac{\sigma_{ci}}{f_{cc}} + \omega (\frac{\sigma_s}{f_{st}} + \frac{\omega_c}{\omega} \frac{\sigma_{sc}}{f_{sc}}) = 0 \qquad (3.3.1)$$

When this method is selected to deal with variation of the compression zone during the load application process, α is a constant. It has therefore been moved outside the summation sign. The ratio σ_{ci}/f_{cc} then remains inside the summation sign. According to Chapter 2, it is this ratio which is read in the non-dimensional stress-strain diagram for a given strain.

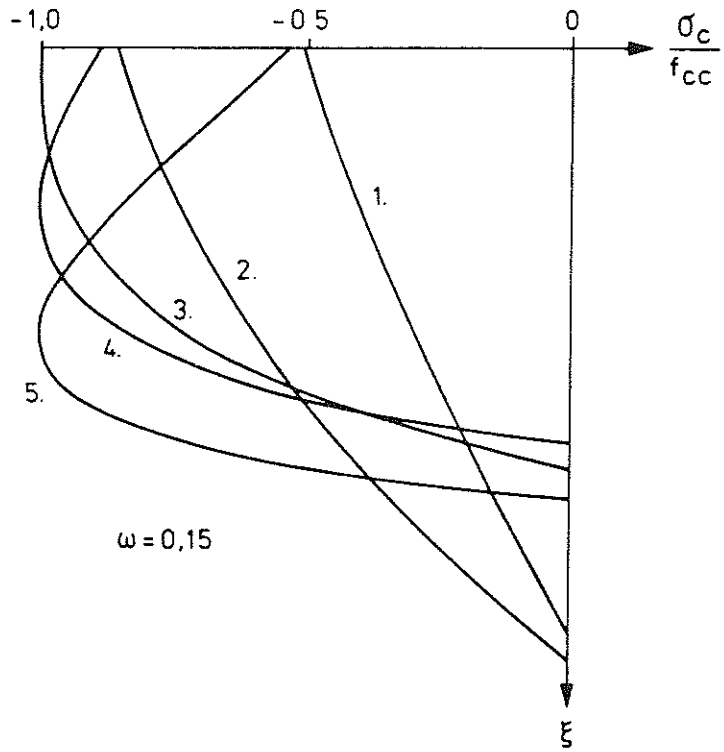

FIG 3.3b Stress distribution over the compression zone of the concrete for five different stages of stressing. The corresponding beam curvatures are shown in FIG 3.3a.

The procedure for determination of the depth of the compression zone during gradual increase in beam curvature will then be as follows.

A fictitious depth ξ_m is first determined. Trial calculations have shown that a convenient value is

$$\xi_m = 1.25\ \xi_o \qquad (3.3.2)$$

where ξ_o is the depth of the compression zone under elastic conditions, calculated from Equation (3.2.11).

The curvature $1/\rho$ is then allowed to increase in equal steps from 0 until, at some value of $1/\rho$, material failure occurs. After each increase in $1/\rho$ an adjustment is made to the strain ε_s in the tension reinforcement, with the value of $1/\rho$ being maintained constant, so that the equilibrium condition (3.3.1) is satisfied within a specified tolerance (2 - 10 ‰ of the force in the tension reinforcement). The iterative process can be described as follows.

1. Increase $1/\rho$ to a new value which is then kept constant during the subsequent calculation steps.

2. Increase the strain in the tension reinforcement by $\Delta\varepsilon_s$ to ε_s, the value of $\Delta\varepsilon_s$ being at first made the same as the increase in strain during the previous change in $1/\rho$.

3. Calculate the relevant strains from Equations (3.1.14), (3.1.15) and (3.1.16) using the values of $1/\rho$ and ε_s applicable during this calculation step.

4. From the calculated strains and the stress-strain curves for the concrete and steel, determine the corresponding non-dimensional stresses σ_{ci}/f_{cc}, σ_{sc}/f_{sc} and σ_s/f_{st}.

5. Substitute the stresses obtained in 4 into Equation (3.3.1). If this is not satisfied within the specified tolerance, adjust the value of $\Delta\varepsilon_s$ and repeat the iteration process from step 2 onwards. Once the specified tolerance is attained in Equation (3.3.1), continue with

6. and calculate the relative depth ξ of the compression zone from Equation (3.1.12).

The results of a calculation according to the procedure described above are illustrated in FIG. 3.3a. The calculation refers to a section without compression reinforcement, and with the quantity of tension reinforcement characterised by $\omega = 0.15$. The reinforcement consists of HR steel and the concrete is of Type B (see Chapter 2). The full line shows variation of the depth ξ of the compression zone as a function of the beam curvature $1/\rho$. The chain line indicates the fictitious depth ξ_m of the compression zone calculated from Equation (3.3.2).

If we assume that the stress block in the compression zone is rectangular and of depth $0.8\,\xi$ at the ultimate stage, we have $\xi = 1.25\omega$. This value is also given in the figure. The ultimate stage, characterised by crushing failure of the concrete, has been marked with a cross at the end of the curve.

The calculated stress distribution in the compression zone is shown in FIG. 3.3b for five values of $1/\rho$. The corresponding positions are marked by the figures 1 ... 5 in FIG. 3.3a.

4 MOMENT-CURVATURE DIAGRAM

Once the depth of the compression zone has been determined according to the procedure described in the previous chapter (as a fundtion fo the curvature $1/\rho$), the moment-curvature diagram can be calculated.

For the purely elastic case it is most convenient to relate the moment equilibrium to the position of the resultant of the concrete stresses. Using the symbols in Chapter 3 and FIG. 3.1a, we thus have

$$M + F_{sc}(\frac{1}{3}x-c) - F_s(d - \frac{1}{3}x) = 0 \qquad (4.1)$$

where M is the bending moment. If we introduce into Equation (4.1) the expressions $F_{sc} = A_{sc}\sigma_{sc}$ and $F_s = A_s\sigma_s$, and divide by the reference moment

$$M_c = N_c d \qquad (4.2)$$

we have the moment in a non-dimensional form

$$\mu = \frac{M}{M_c} = \frac{A_s}{A_c}\frac{f_{st}}{f_{cc}}\frac{\sigma_s}{f_{st}}(1 - \frac{1}{3}\xi) - \frac{A_{sc}}{A_c}\frac{f_{sc}}{f_{cc}}\frac{\sigma_{sc}}{f_{sc}}(\frac{1}{3}\xi-\gamma) \qquad (4.3)$$

Substitution of the effective reinforcement ratios ω and ω_c according to Equations (3.2.7) and (3.2.8) respectively, and of Equation (3.2.5), into Equation (4.3) yields

$$\mu = \omega\frac{\sigma_s}{f_{st}}(1 - \frac{1}{3}\xi) + \omega_c\frac{\sigma_s}{f_{st}}\frac{1}{\nu}\frac{\xi - \gamma}{1 - \xi}(\frac{1}{3}\xi - \gamma) \qquad (4.4)$$

The beam curvature is calculated from the Equation (3.1.11) and Hooke's law, and is written

$$\frac{1}{\rho} = \frac{1}{1 - \xi}\frac{\sigma_s}{f_{st}}\frac{f_{st}}{E_s} = \frac{1}{e_s}\frac{1}{1 - \xi}\frac{\sigma_s}{f_{st}} \qquad (4.5)$$

If the ratio σ_s/f_{st} is eliminated from the expressions (4.4) and (4.5), we have

$$\frac{1}{\rho} = \frac{\mu}{\delta} \qquad (4.6)$$

where the non-dimensional bending stiffness δ is

$$\delta = \omega e_s\{(1 - \frac{1}{3}\xi)(1 - \xi) + \frac{1}{\nu}\frac{\omega_c}{\omega}(\gamma - \frac{1}{3}\xi)(\gamma - \xi)\} \qquad (4.7)$$

Expression (4.6) gives the relation between the curvature $1/\rho$ and the bending moment μ, the stiffness δ for elastic behaviour and the given depth ξ of the compression zone being determined from Equation (4.7).

Under elasto-plastic conditions it is more convenient to relate the moment equilibrium to the bottom edge of the fictitious compression zone, see FIG. 3.1a and b. We then have the relation

$$M - F_c y_c + F_{sc}(x_m - c) - F_s(d - x_m) = 0 \qquad (4.8)$$

where y_c is the ordinate of the position of the resultant F_c of the concrete stresses. Equation (4.8) is re-written as

$$M - \sum_1^n \Delta A_c \sigma_{ci} y_i + A_{sc}\sigma_{sc}(x_m - c) - A_s\sigma_s(d - x_m) = 0$$

which, after division by the reference moment M_c, yields the non-dimensional moment

$$\mu = \sum_1^n \frac{\Delta A_c}{A_c}\frac{\sigma_{ci}}{f_{cc}}\eta_i + \frac{A_s}{A_c}\frac{f_{st}}{f_{cc}}\frac{\sigma_s}{f_{st}}(1-\xi_m) - \frac{A_{sc}}{A_c}\frac{f_{sc}}{f_{cc}}\frac{\sigma_{sc}}{f_{sc}}(\xi_m-\gamma) \qquad (4.9)$$

Substitution of ω, ω_c and η_i according to Equations (3.2.7), (3.2.8) and (3.1.7) into Equation (4.9) yields the expression

$$\mu = \alpha^2\sum_1^n \frac{\sigma_{ci}}{f_{cc}}(\frac{1}{2} - i) + \omega\{(1-\xi_m)\frac{\sigma_s}{f_{st}} + (\gamma-\xi_m)\frac{\omega_c}{\omega}\frac{\sigma_{sc}}{f_{sc}}\} \qquad (4.10)$$

For selected value of $1/\rho$ the procedure in Chapter 3 gives the corresponding depth ξ of the compression zone. The strain distribution is then known and the corresponding stresses σ_{ci}/f_{cc}, σ_s/f_{st} and σ_{sc}/f_{sc} can be determined with the aid of the stress-strain diagrams for the steel and concrete, after which the moment is calculated from Equation (4.10). By successive repetition of this procedure for values of $1/\rho$ increasing in discrete steps, a moment-curvature curve is determined for the section.

As an example of the results obtained according to the calculation technique described above, FIG. 4a shows the moment-curvature curve for a section without compression reinforcement for different values of ω. The calculation refers to HR steel and concrete of Type A.

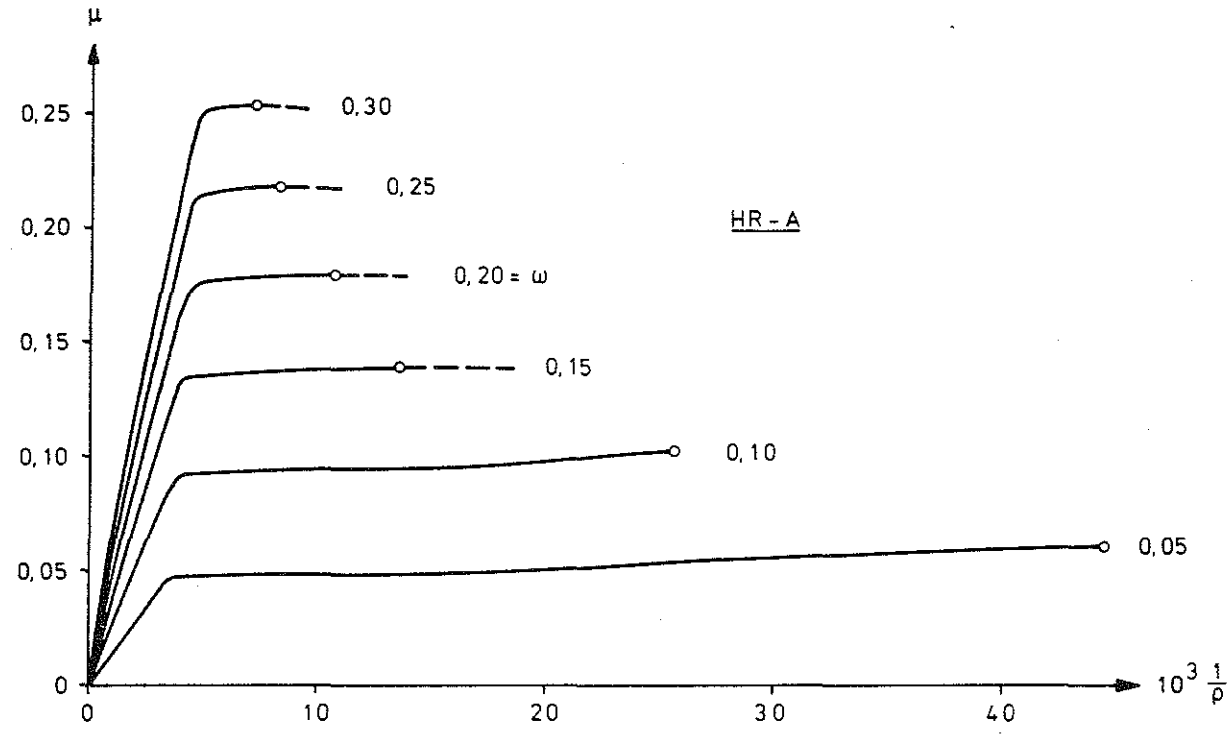

FIG 4a Moment-curvature curves for different values of ω. The curves relate to a cross section with tension reinforcement of HR steel.

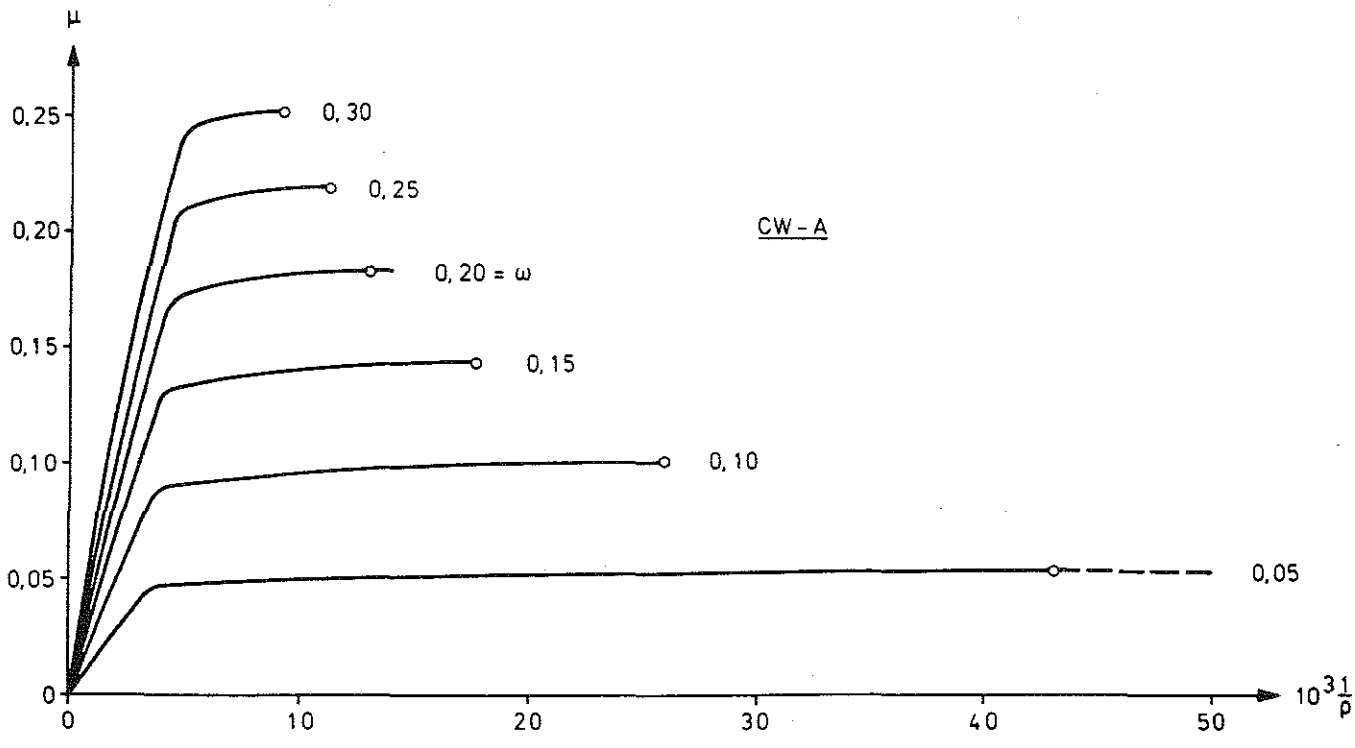

FIG 4b Moment-curvature curves for different values of ω. The curves refer to a cross section with tension reinforcement of CW steel.

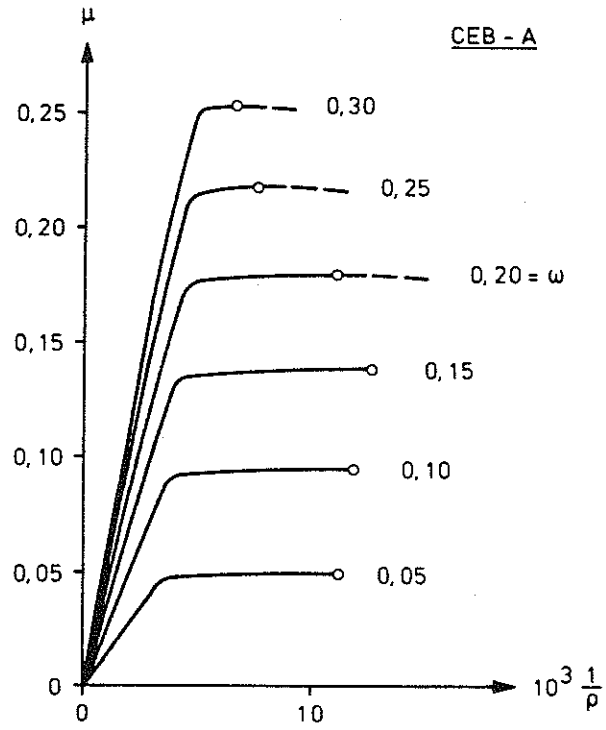

FIG 4c Moment-curvature curves for different values of ω. The curves refer to a cross section with tension reinforcement of CEB steel.

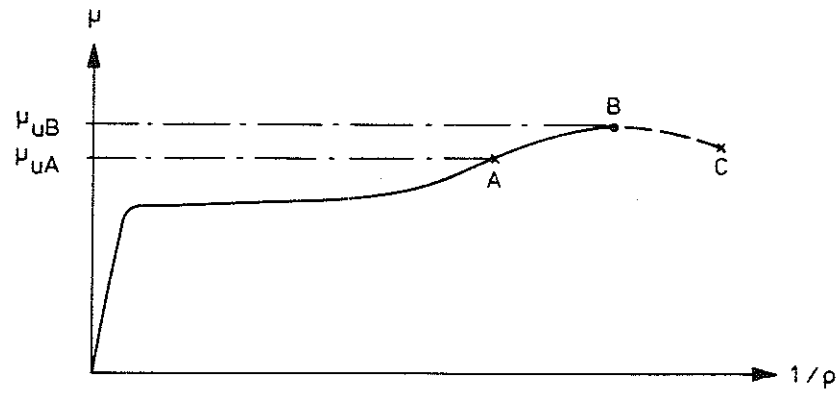

FIG 4d Ordinary shape of moment-curvature curve. This curve permits two alternative definitions of the ultimate moment.

For purposes of comparison, FIG. 4b and 4c show the corresponding moment-curvature-curves for CW steel and CEB steel. All calculations have been carried as far as the ultimate strains of the steel and concrete permit.

When some convenient definition of the ultimate moment has been decided on, this can be read off the moment-curvature diagram. If the loading process is assumed to be force-controlled, and this is the assumption made in the following, then at least two failure criteria can be stipulated. As a rule, the moment-curvature diagram increases monotonically up to a maximum moment after which the moment decreases. The situation is set out schematically in FIG. 4d. Material failure can occur either before or after the maximum moment at point B. If it occurs before this, as at point A, the corresponding moment is taken to be the ultimate moment μ_u ($=\mu_{uA}$). This situation occurs, for instance, in the case of $\omega = 0.010$ in FIG. 4a. If the material failure occurs after the maximum moment, as at point C in FIG. 4d, then the maximum moment is taken to be the ultimate moment μ_u ($=\mu_{uB}$). This is the situation which occurs, for instance, in conjunction with $\omega = 0.15$ in FIG. 4a. These two failure situations occur in conjunction with both HR and CW steel reinforcement.

In certain cases a special situation may occur in conjunction with HR steel. This is illustrated by FIG. 4e. The moment has a first maximum at point A. If, at the same time, the stress in the concrete has reached its minimum value $\sigma_c/f_{cc} = -1.0$ at the upper edge of the compression zone and the steel strain is at incipient yield level then, as curvature continues to increase, the strain in the steel will rise for a constant force in the reinforcement, and at the same time the position of the minimum stress in the concrete is displaced downwards in the compression zone, as shown in FIG. 3.3b. The moment thus drops due to the decrease in the internal level arm while the curvature continues to increase, until the strain in the steel has passed the lower limit of strain hardening, after which the moment again increases. This process is described schematically by curve A-B-C in FIG. 4e. After this the process may be as shown in FIG. 4d. When loading is force-controlled, the above process implies that an instability situation occurs at point A. As the moment continues to rise, the situation changes instantaneously from a position with a higher potential, point A, to one with a lower potential, point C. In other contexts this phenomenon is referred to as "snapping". For a section with the properties described, the moment corresponding to point A is taken to be the ultimate moment μ_{uA} if material failure occurs between points A and C, such as at point

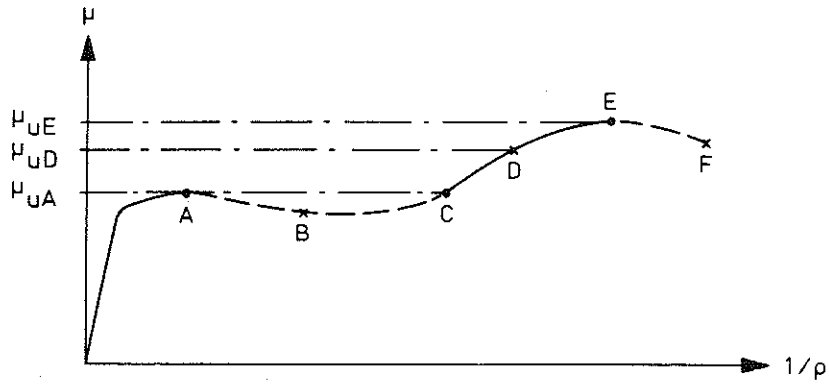

FIG 4e Shape of moment-curvature curve in which instability may occur. This curve permits three alternative definitions of the ultimate moment.

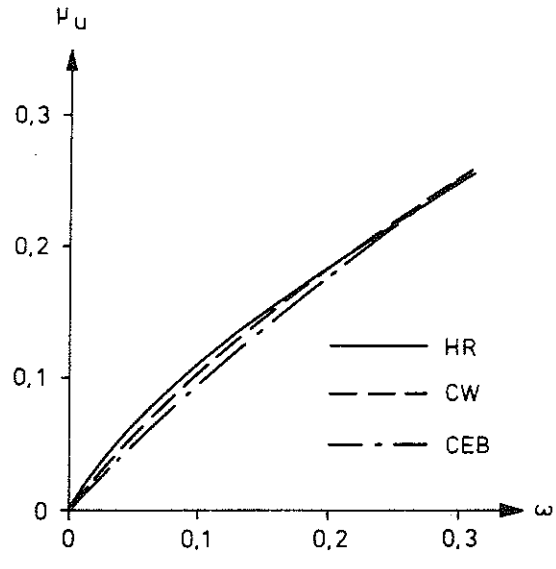

FIG 4f The ultimate moment as a function of the effective reinforcement ratio. The curves relate to a beam section with no compression reinforcement.

B. If material failure occurs along the section C-E, for instance at point D, the corresponding moment is taken to be the ultimate moment μ_{uD}. Finally, it is possible for material failure not to occur until the moment has passed its second maximum, point E, in which case the moment corresponding to the maximum point is considered to be the ultimate moment μ_{uE}.

If the stipulated failure criteria are applied to the moment-curvature diagrams shown in FIG. 4a, 4b and 4c, the relationship between ω and μ_u will be as shown in FIG. 4f. As will be seen, the ultimate moment is practically the same for all three types of steel.

The ultimate moment is often calculated on the basis of a simplified rectangular stress distribution in the compression zone. In such a case, the moment is

$$\mu_u = \omega \left(1 - \frac{\omega}{2}\right) \qquad (4.11)$$

This equation yields a curve which is practically coincident with that for CEB steel in FIG. 4f.

5 DEFORMATION ENERGY

The calculation technique which results in the derivation of the moment-curvature diagram for an arbitrarily selected section in a reinforced con-beam, under elastic and elasto-plastic conditions, was developed in Chapters 3 and 4. This will be complemented below by calculation of the corresponding consumption by the cross section of deformation energy per unit length of the beam, a moment-energy relation being constructed.

The quantity of internal energy Δw per unit length of the beam which is stored during the increase in curvature $\Delta(1/\rho)$, i.e. during one calculation step, is

$$\Delta w = \sum_{1}^{n} \Delta A_c \sigma_{ci} \Delta\varepsilon_i + A_{sc} \sigma_{sc} \Delta\varepsilon_{sc} + A_s \sigma_s \Delta\varepsilon_s \qquad (5.1)$$

where Δw includes both reversible and irreversible energy consumption.

The increments in strain $\Delta\varepsilon_{sc}$ and $\Delta\varepsilon_i$ corresponding to the increase in curvature $\Delta(1/\rho)$ are obtained by partial differentiation of the expressions (3.1.15) and (3.1.16). The following expressions are obtained

$$\Delta\varepsilon_{sc} = -(1-\gamma)\cdot\Delta\left(\frac{1}{\rho}\right)+\Delta\varepsilon_s \qquad (5.2)$$

$$\Delta\varepsilon_i = \left(\alpha\left(\frac{1}{2} - i\right) + \xi_m - 1\right)\cdot\Delta\left(\frac{1}{\rho}\right)+\Delta\varepsilon_s \qquad (5.3)$$

with the increment in strain $\Delta\varepsilon_s$ determined by means of an equilibrium condition according to Chapter 3.

The stresses contained in Equation (5.1) are obtained from the stress-strain diagram of the section component concerned, the stresses being referred to the centre of the corresponding strain interval $\Delta\varepsilon$.

If Δw according to Equation (5.1) is divided by the reference force N_c, the increase in consumed deformation energy per unit length of the beam is obtained in non-dimensional form

$$\Delta\psi = \frac{\Delta w}{N_c} = \sum_{1}^{n} \frac{\Delta A_c}{A_c} \frac{\sigma_{ci}}{f_{cc}} \Delta\varepsilon_i + \frac{A_{sc}}{A_c} \frac{f_{sc}}{f_{cc}} \frac{\sigma_{sc}}{f_{sc}} \Delta\varepsilon_{sc} + \frac{A_s}{A_c} \frac{f_{st}}{f_{cc}} \frac{\sigma_s}{f_{st}} \Delta\varepsilon_s \qquad (5.4)$$

Substitution into the above of Equations (3.1.6), (3.2.7) and (3.2.8) yields

$$\Delta\psi = \Delta\psi_c + \Delta\psi_{sc} + \Delta\psi_s = \alpha \sum_1^n \frac{\sigma_{ci}}{f_{cc}} \Delta\varepsilon_i + \omega_c \frac{\sigma_{sc}}{f_{sc}} \Delta\varepsilon_{sc} + \omega \frac{\sigma_s}{f_{st}} \Delta\varepsilon_s \qquad (5.5)$$

Use of Equations (5.2) and (5.3) yields the following for the contribution of the compressed concrete to the deformation energy per unit length of the beam

$$\Delta\psi_c = \alpha \sum_1^n \frac{\sigma_{ci}}{f_{cc}} \{(\alpha(\frac{1}{2} - i) + \xi_m - 1)\Delta(\frac{1}{\rho}) + \Delta\varepsilon_s\} \qquad (5.6)$$

For the contribution of the compression reinforcement, we have

$$\Delta\psi_{sc} = \omega \frac{\omega_c}{\omega} \frac{\sigma_{sc}}{f_{sc}} ((\gamma - 1)\Delta(\frac{1}{\rho}) + \Delta\varepsilon_s) \qquad (5.7)$$

and for the contribution of the tension reinforcement

$$\Delta\psi_s = \omega \frac{\sigma_s}{f_{st}} \Delta\varepsilon_s \qquad (5.8)$$

The total deformation energy per unit length of the beam consumed at the prevailing state of deformation is obtained by summation from zero up to the appropriate value of the curvature $1/\rho$. We then have

$$\psi = \Sigma\Delta\psi = \Sigma\Delta\psi_c + \Sigma\Delta\psi_{sc} + \Sigma\Delta\psi_s \qquad (5.9)$$

With $1/\rho$ as the governing parameter, associated values of ψ and μ can now be calculated according to Equations (4.10) and (5.9). In this way the moment-energy relation sought is obtained.

As an example of the results of such a calculation, FIG. 5a shows the $\mu - \psi$ relation for a cross section of concrete Type B reinforced with HR steel. The effective reinforcement ratio is $\omega = 0.30$ on the tension side and $\omega = 0.15$ on the compression side. The example chosen includes the effect of creep in the concrete, the creep factor being $\varphi = 3$. The effect of creep on the rotation capacity is studied in Chapter 8. The only reason why creep has been included in this case is that the figure is clearer as a result. The figure shows three curves, of which the bottom one represents the share of the concrete ψ_c in the energy consumption. The centre curve gives the energy consumption in the compression zone of the beam

$$\psi_t = \psi_c + \psi_{sc} \qquad (5.10)$$

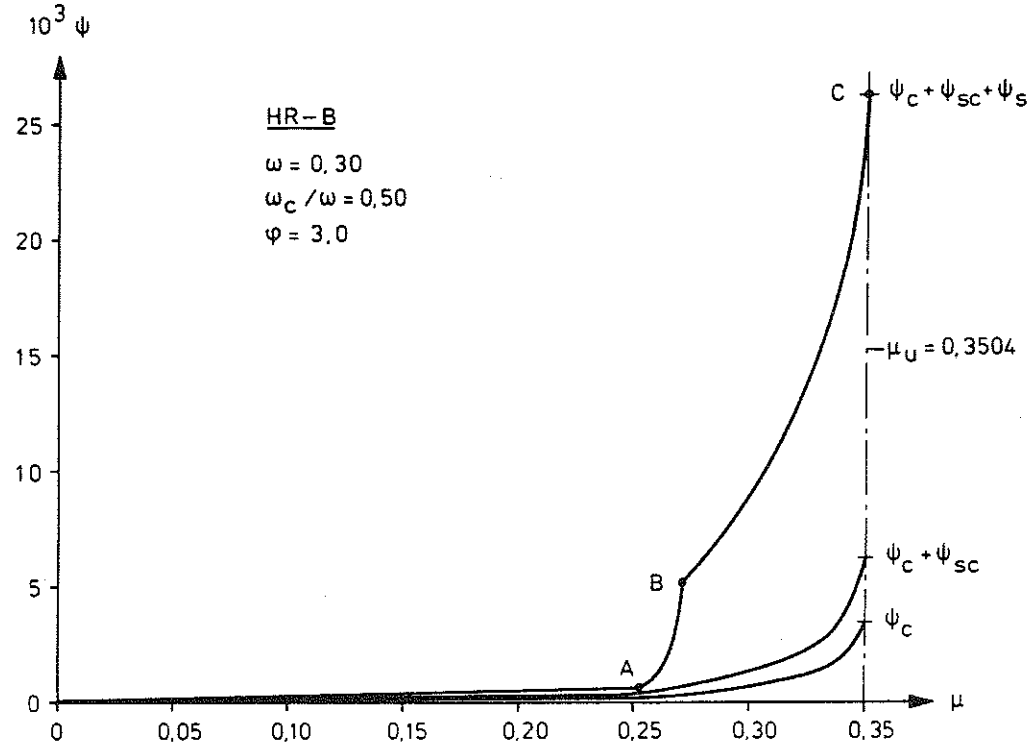

FIG 5a Moment-energy curve for a cross section in a beam reinforced with HR steel.

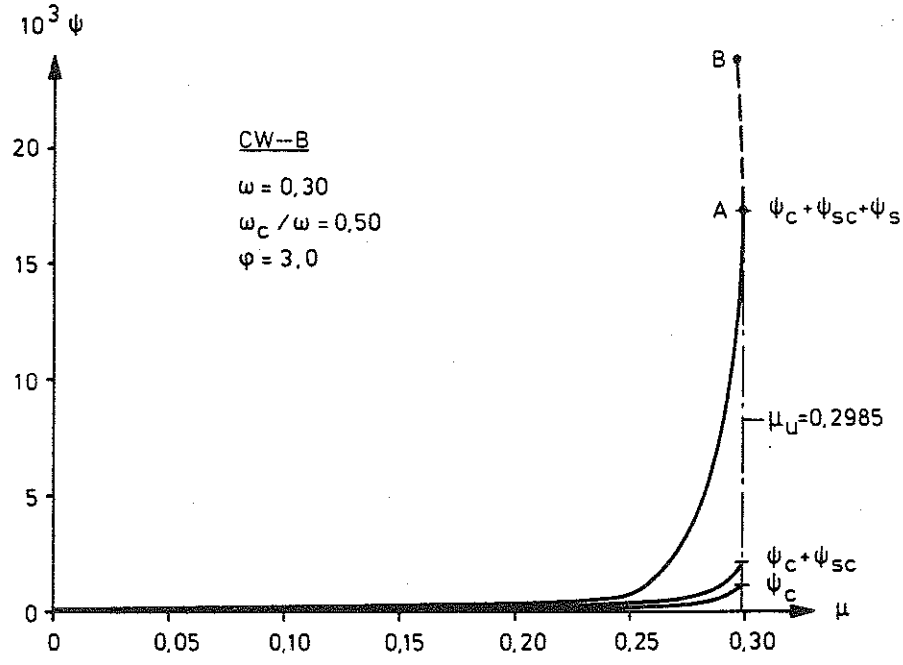

FIG 5b Moment-energy curve for a cross section in a beam reinforced with CW steel.

i.e. the quantity of deformation energy per unit length of the beam which is stored by the compressed concrete and the compression reinforcement taken together.

The top curve shows the total energy consumption of the cross section per unit length of the beam. Point A in the figure represents the state of affairs in the cross section when the tension reinforcement reaches the upper yield stress, i.e. when $\varepsilon_s = \varepsilon_2$. Point B represents the state of affairs when the tension reinforcement reaches the lower strain hardening limit ε_1. Finally, point C represents the ultimate state which in this case is characterised by crushing failure of the concrete.

A corresponding $\mu - \psi$ curve for a beam reinforced with CW steel but in other respects similar to the previous case is shown in FIG. 5b. The tension reinforcement fails at point B. However, this diagram is utilised only up to point A which is characterised by the fact that the ultimate moment μ_u here is equal to the maximum moment.

6 ENERGY BALANCE

In the following, the rotation span of a plastic hinge refers to the part of the beam between the plastic hinge and the nearest point where the moment is zero. A discontinuous plastic hinge has two rotation spans, one on each side of the hinge, while a continuous plastic hinge, for instance one at a fixed end, has only one rotation span. In the following, only conditions on one side of a plastic hinge will be studied, whether it is a discontinuous or continuous hinge.

The length of the rotation span is detoned l_o. The value of l_o generally varies somewhat during application of the load. However, the simplifying assumption is made here that l_o is constant and equal to the length corresponding to the ultimate moment M_u of the plastic hinge. Most of the energy interchange during a complete loading process occurs for moments of this magnitude, and the variation in the length of the rotation span which occurs in the region around the zero moment can therefore be considered to have a negligible effect on the total energy situation of the span.

In the following, a calculation is first made of the external work required for deformation of the rotation span, the deformation energy simultaneously stored in the span is then determined according to Chapter 5, and finally an energy balance is drawn up from which the elasto-plastic rotation, the rotation capacity, is calculated.

6.1 The external work

FIG. 6.1a shows the rotation span of length l_o between a plastic hinge PH to the right and a point of zero moment to the left. At its left-hand end, the part of the beam is acted upon by the shear force V_n. At its right-hand end it is acted upon by the ultimate moment M_u and the shear force V_o. The span is assumed to carry a uniformly distributed load q. The variation of moment over the length of the span is thus parabolic, as shown in the upper moment diagram in the figure. Under this assumption, the moment variation is uniquely characterised by a coefficient β according to the figure, which expresses the difference between this moment variation and a linear variation shown dashed in the figure.

The above method of describing the moment variation does not cover all conceivable situations. Examples of such cases are a uniformly distributed load over part of the span, and one or more point loads placed between the

plastic hinge and the point of zero moment. On the other hand, this method permits uncomplicated treatment of the loading situations which most often occur in practice.

The following values of β can occur. See FIG. 6.1b.

$\beta = -0.06$ represents the moment variation adjacent to a plastic hinge near a support section when the beam carries a uniformly distributed load.

$\beta = 0$ represents the variation adjacent to a plastic hinge which is situated either near a support section or in the span when the beam is acted upon by point loads.

$\beta = 0.25$ represents the moment distribution near a plastic hinge in the span when the beam carries a uniformly distributed load.

The moment distribution can be written as

$$M = (1 - \frac{z}{l_o})(1 + 4\beta \frac{z}{l_o})M_u \qquad (6.1.1)$$

If the rotation span is divided into n equal parts each of length Δl_o, as shown in FIG. 6.1a, the relation

$$\frac{z}{l_o} = \frac{i}{n} \qquad (6.1.2)$$

applies at point No i.

Substitution of Equation (6.1.2) into Equation (6.1.1), and simultaneous division by the reference moment M_c according to Equations (3.2.6) and (4.2) gives the non-dimensional moment at point No i as

$$\mu_i = \frac{M_i}{M_c} = \mu_u(n-i)(n+4\beta i)/n^2 \qquad (6.1.3)$$

where $\mu_u = M_u/M_c$.

The relation between β and q is written according to the figure

$$\frac{1}{8} q l_o^2 = \beta M_u$$

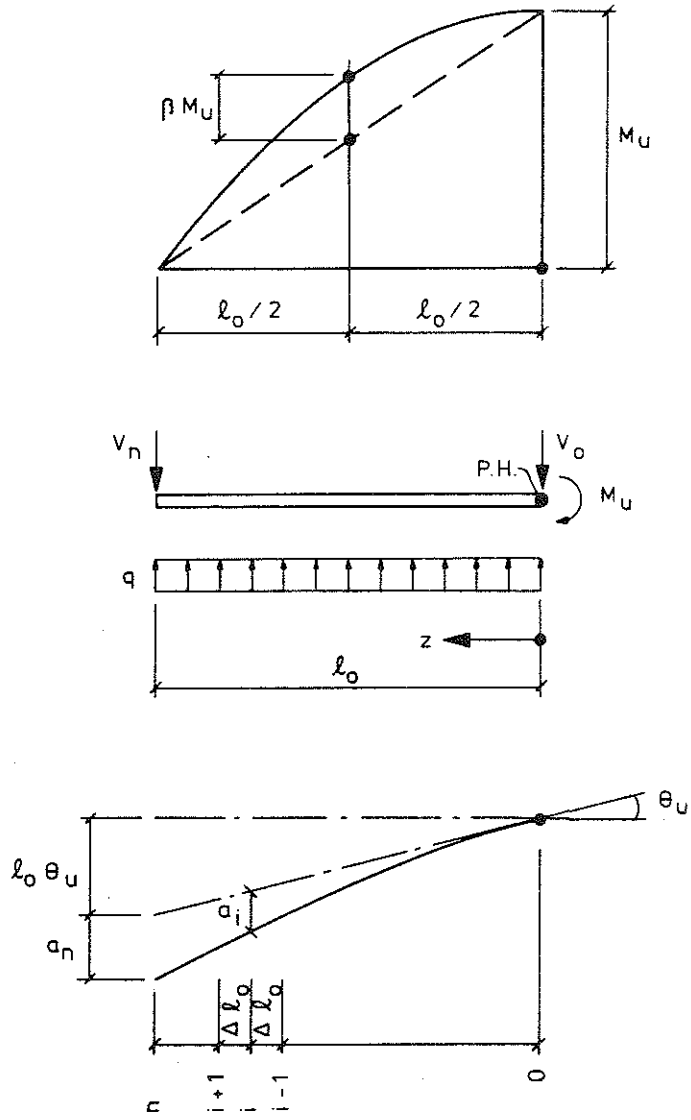

FIG 6.1a Moment distribution at the ultimate stage over the length l_o of the rotation span. The internal and external forces acting on the rotation span. The deformation of the rotation span divided into a plastic and an elastic portion.

or

$$q l_o^2 = 8\beta M_u \tag{6.1.4}$$

Moment equilibrium for the part of the beam under consideration gives

$$M_u + \frac{1}{2} q l_o^2 - V_n l_o = 0 \tag{6.1.5}$$

from which, by making use of Equation (6.1.4), we calculate

$$V_n = (1+4\beta)\frac{M_u}{l_o} \tag{6.1.6}$$

Under the influence of the forces acting on the beam, the rotation span is deformed according to the lower figure in FIG. 6.1a. The deflection is divided into an inelastic and an elastic part.

In an initial phase, all deformations are elastic. During this phase the external load rises from zero to a value q_y which is attained when plastic flow begins in the section where the moment is a maximum, i.e. at the theoretical plastic hinge. At the same time as this occurs, the bending moment at the plastic hinge is M_y and the shear force at the point of zero moment is V_y. In this situation, the relations corresponding to Equations (6.1.4) and (6.1.6) are

$$q_y l_o^2 = 8\beta M_y \tag{6.1.7}$$

and

$$V_y = (1+4\beta)\frac{M_y}{l_o} \tag{6.1.8}$$

As the external load increases from the yield value q_y to the ultimate value q, there is plastic rotation about the plastic hinge, and at the same time the elastic deflection at the point of zero moment increases to its maximum value a_n. The elastic part of the deflection at the arbitrary point No i is corresponding denoted a_i.

Computationally, the inelastic deformation is treated as a rotation of the rotation span, considered as a rigid body, through an angel θ_u about the plastic hinge. According to the definition, θ_u represents the rotation capacity of the plastic hinge on the side being considered. When failure occurs, the maximum inelastic deflection at the point of zero moment is $l_o\theta_u$.

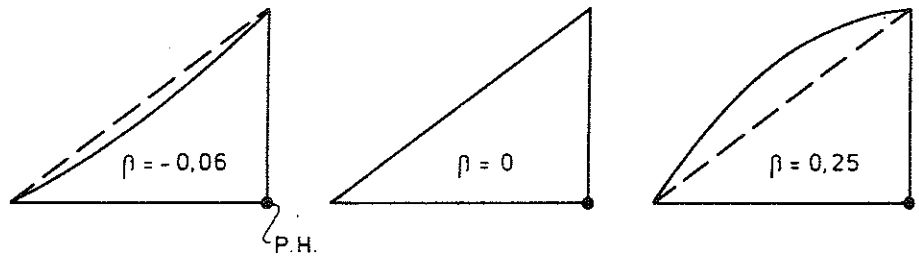

FIG 6.1b Three moment distributions over the length of the rotation span. The form of the moment distribution is determined by the parameter β.

The relationship between beam deformation and plastic hinge moments over the moment interval M_y - M_u, i.e. over the elasto-plastic loading range, is dependent on a number of factors among which the shape of the stress-strain diagram of the reinforcing steel is dominant. In view of all the other uncertainty which is associated with this type of calculation, the following derivation has been based on the approximate assumption that the above relationship is linear.

The total external work which is performed during the loading phase up to failure is thus

$$W_e = \frac{1}{2}V_n a_n + \frac{1}{2}(V_y+V_n)\theta_u l_o - \frac{1}{2}\sum_1^n q\Delta l_o a_i - \frac{1}{2}(q_y+q)l_o \cdot \frac{1}{2}\theta_u l_o \qquad (6.1.9)$$

With reference to FIG. 6.1a the following comments are made concerning the various terms in this relation.

The first term refers to the elastic work performed by the shear force at the point of zero moment as the force rises from zero to its maximum value V_n, and at the same time the elastic part of the deflection at the same section increases to its final value a_n.

The second term refers to the plastic work performed by the shear force at the point of zero moment. Up to the value V_y no plastic work is done. As the shear force then increases from V_y to V_n, the mean force during the plastic loading phase is $(V_y + V_n)/2$. This acts over the plastic part of the deflection $\theta_u l_o$.

The third term refers to the elastic work performed by the ultimate load q when the elastic part of the beam deflection, as the load increases, rises to the final value a_i at the point No i.

The fourth term, finally, refers to the plastic work performed by the distributed load. Up to the value q_y no plastic work is done. As the load then rises from the yield value q_y to the ultimate value q, the resultant of the mean load during the plastic loading phase is $(q_y + q)l_o/2$. This resultant, which acts at the centre of this part of the beam, acts over the deflection $\theta_u l_o/2$.

The section forces V_o and M_u are also shown in FIG. 6.1a. All displacements have been related to the plastic hinge which, in this derivation, has been assumed to be a point incapable of displacement. The work done by the shear force is therefore equal to zero. Nor has the ultimate moment M_u which acts at the plastic hinge been included in Equation (6.1.9) because, in this context, M_u may be considered to be an internal moment. That this is so is evident if we imagine that the plastic hinge being considered occurs over an intermediate support in a continuous beam, and consequently envisage the part of the beam being considered to comprise the section $2l_o$, placed symmetrically with regard to the plastic hinge.

Substitution of $q_y l_o^2$ according to Equation (6.1.7), ql_o^2 according to Equation (6.1.4), and V_n and V_y according to Equations (6.1.6) and (6.1.8) respectively into Equation (6.1.9) yields

$$W_e = \frac{1}{2}(1 + \frac{M_y}{M_u})M_u\theta_u + \frac{1}{2}(1+4\beta)M_u\frac{a_n}{l_o} - 4\beta M_u \frac{\Delta l_o}{l_o}\sum_1^n \frac{a_i}{l_o} \qquad (6.1.10)$$

If this is divided by the reference moment M_c and it is noted that $\Delta l_o/l_o = 1/n$, we have the external work in a non-dimensional form

$$\phi_e = \frac{W_e}{M_c} = \frac{1}{2}(1 + \frac{\mu_y}{\mu_u})\mu_u\theta_u + \frac{1}{2}(1+4\beta)\mu_u \frac{d}{l_o}\frac{a_n}{d} - 4\beta\mu_u \frac{d}{l_o}\frac{1}{n}\sum_1^n \frac{a_i}{d} \qquad (6.1.11)$$

where $\mu_y = M_y/M_c$.

If we introduce the symbol

$$\lambda = \frac{l_o}{d} \qquad (6.1.12)$$

for the non-dimensional length of the rotation span (the slenderness of the span), the relation (6.1.11) can be written as

$$\phi_e = \{\frac{1}{2}(1 + \frac{\mu_y}{\mu_u})\theta_u + \frac{1}{2}(1+4\beta)\frac{1}{\lambda}\frac{a_n}{d} - 4\beta\frac{1}{\lambda}\frac{1}{n}\sum_1^n \frac{a_i}{d}\}\mu_u \qquad (6.1.13)$$

The elastic deflection a_i and a_n are calculated with the aid of finite differences. We thus have the relation

$$\frac{a_{i-1} - 2a_i + a_{i+1}}{(\Delta l_o)^2} = \frac{1}{r_i} \qquad (6.1.14)$$

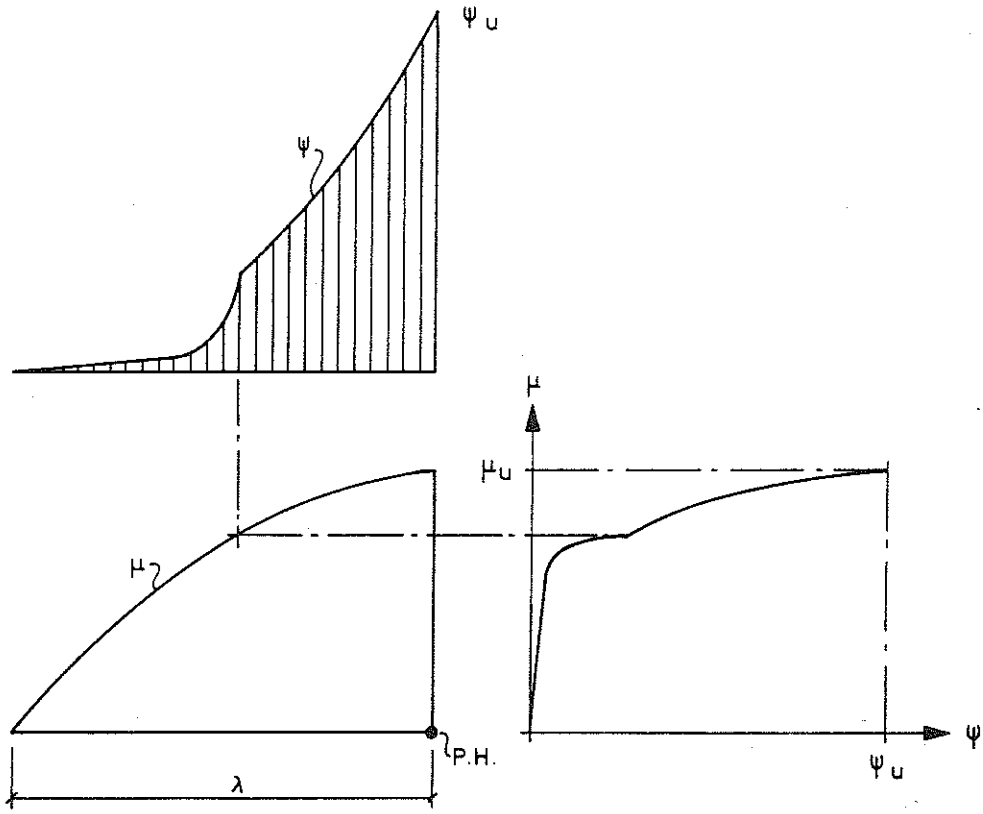

FIG 6.2a Transformation of the moment-energy curve by means of the moment curve. The transformation yields the distribution of consumed deformation energy ψ per unit length of beam along the rotation span.

where r_i is the radius of curvature at point No i under elastic conditions. The relation is re-written as

$$\left(\frac{a}{d}\right)_{i-1} - 2\left(\frac{a}{d}\right)_i + \left(\frac{a}{d}\right)_{i+1} = \left(\frac{\Delta l_o}{l_o}\right)^2 \left(\frac{l_o}{d}\right)^2 \frac{d}{r_i} = \frac{\lambda^2}{n^2} \frac{1}{\rho_i} \qquad (6.1.15)$$

where $\rho_i = r_i/d$ is the non-dimensional radius of curvature at point No i.

If we introduce the non-dimensional deflection

$$\kappa_i = \frac{a_i}{d} \frac{n^2}{\lambda^2} \qquad (6.1.16)$$

into Equation (6.1.14), we have the difference equation

$$\kappa_{i-1} - 2\kappa_i + \kappa_{i+1} = \frac{1}{\rho_i} \qquad (6.1.17)$$

Since the portion of the beam is rigidly fixed at the plastic hinge with respect to elastic deflection, the boundary conditions

$$\kappa_o = 0 \qquad \kappa_1 = \kappa_{-1}$$

apply there, and when these are substituted into Equation (6.1.17), we have the deflection at the first subdivision point (i = 1) as

$$\kappa_1 = \frac{1}{2} \frac{1}{\rho_o} \qquad (6.1.18)$$

From Equation (6.1.17) we obtain the recursion formula

$$\kappa_{i+1} = 2\kappa_i - \kappa_{i-1} + \frac{1}{\rho_i} \qquad (6.1.19)$$

for successive calculation of the elastic part of the deflection.

When the elastic beam curvature required for calculation of a_i and a_n in Equation (6.1.13) is to be determined, the calculation cannot be based on the depth of the compression zone which corresponds to purely elastic behaviour of the cross section. It must be borne in mind that, in actual fact, conditions are elasto-plastic, and the corresponding compression zone depth must be used. It was shown in Chapter 3 how the depth ξ to the compression zone can be determined as a function of the elasto-plastic curvature. Chapter 4 describes the corresponding determination of the bending moment μ. Using the elasto-plastic curvature as the governing parameter, a μ - ξ relation can be calculated in this way.

It is now possible to calculate the moment μ_i from the expression (6.1.3) for every subdivision point in the rotation span, and then to determine the corresponding value of ξ from the μ - ξ relation obtained as above. This, when substituted into Equation (4.7), gives the bending stiffness δ. The sought elastic curvature is then obtained from Equation (4.6).

Finally, substitution of the non-dimensional elastic deflection according to Equation (6.1.16) into Equation (6.1.13) gives the non-dimensional external work in the form

$$\phi_e = \frac{1}{2}(1 + \frac{\mu_y}{\mu_u})\theta_u\mu_u + \frac{\lambda}{2n^2}((1+4\beta)\kappa_n - 8\beta\frac{\Sigma\kappa_i}{n})\mu_u \qquad (6.1.20)$$

6.2 The consumed deformation energy

The way in which the relation between the non-dimensional deformation energy ψ per unit length of beam and the non-dimensional bending moment μ can be determined was shown in Chapter 5. Such a relation is shown, for instance, in FIG. 5a. This relation is reproduced in principle, but with another orientation, in FIG. 6.2a along the moment diagram of the rotation span. The way the μ - ψ relation can be transformed via the moment diagram so as to give the distribution of ψ along the length λ of the rotation span is evident from the figure. The total deformation energy consumed within the beam volume of the rotation span is thus equivalent to the dashed area in FIG. 6.2a. With the same subdivision of the span as that applied in Section 6.1, we obtain the following relation for the total energy - see also Equation (5.4)

$$W_i = \Sigma N_c\psi_i\Delta l_o = N_c\Delta l_o\Sigma\psi_i = N_c\frac{l_o}{n}\Sigma\psi_i \qquad (6.2.1)$$

If this expression is divided by the reference moment $M_c = N_c d$, the total consumed deformation energy is obtained in non-dimensional form as

$$\phi_i = \frac{W_i}{M_c} = \frac{l_o}{d}\frac{1}{n}\Sigma\psi_i = \frac{\lambda}{n}\sum_1^n\psi_i \qquad (6.2.2)$$

6.3 Energy balance

The total consumed deformation energy ϕ_i is equal to the work ϕ_e performed by the external forces within the rotation span, i.e.

$$\phi_e = \phi_i \qquad (6.3.1)$$

If we substitute into this expression ϕ_e according to Equation (6.1.20) and ϕ_i according to Equation (6.2.2), we have

$$\frac{1}{2}\left(1+\frac{\mu_y}{\mu_u}\right)\theta_u\mu_u+\frac{\lambda}{2n^2}\left\{(1+4\beta)\kappa_n-8\beta\frac{\Sigma\kappa_i}{n}\right\}\mu_u=\frac{\lambda}{n}\Sigma\psi_i$$

from which the rotation capacity is calculated as

$$\frac{\theta_u}{\lambda}=\left\{\frac{1}{\mu_u}\frac{\Sigma\psi_i}{n}+\frac{1}{2n^2}\left(8\beta\frac{\Sigma\kappa_i}{n}-(1+4\beta)\kappa_n\right)\right\}\frac{2}{1+\frac{\mu_y}{\mu_u}} \qquad (6.3.2)$$

Equation (6.3.2) has been used as the basis for the development of a computer program. Results of calculations using this program are set out in the following.

7 DEPENDENCE OF THE ROTATION CAPACITY ON THE SHAPES OF THE STRESS-STRAIN DIAGRAMS FOR THE STEEL AND CONCRETE

The rotation capacities for the three typical steels HR, CW and CEB, combined with the two concrete types A and B described in Chapter 2, are first calculated. The calculation is made for three moment distributions corresponding to $\beta = 0.25$, $\beta = 0$ and $\beta = -0.06$ according to Chapter 6. The object of this investigation is to show the general effect on the rotation capacity due to the different shapes of the stress-strain diagrams for the steel and concrete.

The way the rotation capacity changes when there are deviations from the parameter values selected in Chapter 2 for the description of the stress-strain diagrams of the three typical steels and the two concrete types is then demonstrated. For the sake of clarity, results are only shown for a moment distribution corresponding to $\beta = 0.25$, i.e. the moment distribution which occurs in conjunction with a plastic hinge which is not acted upon by large shear forces.

The results are set out in the form of diagrams, with the effective reinforcement ratio as the abscissa and θ_u/λ as the ordinate. The value of ω is made to vary between the limits 0.04 and 0.31, which ought to cover all situations that normally occur.

7.1 Different combinations of typical steels and concrete types

If HR steel is combined with concrete types A and B, results according to FIG. 7.1a are obtained. The two families of curves have the same general form, characterised by the existence of a critical value of ω, ω_{cr}, at which there is a change in the shape of the curves.

For $\omega < \omega_{cr}$, there is a marked increase in rotation capacity with decreasing ω, while for $\omega > \omega_{cr}$ the value of ω is low and practically constant. If detailed calculations are made in order to find an explanation of this phenomenon, it is seen that at ω_{cr} failure occurs exactly when the strain in the steel coincides with the lower strain hardening limit ε_1 of the steel in FIG. 2.2b. When $\omega < \omega_{cr}$, failure occurs within the strain hardening region of the steel.

When $\omega > \omega_{cr}$, failure occurs at the yield level of the steel. This shows that the concepts of over-reinforcement and normal reinforcement must be given different meanings depending on whether it is the ultimate moment or the rotation capacity that is being studied. The boundary between over-reinforcement and normal reinforcement is at the steel strain $\varepsilon_2 = 1/e_s$ for calculation of the ultimate moment, while for calculation of the rotation capacity it may be considered to be situated at the end point of the yield level, at the strain ε_1. The statement sometimes encountered, that the rotation capacity is at all times sufficient provided that the beam is normally reinforced, is thus rather rash.

FIG. 7.1a also shows the effect due to variation of the mechanical properties of concrete. For concrete type A, $\omega_{cr} = 0.15$, while for type B $\omega_{cr} = 0.21$. In this context it is primarily the ultimate compressive strain ε_{cu} of the concrete which is critical with regard to the position of ω_{cr}.

A corresponding calculation relating to CW steel gives results according to FIG. 7.1b. In this case there is no ω_{cr} since this steel has no pronounced boundary between the yield region and the strain hardening region. The rotation capacity of a concrete beam with CW steel is consistently lower than that of a beam with HR steel.

The results of a calculation relating to CEB steel are shown in FIG. 7.1c. As may have been expected after a study of the moment-curvature diagram for this hypothetical steel, the rotation capacity is extremely low. This shows that it is unrealistic to apply the stress-strain curve suggested by the CEB for reinforcing steel in conjunction with calculation of the rotation capacity. On the other hand, as shown in Chapter 4, this truncated stress-strain curve does not exhibit any palpable disadvantages in conjunction with the calculation of the ultimate moment of a cross section.

It is a common feature of the results set out that the moment distribution $\beta = 0.25$ gives a larger rotation capacity than the distributions $\beta = 0$ and $\beta = -0.06$, which is to be expected in view of the general discussion in relation to FIG. 1.3a. It must however be noted that any effect due to shear force is not taken into consideration here. The presence of shear force can change the results in a direction favourable for the distributions $\beta = 0$ and $\beta = -0.06$.

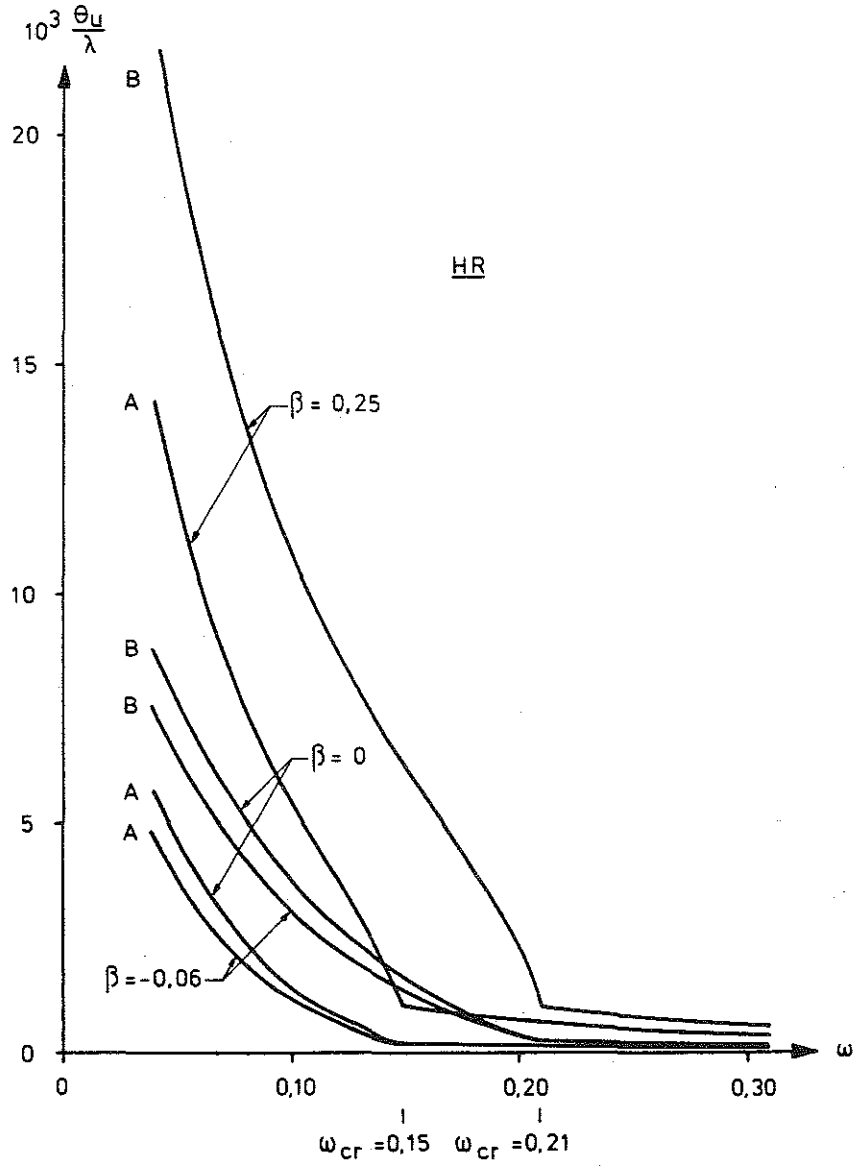

FIG 7.1a Rotation capacity expressed in terms of the ratio θ_u/λ as a function of ω. The curves relate to HR steel combined with concrete types A and B for three different moment distributions.

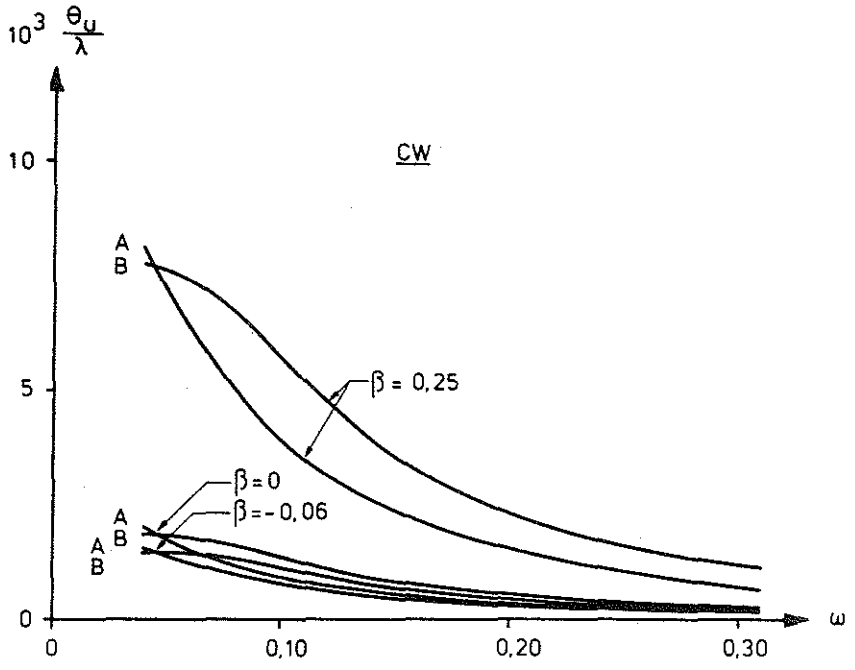

FIG 7.1b Rotation capacity expressed in terms of the ratio θ_u/λ as a function of ω. The curves relate to CW steel combined with concrete types A and B for three different moment distributions.

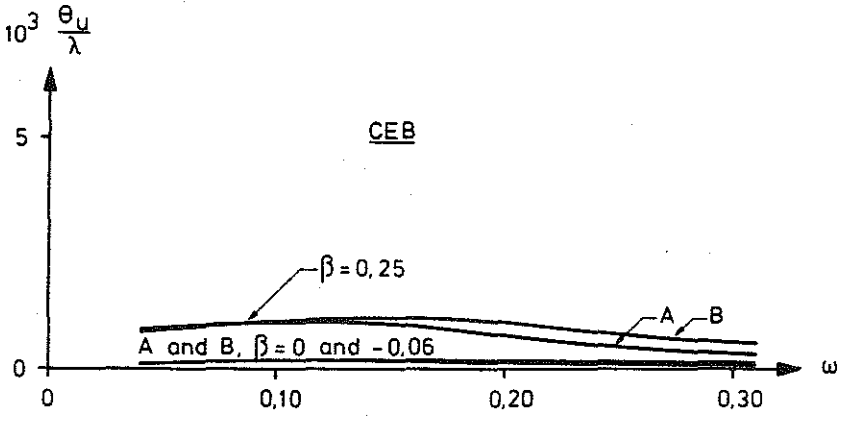

FIG 7.1c Rotation capacity expressed in terms of the ratio θ_u/λ as a function of ω. The curves relate to CEB steel combined with concrete types A and B for three different moment distributions.

7.2 Deviations from the parameter values selected for the typical steels and the concrete types

All the calculation results given in this section refer to the moment distribution $\beta = 0.25$.

In Section 2.1 representative parameters were determined for the description of concretes type A and B. The value $e_c = 1200$ was chosen for the non-dimensional initial modulus of elasticity of the concrete. It is interesting to see what the effect of deviations from the selected value is for the rotation capacity. In order to investigate this, two calculations have been made for CW steel, in one case combined with concrete type A, with $e_c = 1800$, and in the other combined with concrete type B, with $e_c = 800$. The results are shown in FIG. 7.2a where corresponding results using the normal value $e_c = 1200$ are also shown with dashed lines for purposes of comparison. As will be seen from this figure, the effect of variations in e_c on the rotation capacity is insignificant, and for this reason e_c can be omitted as a variable parameter in the following, and the constant value of $e_c = 1200$ used.

In section 2.2 a value $e_s = 350$ was chosen as the non-dimensional modulus of elasticity of the steel, and this was then applied as normal value for all three typical steels, HR, CW and CEB. In order to see what effect deviations from the selected value have on the rotation capacity, two calculations have been made for HR steel and concrete type B, with $e_s = 250$ in one case and $e_s = 700$ in the other. See FIG. 2.2c. The results obtained are shown in FIG. 7.2b. Compared with the results for the normal value of $e_s = 350$, the differences are small, and for this reason it may be considered justified to omit e_s also as a variable parameter and to use the constant value $e_s = 350$ irrespective of steel type and the value of f_{st}.

For HR steel, the lower strain hardening limit $\varepsilon_1 = 0.015$ was chosen as normal value in Section 2.2. Comparative calculations for this value and the alternative values $\varepsilon_1 = 0.005$ and $\varepsilon_1 = 0.025$ are of interest, during which process the entire strain hardening region of the steel between ε_1 and ε_0 is given a corresponding sideways displacement as shown in FIG. 7.2c. The results of calculations using the alternative stress-strain curves for the HR steel in combination with concretes types A and B are shown in the same figure. In view of the above explanation concerning the physical meaning of a critical value ω_{cr} for the effective reinforcement ratio, it may be expected that a variation in ε_1 will be reflected in a corresponding variation in ω_{cr}. The figure shows that this is actually the case. The value of ω_{cr} changes from approx. 0.10 to

0.29 when ε_1 is changed from 0.025 to 0.005 in combination with concrete type A. In combination with concrete type B, the corresponding change in ω_{cr} is from about 0.15 to a value in excess of 0.31.

In order to throw further light on this subject, $\eta = f_{stu}/f_{st}$ is varied for an HR steel as shown in FIG. 7.2d, the value of the lower strain hardening limit being maintained at $\varepsilon_1 = 0.015$. Two values of η, 1.2 and 1.6, are combined with concretes types A and B. A variation in η has no effect on the position of ω_{cr}, nor on the rotation capacities corresponding to $\omega > \omega_{cr}$, since failure then occurs at steel strains less than the lower strain hardening limit. The calculation results set out in the figure also show that the variation in rotation capacity with η is moderate for $\omega < \omega_{cr}$.

Finally, FIG. 7.2e shows what change is obtained in the rotation capacity when η for a CW steel is increased from the selected normal value of 1.1 to 1.2. Calculated results are set out in the figure for the CW steel in combination with concretes types A and B. It is seen from the figure that the variation studied causes a moderate change in the rotation capacity.

Tho following conslusions may be drawn from the above analysis.

The non-dimensional initial modulus of elasticity of concrete may be considered constant and equal to $e_c = 1200$ in all contexts.

For both HR and CW steels, the non-dimensional modulus of elasticity of steel may be considered constant and equal to $e_s = 350$.

The stress-strain curve suggested by the CEB for reinforcing steel is not applicable in conjunction with determination of the rotation capacity.

The boundary between over-reinforcement and normal reinforcement, which for calculation of the ultimate moment is put at the steel strain $\varepsilon_2 = 1/e_s$, should instead be related to the lower strain hardening limit ε_1 when the rotation capacity is calculated.

The magnitude of the rotation capacity, within certain values of ω, is greatly dependent on the position of the lower strain hardening limit of the steel. The value of the ratio $\eta = f_{stu}/f_{st}$ does not have the same significance.

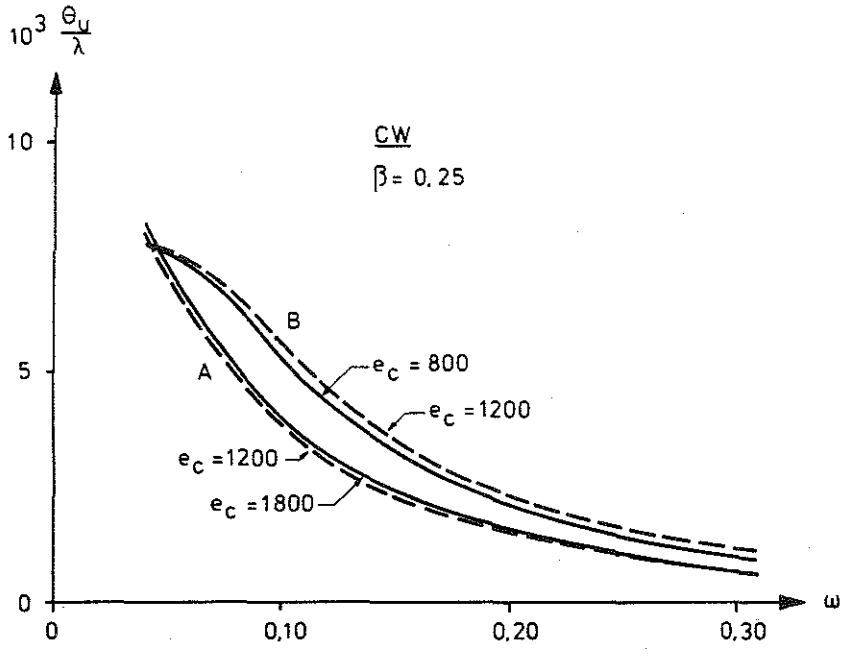

FIG 7.2a Rotation capacity as a function of the non-dimensional modulus of elasticity e_c of the concrete.

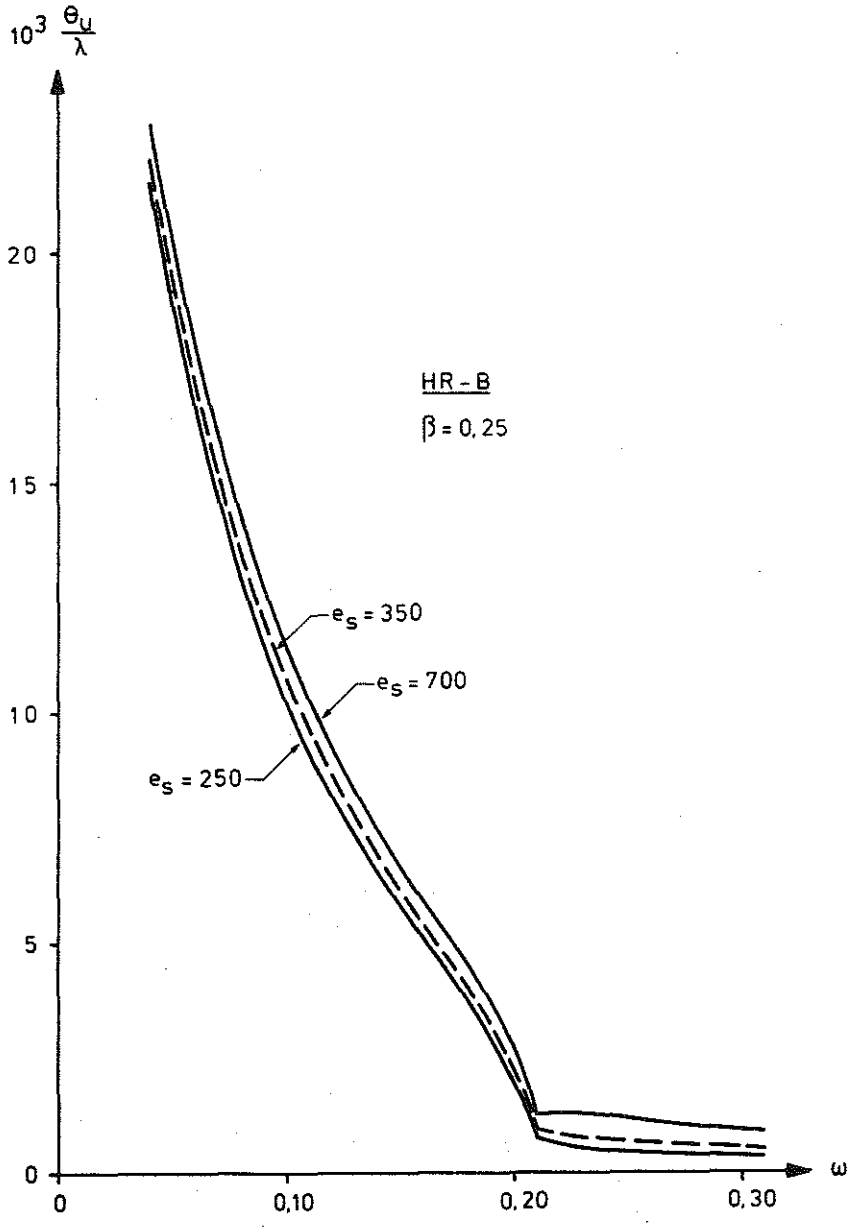

FIG 7.2b Rotation capacity as a function of the non-dimensional modulus of elasticity e_s of the reinforcing steel.

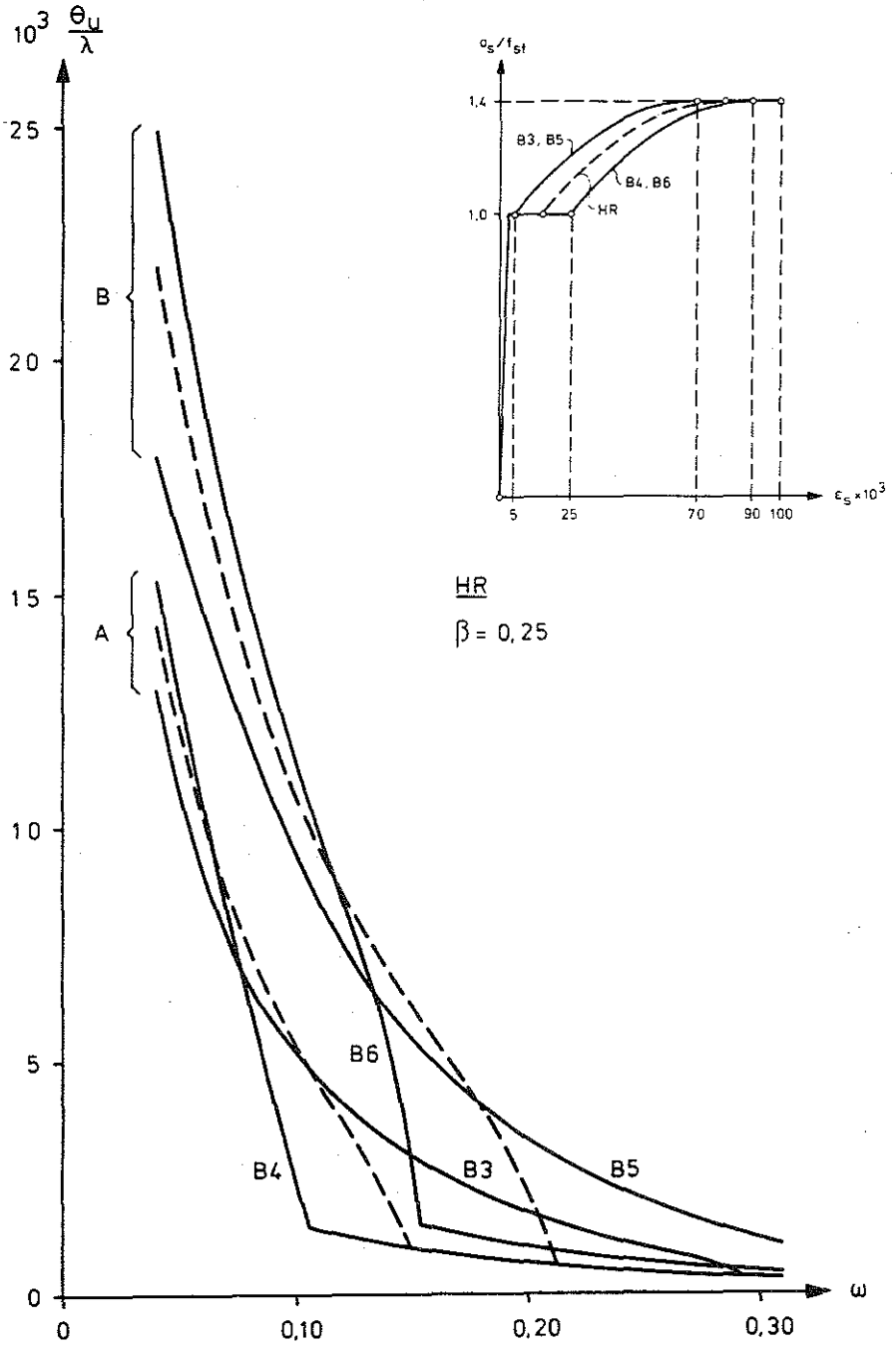

FIG 7.2c Stress-strain curve for HR steel modified by variation of the lower strain hardening limit of the steel. The ratio θ_u/λ as a function of ω for combinations of the modified curves with concrete types A and B.

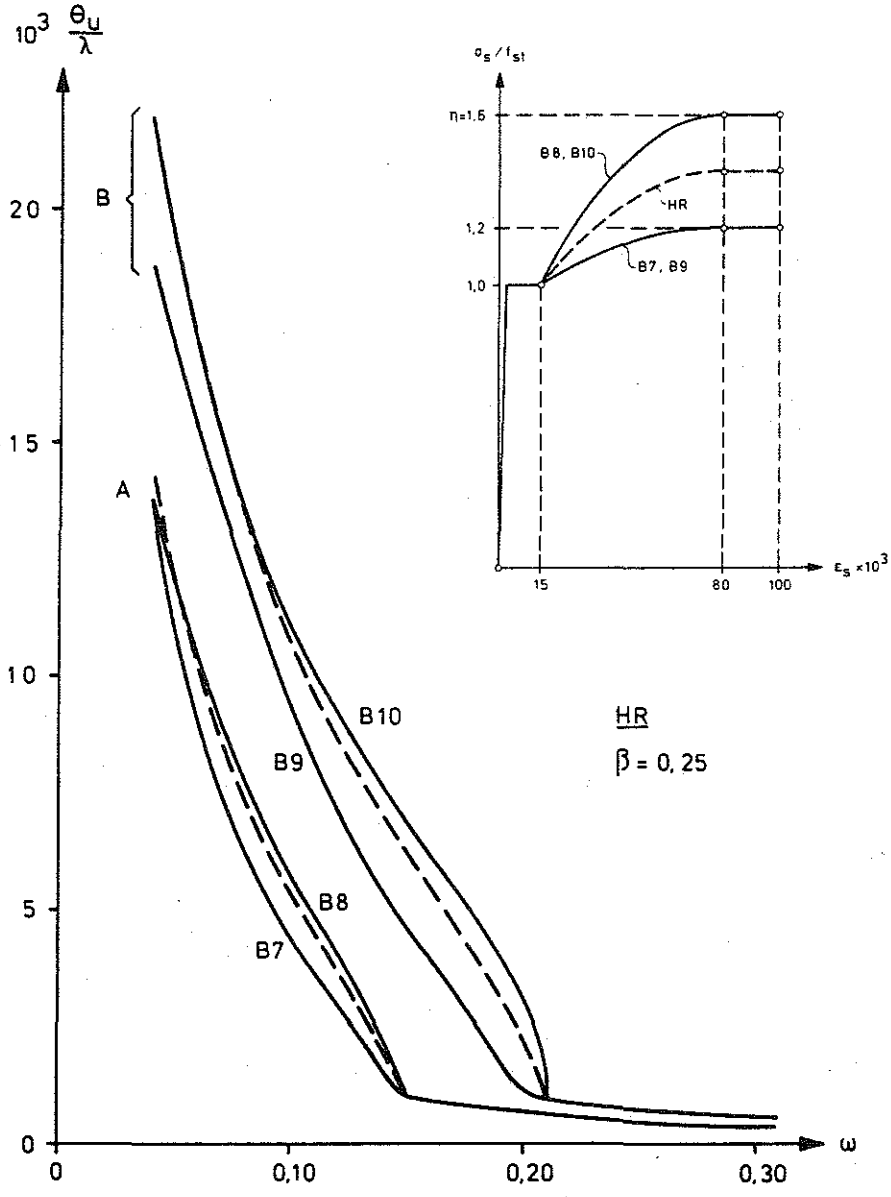

FIG 7.2d Stress-strain curve for HR steel modified by variation of the coefficient η. The ratio θ_u/λ as a function of ω for combinations of the modified curves with concrete types A and B.

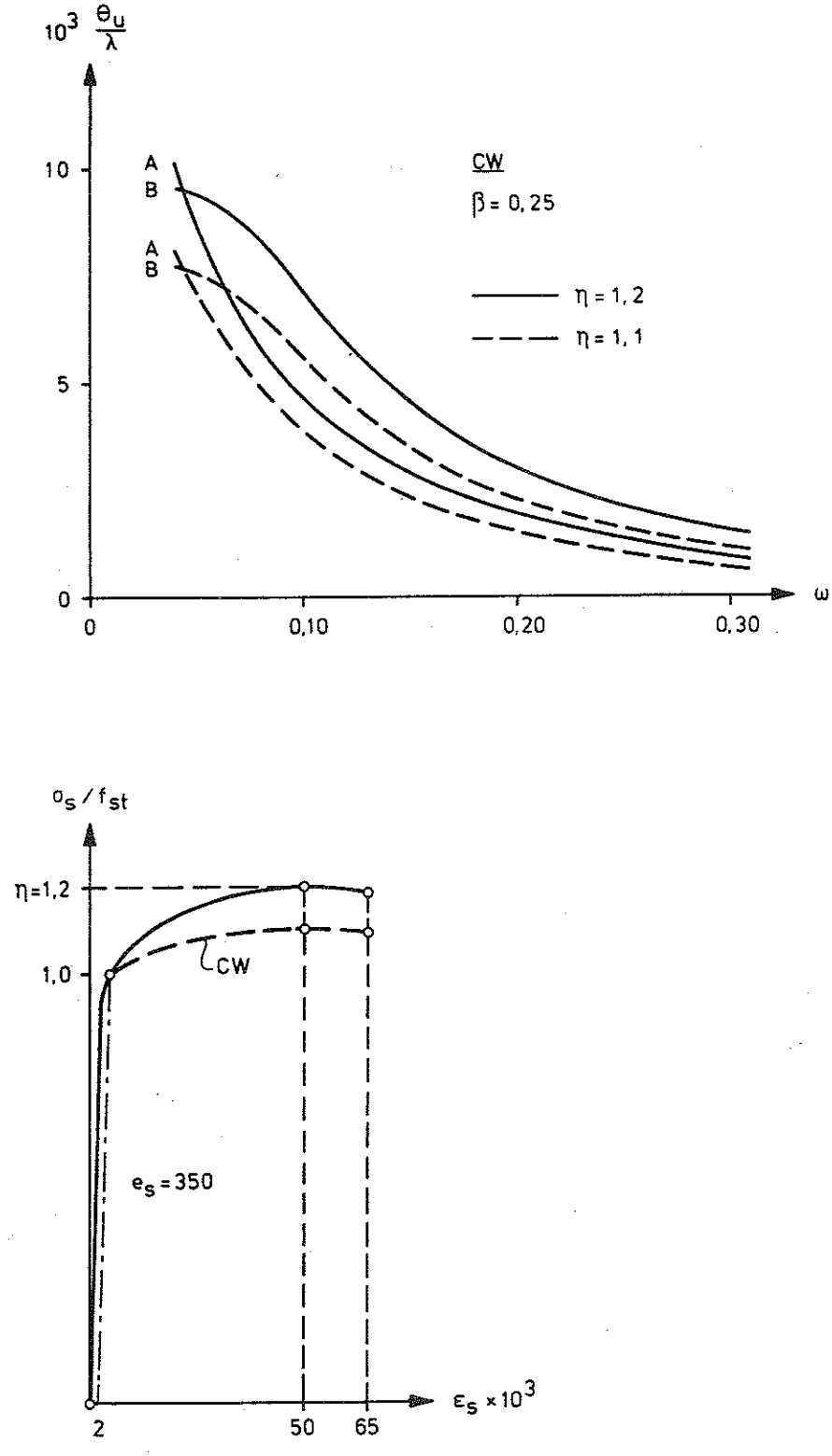

FIG 7.2e Stress-strain curve for CW steel modified by alteration of the coefficient η from 1.1 to 1.2. The ratio θ_u/λ as a function of ω for combinations of the modified curve with concrete types A and B.

The value of the rotation capacity is consistently somewhat greater when the calculations are based on concrete type B, which is more in conformity with actual conditions, than when the calculations are based on concrete type A which is more restrictive as regards deformations.

8 CREEP OF THE CONCRETE

As a rule, the effect due to creep of the concrete is not taken into consideration when the rotation capacity of a concrete beam is calculated. In cases when an accurate check is made on the compatibility conditions and the effect of creep is thus taken into account in determining the rotation requirement of the plastic hinge, inclusion of the effect of creep in calculating the rotation capacity is also warranted.

Computationally, the effect of creep can be allowed for by transforming the compressive stress-strain curve of the concrete by means of changing the scale along the ε_c axis, as shown in FIG. 8a. The scale factor is $1+\varphi$, where φ is the creep factor. Computationally, this implies that the appropriate strain ε_i in strip No i must be divided by $1+\varphi$ and the modified strain thus obtained used for determination of the stress in the untransformed stress-strain diagram for the compressive stresses in the concrete. In consequence of this, the modulus of elasticity of concrete must be divided by $1+\varphi$ in the previously derived formulae for calculation of the rotation capacity.

Calculations which take the creep of concrete into account give the results shown in FIG. 8b and 8c. In FIG. 8b the effect of creep on concrete type A, in combination with reinforcing steels of both types HR and CW, is studied. FIG. 8c shows the corresponding results for concrete type B in combination with the same reinforcing steels.

The figures show that an increase in the creep factor consistently raises the rotation capacity. The reason for this is that the greater value of ε_{cu} applicable in conjunction with creep allows a greater strain in the tension reinforcement before the concrete undergoes crushing failure. As a result, a greater quantity of deformation energy can be stored within the volume of the rotation span. In particular, the value of ω_{cr} for HR steel becomes progressively higher as the creep factor increases.

When there is compression reinforcement within the section, creep of the concrete causes a change in the distribution of force between the compression reinforcement and the compressed concrete. If, prior to creep of the concrete, the stress in the compression reinforcement is below the yield stress, the concrete will be relieved of load and a greater proportion of the force will be transferred to the steel. If the compression reinforcement has already attained its yield stress before the concrete begins to creep, there is no

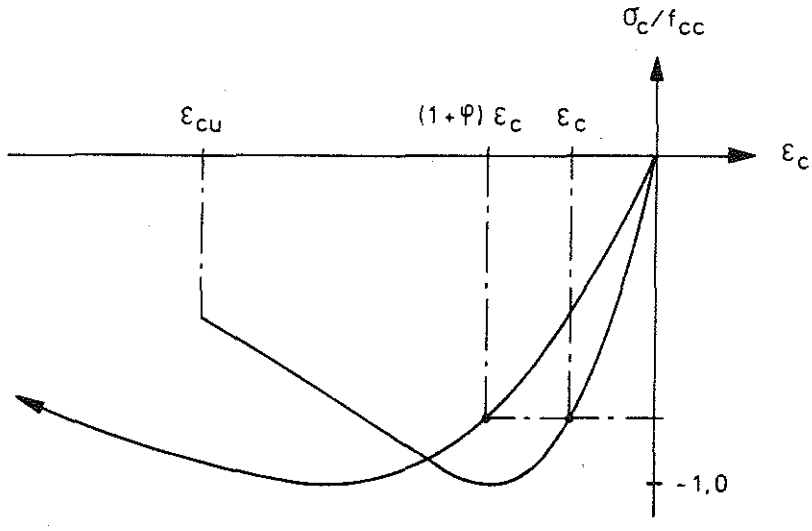

FIG 8a Stress-strain curve for concrete in compression, with and without consideration of the creep of concrete.

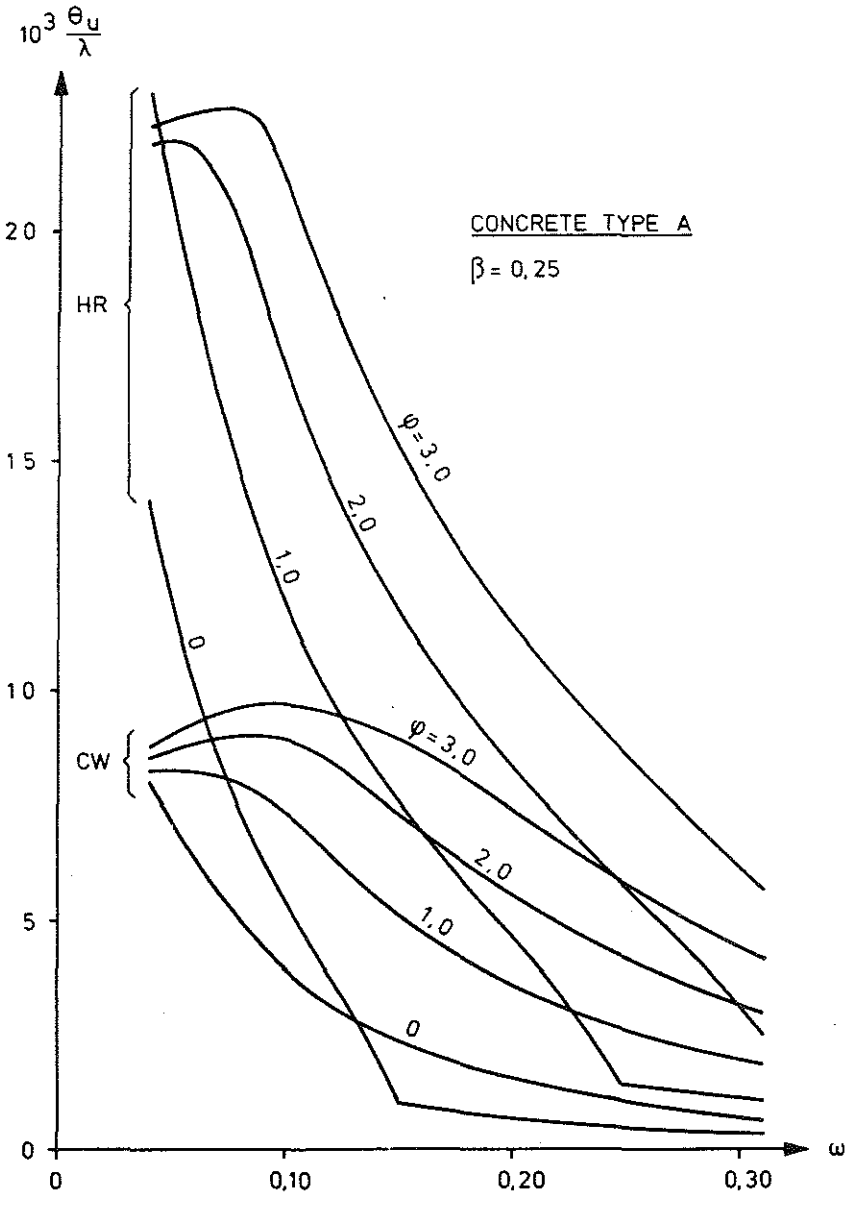

FIG 8b The ratio θ_u/λ as a function of ω for different values of the creep factor φ for concrete. The figure relates to concrete type A in combination with both HR and CW steel.

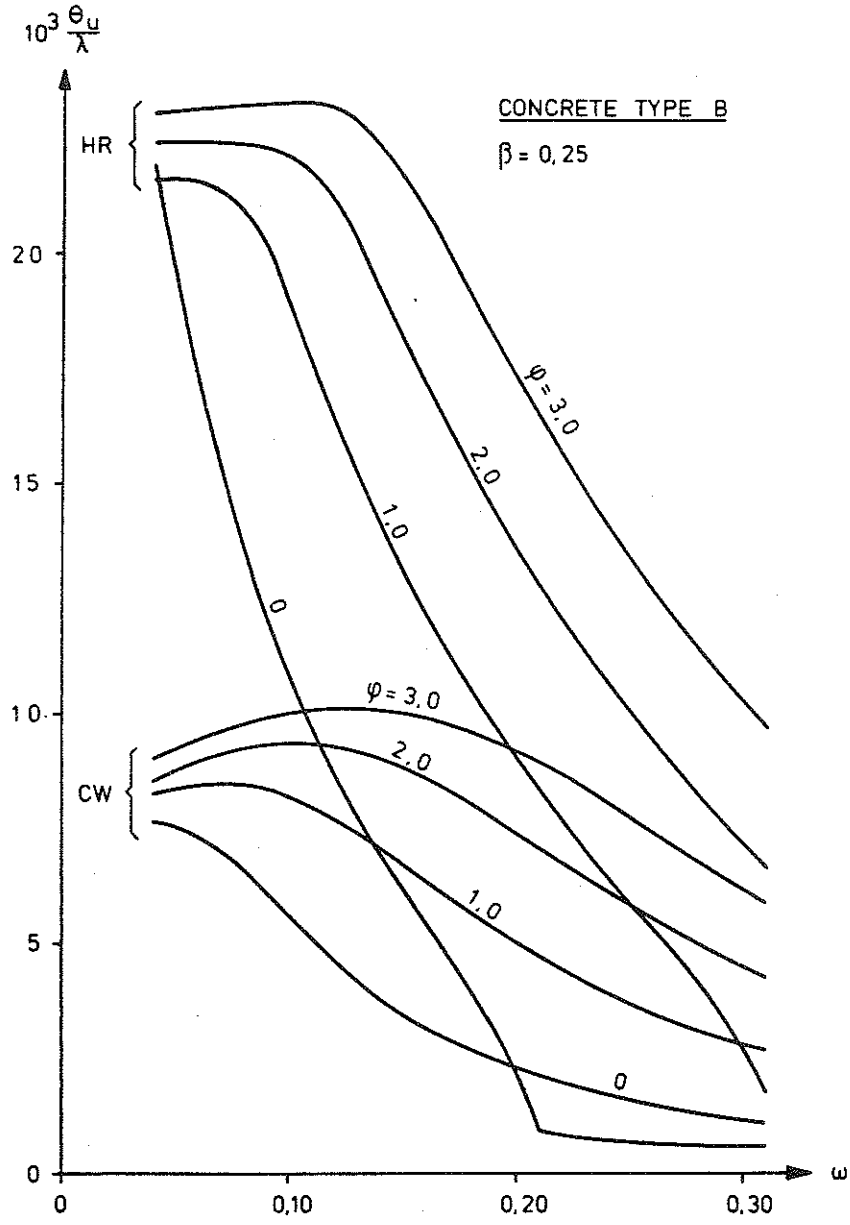

FIG 8c The ratio θ_u/λ as a function of ω for different values of the creep factor φ for concrete. The figure relates to concrete type B in combination with both HR and CW steel.

redistribution of force. It may therefore be expected that creep of the concrete in a section containing compression reinforcement will cause a greater increase in rotation capacity for larger values of ω than for small ones. See also Chapter 9.

9 THE EFFECT OF COMPRESSION REINFORCEMENT

When compression reinforcement is used, the compression force on the cross section is sustained jointly by the compression reinforcement and the concrete. The depth of the compression zone is then somewhat less than in a comparable beam without compression reinforcement. Reduction in the depth of the compression zone results in an increase in strain in the tension reinforcement before the ultimate moment is reached, which, in turn, means that more deformation energy is stored within the volume of the rotation span and the rotation capacity is therefore greater.

A calculation for HR steel and concrete type B, with the position of the compression reinforcement in the section determined by $\gamma = c/d = 0.1$, gives the rotation capacity shown in FIG. 9a. For $\omega = 0.055$ the rotation capacity is independent of the quantity of compression reinforcement, the reason being that, at this value of ω, the neutral axis is at the same level as the compression reinforcement. For larger values of ω the rotation capacity increases with ω_c/ω. It may also be noted that ω_{cr} increases as the value of ω_c/ω increases.

The results of corresponding calculations for CW steel, with the same conditions regarding concrete type and the position of the compression reinforcement, are set out in FIG. 9b. In this case the neutral axis and the compression reinforcement coincide at $\omega = 0.068$. It will be seen that for $\omega_c/\omega \geq 0.8$ the rotation capacity is practically independent of ω within the range studied.

The results given in FIG. 9a and 9b are based on the assumption that the steel in the tension and compression reinforcement is of the same type, and that f_{st} for the tension reinforcement is equal to f_{sc} for the compression reinforcement, i.e. $\nu = f_{sc}/f_{st} = 1.0$. In other respects there is no need to make any further assumptions concerning identity of the properties of the tension and compression reinforcement, for instance concerning the position of the lower strain hardening limit. The reason for this is that while the tension reinforcement can develop strains beyond the lower strain hardening limit, this is impossible in the case of the compression reinforcement. Even in extreme cases, the strain in the compression reinforcement is at the beginning of the yield range, determined by the ultimate compressive strain ε_{cu} of the surrounding concrete.

In order to investigate what the effect is on the rotation capacity when different grades of steel are chosen for the tension and compression reinforcement, comparative calculations have been made using $\nu = 0.7$ and 1.3. The other conditions are: HR steel, concrete type B, $\gamma = 0.1$ and $\omega_c/\omega = 0.5$ and 1.0. With the boundaries of ω equal to 0.05 and 0.30, in no case was the difference found between the calculated rotation capacities for $\nu = 0.7$ and 1.3 greater than 0.1%. This demonstrates that the coefficient ν need not be regarded a variable parameter, but can be given the fixed value $\nu = 1.0$. This is the value which has been applied in all other calculations concerning compression reinforcement.

The results set out in FIG. 9a and 9b are based on a position of the compression reinforcement corresponding to the value $\gamma = 0.1$. In order to see how sensitive the rotation capacity is to variations in the placing of the compression reinforcement within the cross section, calculations have been made for the values $\gamma = 0.05$, $\gamma = 0.10$ and $\gamma = 0.20$. The other conditions are: HR steel, concrete type B, $\omega_c/\omega = 0.5$. The results are shown in FIG. 9c. When the compression reinforcement is placed high up in the section, $\gamma = 0.05$, there is some increase in rotation capacity, for values of ω less then 0.18, compared with the position given by $\gamma = 0.10$. For greater values of ω the rotation capacity obtained is about the same in both cases. For compression reinforcement placed low in the section, $\gamma = 0.20$, there is a considerable reduction in rotation capacity over the entire range of ω studied. The rotation capacity calculated under similar conditions but without consideration of the compression reinforcement has been plotted in the figure with a dashed line. As will be seen, the results for the compression reinforcement situated low in the section are in some cases less favourable that for no compression reinforcement at all. This is due to the fact that for low values of ω the compression reinforcement drops below the neutral axis of the section and will be in tension instead of in compression. If, therefore, compression reinforcement is chosen as a means of elevating the rotation capacity, care must be taken to ensure that the reinforcement is properly placed in the formwork and that it is not displaced downwards when the concrete is poured.

In ordinary calculations of the ultimate moment of a reinforced concrete cross section, based on the assumption that the distribution of stress in the compressed concrete is rectangular, it is generally assumed that the depth of the compression zone can be calculated from the expression

$$\xi = 1{,}25\ (\omega - \omega_c) \qquad (9.1)$$

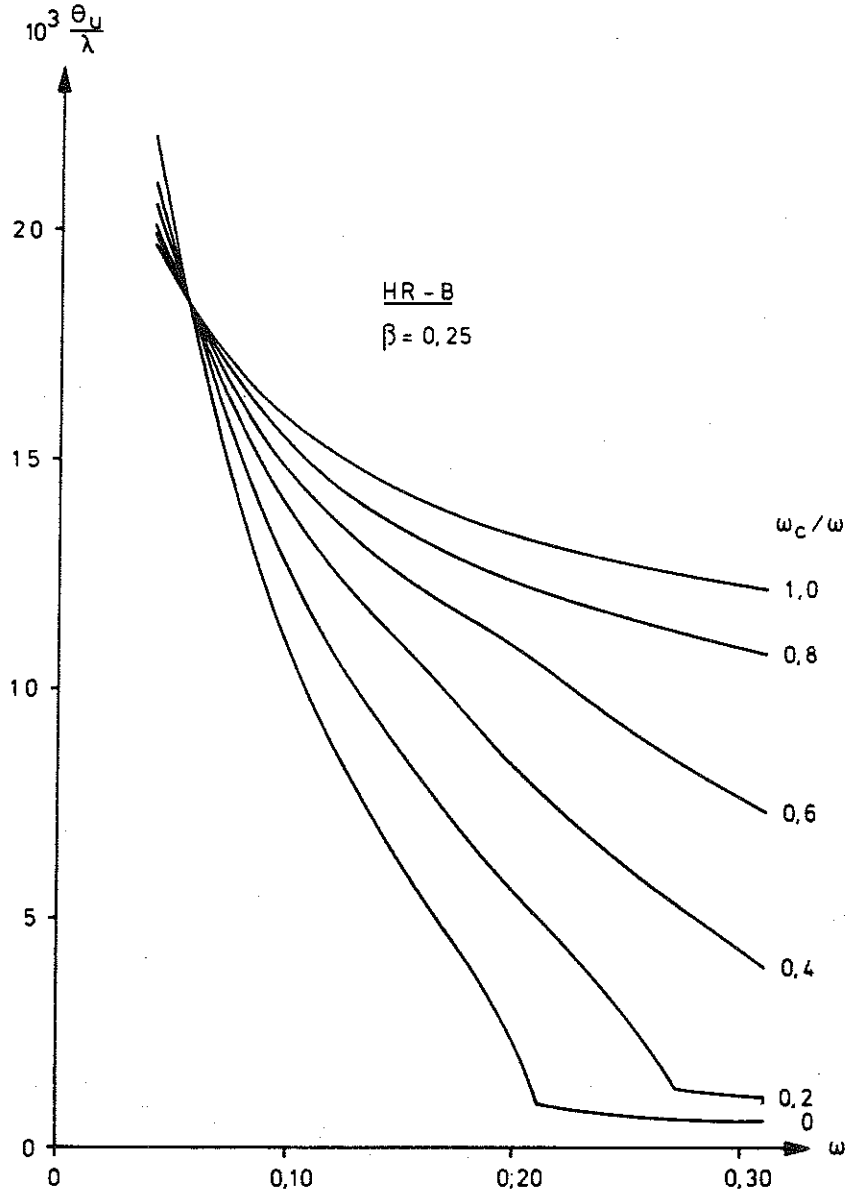

FIG 9a Rotation capacity expressed in terms of the ratio θ_u/λ as a function of ω and ω_c. The diagram relates to HR steel and concrete type B.

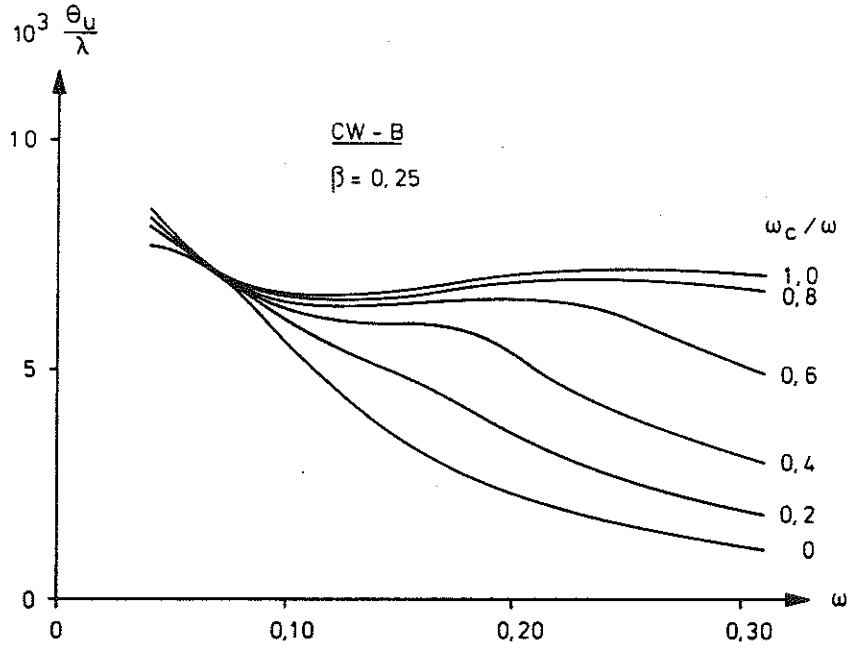

FIG 9b Rotation capacity expressed in terms of the ratio θ_u/λ as a function of ω and ω_c. The diagram relates to CW steel and concrete type B.

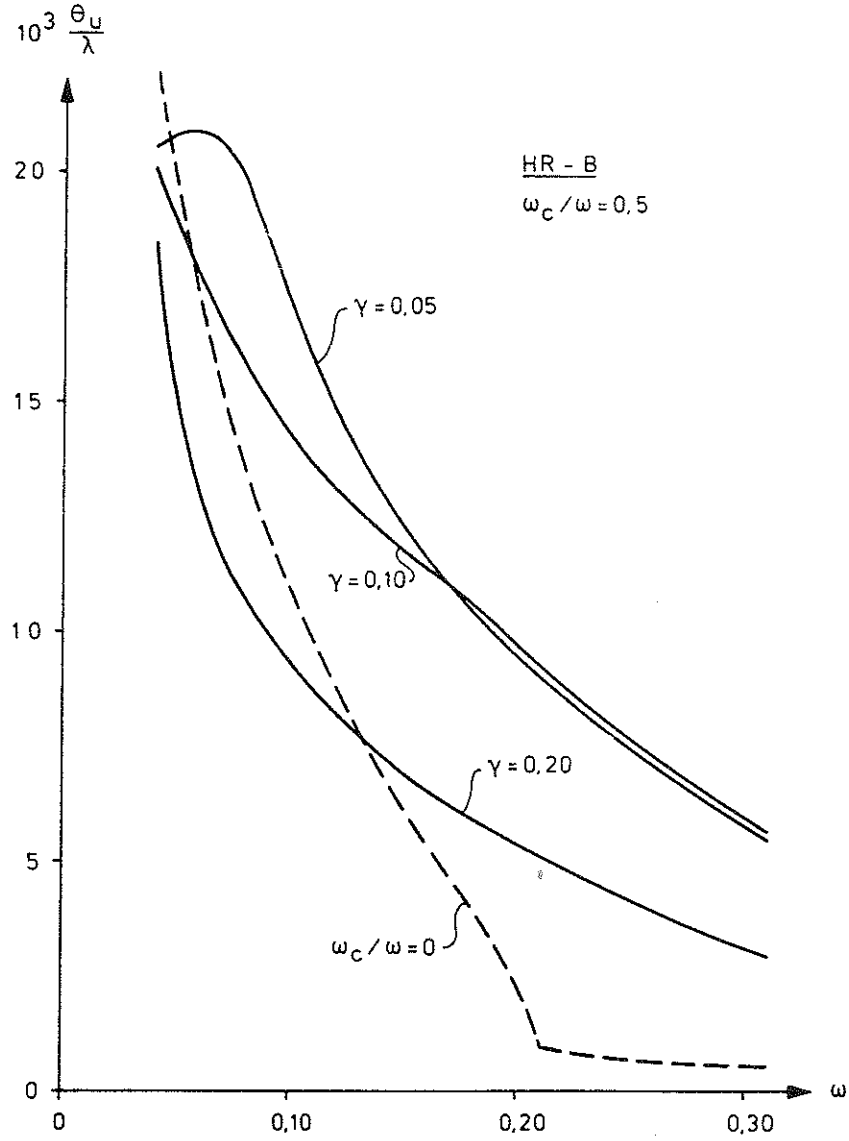

FIG 9c Rotation capacity as a function of the placing of the compression reinforcement in the cross section.

This assumes that the compression reinforcement takes up that proportion of the resultant compressive force which corresponds to the yield stress of the reinforcement. For calculation of the ultimate moment, this approach can be accepted, since the resulting force in the compression reinforcement is generally practically coincident with the resultant of the compressive stresses in the concrete. The calculation results are therefore insensitive to the way in which the total compressive force is divided between the two resultant components. If, for instance, expression (9.1) is applied for $\omega_c = \omega$, $\xi = 0$ is obtained, i.e. it is assumed that the entire compressive force is resisted by the compression reinforcement, and the concrete is therefore unstresses. Naturally, this is functionally unreasonable, but still gives a fairly correct value of the ultimate moment. On the other hand, application of the same approach for calculation of inelastic deformations yields meaningless results. Some authors claim that the rotation capacity can be expressed as a function of only the depth ξ of the compression zone. Quite apart from the fact that this assumption has no meaning, application of Equation (9.1) will give completely erroneous results if there is a large quantity of compression reinforcement. This problem is illustrated by FIG. 9d in which (9.1) is plotted with dashed lines for $\omega = 0.10$ and $\omega = 0.20$. The full lines show the calculated variation in the actual depth of the compression zone at failure as a function of the ratio ω_c/ω. The calculation relates to HR steel and concrete type B. As will be seen from the figure, for large values of ω_c/ω there is a considerable difference between the depth of the compression zone calculated on the basis of realistic stress-strain curves and that obtained from Equation (9.1).

When failure occurs under the influence of long-term loading, creep takes place in the compressed concrete. This causes a certain redistribution of forces in the compressed portion of the cross section. For low values of ω this redistribution is moderate, since the stress in the compression reinforcement will already have reached, or is very near, the compressive yield stress of the steel before creep commences. For larger values of ω, the stress in the compression reinforcement is substantially below the yield point when creep begins, and it ts therefore possible for this stress to increase during creep, while at the same time the stress in the concrete in the compression zone decreases. During this process there is some reduction in the depth of the compression zone, and the rotation capacity therefore increases in the corresponding degree. The final results on completion of creep are given in FIG. 9e for both HR and CW steels in combination with

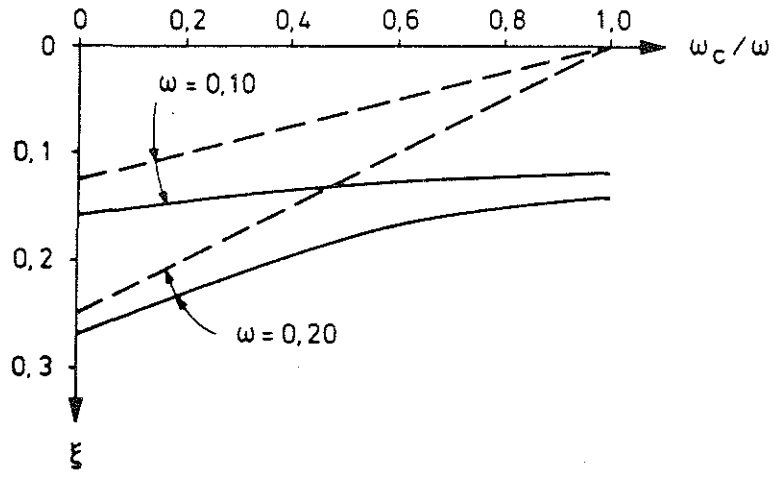

FIG 9d The non-dimensional actual depth ξ of the compression zone at beam failure as a function of ω_c/ω for two fixed values of ω. The dashed lines represent the depth of the compression zone calculated by the expression $\xi = 1.25(\omega - \omega_c)$

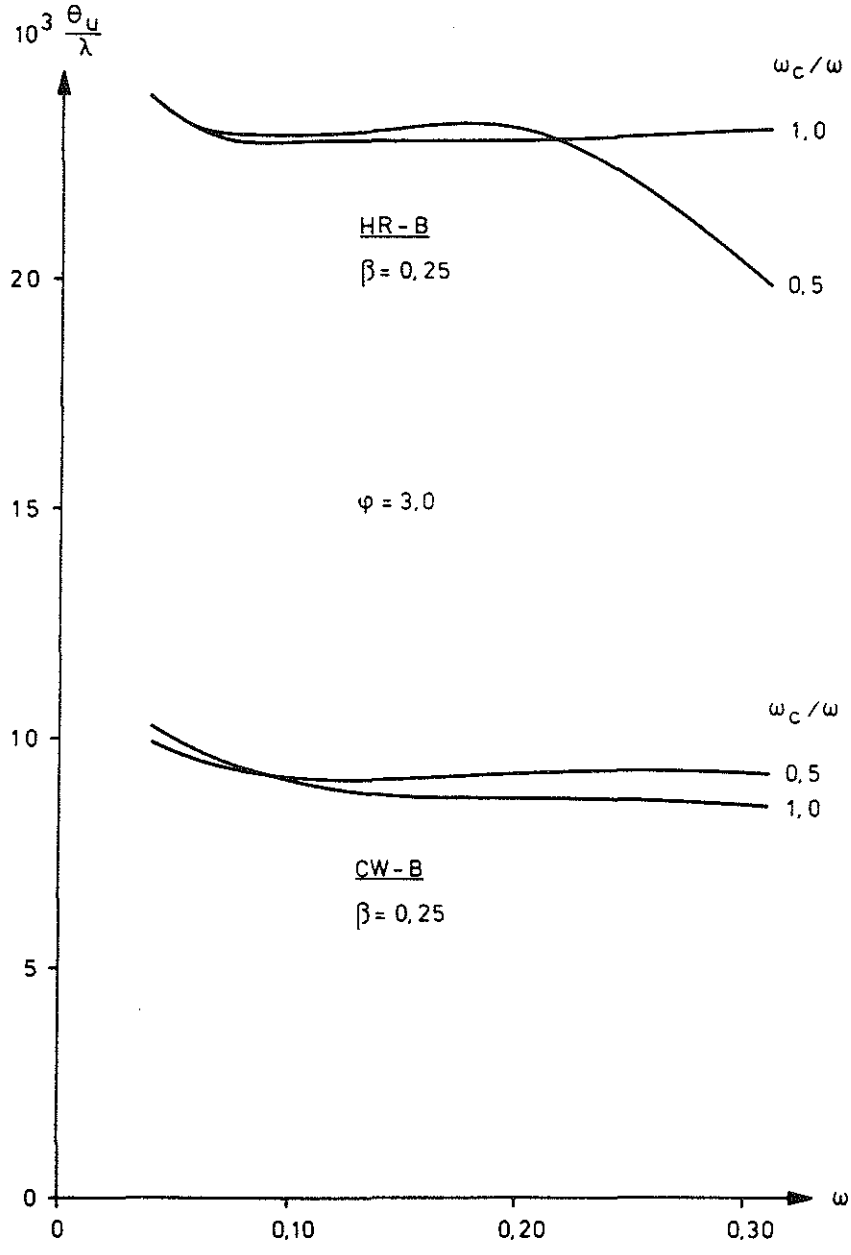

FIG 9e Rotation capacity in conjunction with creep of the concrete in a cross section with heavy compression reinforcement.

concrete type B. The creep factor is $\varphi = 3.0$, and the compression reinforcement corresponds to $\omega_c/\omega = 0.5$ and 1.0. As will be seen, the rotation capacity obtained for both steel types is practically constant within the range of ω considered.

The analytical model is based on the assumption that the compression reinforcement is rigidly fixed in the stipulated position during the entire loading process. In experimental investigations of concrete beams with compression reinforcement, it is sometimes noted that local deflection of the compression reinforcement occurs at moments near the ultimate moment. With regard to the rotation capacity, in such cases the compression reinforcement does more harm than good, since the deflected reinforcement causes splitting of the concrete in the compression zone and thus accelerates crushing failure. In order therefore that the rotation capacity calculated by means of the analytical model may be considered reliable, it is essential that the compression reinforcement is restrained by stirrups of suitably close spacing.

10 THE EFFECT OF SHEAR FORCE

The calculations set out so far have been consistently based on the validity of e.g. Bernoulli's hypothesis, which indirectly implies that the effect on the rotation capacity due to shear force acting simultaneously with the ultimate moment has been ignored. Experiments reported in the literature show that the incidence of a large shear force in the vicinity of the plastic hinge increases the rotation capacity. An attempt should therefore be made to modify the analytical model developed in such a way that the favourable effect of shear force may be included, if only approximately.

10.1 Analytical model

When the effect of shear force is to be included in the analytical model, application of the Ritter-Mörsch truss model is the obvious choice, and this is therefore used as the basis of the following line of reasoning.

If the analytical model derived in the provious section is supplemented by diagonals between the tension and compression zones in such a way that a truss is formed, and the model thus constructed is acted upon by shear force, two principal phenomena occur,

a. The diagonals of the truss are deformed under the action of the applied forces, and thus store deformation energy.

b. The variation of force along the compression and tension zones of the analytical model is different from that in the original model, and the energy stored in these zones is therefore also modified correspondingly.

With regard to the effect in a, the following may be stated. If stirrups which in actual fact are uniformly distributed are assumed in the model to be concentrated into discrete diagonals in tension, then the stresses, deformations and the associated energy storage in these can, in principle, be calculated with reasonable accuracy. However, the calculations presuppose that the distance between the diagonals in tension is known. For a given stirrup inclination, this distance is dependent on the inclination of the compressed concrete diagonals postulated in the truss model, i.e. dependent on the directions of the bending shear cracks which occur. Correct treatment of this problem thus demands knowledge and consideration of the variation in crack direction along the rotation span. If this is to be applied in the analytical model, the number of primary parameters will be increased very considerably, and the results will lose the clarity hitherto achieved. It is therefore desirable that this situation be avoided by the use of some appro-

riate approximation.

It is a general rule in the design of a reinforced concrete beam that the factor of safety with regard to shear failure should be greater than that with regard to bending failure. In view of this it is not unreasonable to introduce the assumption that, when bending failure occurs subsequent to plastic flow, if any, the steel in the stirrups will just about have attained its yield stress. All the deformation in the diagonals in tension will then have been elastic, and the deformation energy stored in these is therefore balanced by some of the work which the shear force performs during shear deformation. The rotation capacity of the plastic hinge is therefore unaffected by this.

As regards the compressed concrete diagonals in the model, the problem arises as to what formal cross sectional area is to be assumed for these. It is possible to assume a large area and small compressive stress, or vice versa, within limits determined by beam geometry and the compressive strength of the concrete. Whichever course is adopted, however, the total deformation energy stored by these compressed diagonals will be very much less than that stored by the diagonals in tension, and can therefore be ignored.
The conclusion drawn concerning the effect according to a is therefore that the rotation capacity of the plastic hinge can be calculated without consideration of the contribution of the diagonals to the deformation energy, with no major error being introduced in consequence.

The following may be said with regard to the effect according to b. Without consideration of the shear force, the extent a_y of the plastic hinge, i.e. the region over which the reinforcement yields, is determined according to figure a in FIG. 10.1a by the ratio of the ultimate moment μ_u to the yield moment μ_y. For purposes of simplicity, it is assumed that variation of moment over the length of the rotation span is linear. If inclined shear cracks are formed along the rotation span, conditions are altered, as will be seen from FIG. 10.1b which shows the portion of the beam between the point of zero moment and an inclined shear crack. It is evident from the figure that deformations and stresses in the tension reinforcement at section 2 are determined by the moment μ_1 at section 1, and that the corresponding stresses and deformations in the compression zone of the concrete at section 1 are determined by the moment μ_2 at section 2. For a constant shear crack direction along the rotation span, this means that the moment curve must be shifted a distance a to the left for calculation of the state of affairs in the tension reinforcement,

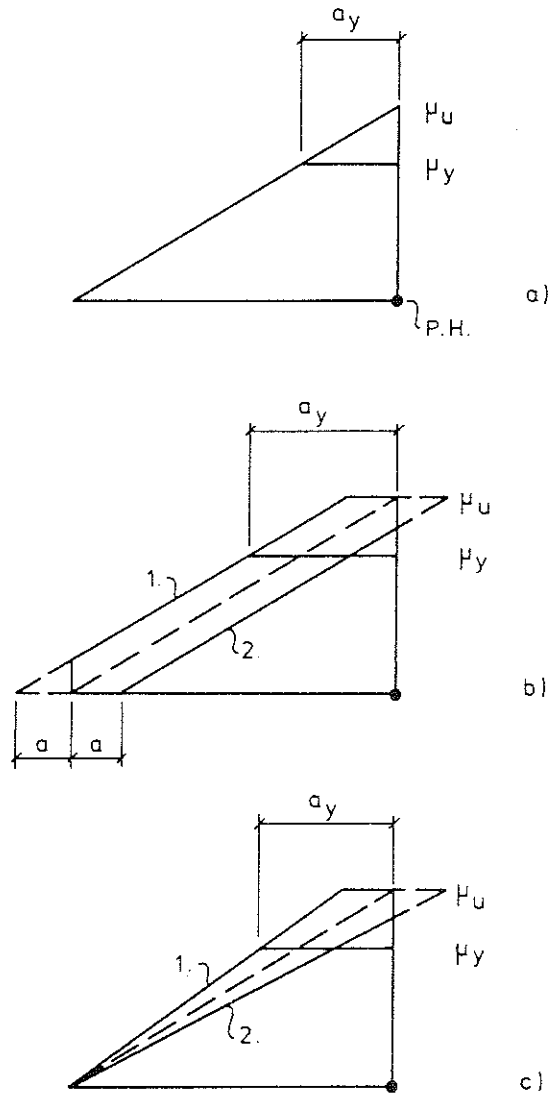

FIG 10.1a Moment shift as a result of inclined shear cracks.

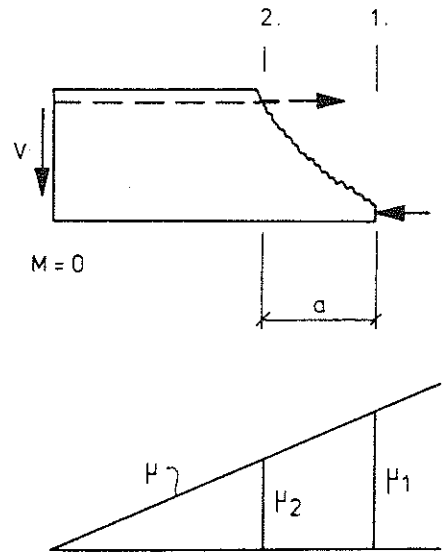

FIG 10.1b Portion of beam bounded by point of zero moment and an inclined shear crack.

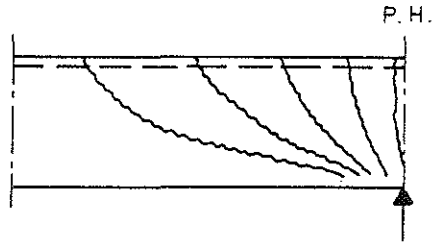

FIG 10.1c Fan shaped crack pattern in the region near a plastic hinge above a point load.

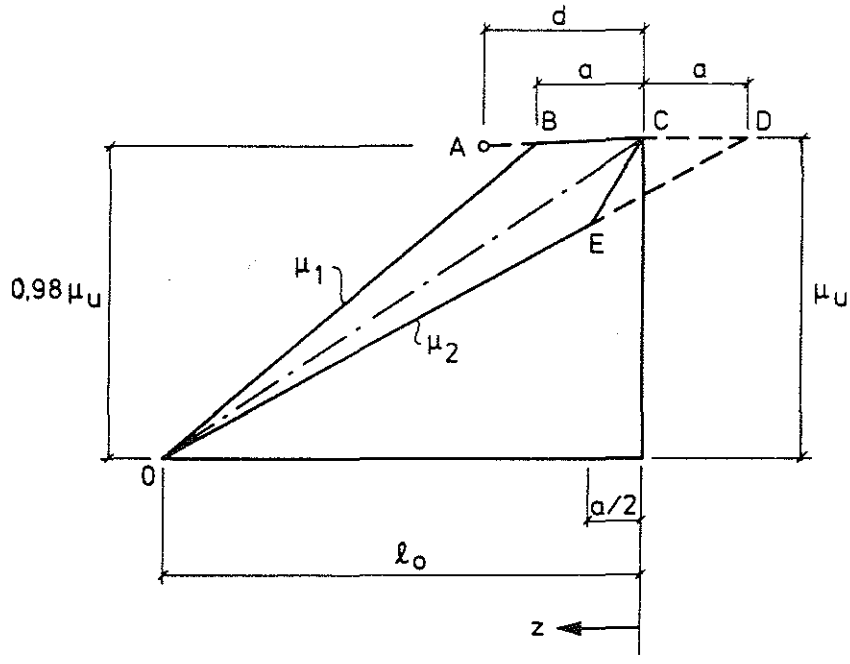

FIG 10.1d The moment shifts assumed in the analytical model. The moment variation μ_1 relates to the tension reinforcement. The moment variation μ_2 relates to the compression zone.

and to the right for calculation of the state of affairs in the compression zone. Owing to this, the extent of the yield region is increased by the distance a, as shown in figure b in FIG. 10.1a. However, the directions of the cracks are not constant along the rotation span, since the state of affairs is characterised by simultaneous occurrence of a large shear force and a linear moment distribution with a large maximum moment. This gives rise to the fan-shaped crack configuration, radiating from the point of action of the point load, shown in FIG. 10.1c. In order that this may be taken into account, the fictitious moment curves are modified as shown in figure c in FIG. 10.1a. The advantage gained by this modification is that the zero moment is now clearly defined. For a realistic value of the ratio μ_u/μ_y, the change in the length a_y of the yield region from figure b to figure c is insignificant.

This approach gives rise to the fictitious moment distribution shown in FIG. 10.1d, in which some more modifications have been introduced. For the crack configuration in FIG. 10.1c, most of the strain in the reinforcement and thus the consumption of energy take place in the cracks and in the region in the immediate vicinity of the cracks. In the reinforcement between two cracks the strain and energy consumption are less. For a constant moment μ_u over the distance a, see FIG. 10.1d, this is not taken into account, and calculations yield an excessive energy consumption over the distance a. This can be compensated for by making this distance inclined instead of horizontal. In view of the fact that the gradient $\partial\psi/\partial\mu$ is very large at the section where μ_u occurs, even a slight inclination should produce a reasonable reduction in the calculated energy consumption. According to FIG. 10.1d, it is decided here to reduce the moment from μ_u to 0.98 μ_u over the distance d. The fictitious moment curve OBC thus determined is used as the basis for calculation of the contribution of the tension reinforcement to the deformation energy.

The following may be noted with regard to the compression zone. According to figure c in FIG. 10.1a, the moment curve 2 for calculation of the state of affairs in the compression zone produces at the section where the formal plastic hinge occurs a moment which is less than the maximum moment μ_u; this is contrary to the equilibrium condition. However, it is evident from FIG. 10.1c that the concrete struts approaching the plastic hinge at an inclination are gradually relieved of load over a relatively short distance. It may therefore be expected that the strains in the compression zone will rapidly increase over this distance until, at the plastic hinge section, they attain a value corresponding to the moment μ_u. It is assumed here that this transition at a high strain gradient takes place over a region of the

selected length a/2, and that the contribution by the compression zone to the deformation energy can therefore be based on the fictitious moment curve OEC in FIG. 10.1d.

The fictitious moment curves OBC and OEC introduced here may be regarded as approximations to more correct curves which are probably of a continually variable curvature and pass between points O and C.

Application of these fictitious moment curves produces the conditions shown in FIG. 10.1e. This figure shows the fictitious moment curves μ_1 and μ_2 and the way in which the energy variation ψ_1 in the tension zone is transformed by means of the moment curve μ_1 of the tension zone into a corresponding energy variation over the length λ of the rotation span. In the same way, it is shown how the energy variation ψ_2 in the compression zone is transformed by means of the moment variation μ_2 in the compression zone. The vertically shaded area thus represents, for the rotation span, the total energy consumption within the tension zone, and the area with inclined shading represents the total energy consumption within the compression zone.

For the sake of simplicity, the derivation here has been based on a linear moment distribution over the rotation span. The reasons for this are as follows. According to Chapter 6, $\beta = 0.25$ represents a moment distribution at a plastic hinge in the span when the beam is acted upon by a uniformly distributed load. In this situation, the shear force is zero at the plastic hinge and small within the rotation span. This situation is therefore not appropriate in this context. For the other two moment distribution alternatives, $\beta = 0$ and $\beta = -0.06$, large shear forces can occur at the plastic hinge. However, from the calculation results set out in Chapter 7 it is evident that the difference between the values θ_u/λ calculated for $\beta = 0$ and $\beta = -0.06$ is insignificant. For this reason, only the case $\beta = 0$, i.e. linear moment distribution, is studied in the following.

The analytical expressions for the fictitious moment variations OBC and OEC in FIG. 10.1d, which are necessary for the calculation, are as follows.

According to the figure, for the tension zone

$$\mu = (1-0{,}02\,\frac{z}{d})\mu_u \qquad \text{för } z < a \qquad (10.1.1)$$

$$\mu = \frac{\lambda - \frac{z}{d}}{\lambda - \alpha}\,(1-0{,}02\alpha)\mu_u \qquad \text{för } a \le z \le l_o \qquad (10.1.2)$$

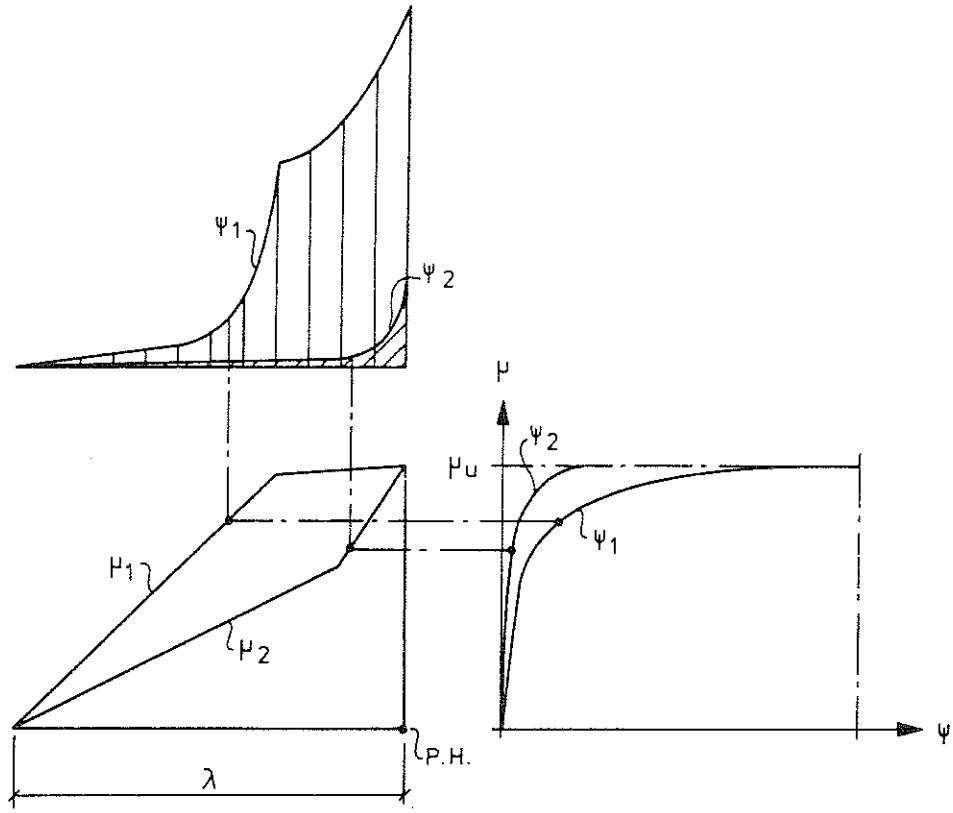

FIG 10.1e Transformations of the moment-energy curves by means of the moment curves μ_1 and μ_2. The distributions of ψ_1 and ψ_2 along the rotation span are obtained as a result.

where $\lambda = l_o/d$ and $\alpha = a/d$.

For the compression zone, similarly,

$$\mu = \frac{\lambda+\alpha-3\frac{z}{d}}{\lambda+\alpha}\mu_u \qquad \text{för } z < \frac{a}{2} \qquad (10.1.3)$$

$$\mu = \frac{\lambda-\frac{z}{d}}{\lambda+\alpha}\mu_u \qquad \text{för } \frac{a}{2} \le z \le l_o \qquad (10.1.4)$$

When the rotation span is divided into n equal parts according to FIG. 6.1a, with the subdivision points numbered from 0 to n, the expression for the moment μ_i at point No i is as follows for the moment curve in the tension zone:

$$\mu_i = (1-0{,}02\frac{\lambda}{n}i)\mu_u \qquad \text{för } i < \frac{\alpha}{\lambda}n \qquad (10.1.5)$$

$$\mu_i = \frac{1-i/n}{1-\alpha/\lambda}(1-0{,}02\alpha)\mu_u \qquad \text{för } \frac{\alpha}{\lambda}n \le i \le n \qquad (10.1.6)$$

and for the moment curve in the compression zone,

$$\mu_i = (1-\frac{3}{1+\alpha/\lambda}\frac{i}{n})\mu_u \qquad \text{för } i < \frac{1}{2}\frac{\alpha}{\lambda}n \qquad (10.1.7)$$

$$\mu_i = \frac{1-i/n}{1+\alpha/\lambda}\mu_u \qquad \text{för } \frac{1}{2}\frac{\alpha}{\lambda}n \le i \le n \qquad (10.1.8)$$

Equation (6.3.2) for calculation of the rotation capacity θ_u can now be modified, in view of the inclusion of the effect of shear force, by multiplication by λ which can no longer be isolated on the left-hand side of the equation since the μ - ψ relation has been made dependent on the value of λ. We thus have, with $\beta = 0$ substituted into Equation (6.3.2),

$$\theta_{uv} = \lambda(\frac{1}{\mu_u}\frac{\Sigma\psi_i}{n} - \frac{\kappa_n}{2n^2})\frac{2}{1+\mu_y/\mu_u} \qquad (10.1.9)$$

The symbol θ_u has now been augmented by the subscript v to indicate that the rotation capacity obtained in this way includes the effect of shear force.

10.2 The length of the yield region

What remains now is to choose an appropriate value of the moment shift a. It is reasonable to assume in this connection that a/d is proportional to the non-dimensional shear force V_n/N_c, where V_n is the constant shear force in the rotation span, see FIG. 6.1a. We therefore write

$$\frac{a}{d} = \kappa \frac{V_n}{N_c} \qquad (10.2.1)$$

or, since $M_u = l_o V_n$ and $M_c = dN_c$,

$$\alpha = \kappa \frac{\mu_u}{\lambda} \qquad (10.2.2)$$

In an extreme case, this relation yields $\alpha = 0$ for $\lambda = \infty$, which means that the moment shift is equal to zero when the shear force is zero.

An approximate value of the coefficient κ is determined as follows. The length a_y of the yield region is obtained according to figure c in FIG. 10.1a from the relation

$$a_y = \frac{\mu_y}{\mu_u} a + \frac{\mu_u - \mu_y}{\mu_u} l_o$$

or, in non-dimensional form,

$$\alpha_y = \frac{\mu_y}{\mu_u} \alpha + (1 - \frac{\mu_y}{\mu_u})\lambda \qquad (10.2.3)$$

Substitution of Equation (10.2.2) into this gives

$$\alpha_y = \kappa \frac{\mu_y}{\lambda} + (1 - \frac{\mu_y}{\mu_u})\lambda \qquad (10.2.4)$$

At the Department of Structural Engineering, Division of Concrete Structures, Chalmers University of Technology, experiments have been carried out concerning the rotation capacity of plastic hinges in reinforced concrete beams. In these tests observations were made regarding the extent of the yield region along the beam. For a few beams the determination was made with the aid of strain gauges attached to the tension reinforcement. For the other beams the determiantion was made more approximately by measuring the distance between the outermost large cracks in the tension zone level with the tension reinforcement. From these tests, 22 were chosen for assessment of the value of the coefficient κ.

The beams were simply supported and acted upon by a point load at the centre, i.e. the moment distribution corresponds to the case $\beta = 0$.

The beam data of interest in this context - type of reinforcement and the slenderness λ of the rotation span - are given in Table 10.2a together with the values of μ_y, μ_y/μ_u and $\alpha_{y,obs}$ measured during the tests. The latter

TABLE 10,2a Comparison of experimentally determined and calculated yield lengths

Beam	Reinforcement	λ	μ_y	μ_y/μ_u	$\alpha_{y,obs}$	$\alpha_{y,calc}$	$\alpha_{y,obs}/\alpha_{y,calc}$
902-1	Ks 40	11,0	0,150	0,944	0,83	0,75	1,10
-2	Ps 50	11,4	0,175	0,896	0,49	1,34	0,37
-3	Ks 80	10,8	0,121	0,949	0,54	0,66	0,81
-3A	Ks 60	10,9	0,141	0,943	1,27	0,75	1,69
-4	Ks 40	11,8	0,208	0,954	1,18	0,72	1,64
-5	Ps 50	11,9	0,218	0,935	0,99	0,96	1,03
-6	Ks 80	10,9	0,157	0,982	0,67	0,34	1,97
-6A	Ks 60	11,0	0,175	0,917	0,97	1,07	0,90
-7	Ks 40	5,8	0,239	0,722	1,54	2,02	0,76
-8	Ps 50	5,9	0,225	0,898	0,99	0,98	1,01
-13	Ks 60	9,1	0,065	0,788	1,64	2,00	0,82
-14	Ks 60	7,3	0,060	0,787	1,91	1,64	1,17
-15	Ks 60	5,5	0,061	0,769	1,83	1,38	1,33
-16	Ks 60	4,6	0,065	0,649	1,37	1,76	0,78
-17	Ks 60	3,7	0,057	0,675	1,23	1,36	0,91
-18	Ks 60	9,1	0,101	0,847	1,33	1,50	0,88
-19	Ks 60	7,4	0,124	0,885	0,94	1,02	0,92
-20	Ks 60	5,5	0,090	0,820	0,62	1,15	0,47
-21	Ks 60	4,6	0,107	0,862	1,31	0,87	1,51
-22	Ks 60	3,6	0,101	0,841	1,36	0,85	1,59
-23	Ks 60	9,2	0,190	0,971	0,86	0,47	1,88
-27	Ks 60	3,7	0,176	0,926	1,17	0,75	1,56

quantity refers to the observed non-dimensional length of the yield region determined as a mean value on each side of the plastic hinge.

The corresponding length $\alpha_{y,calc}$ of the yield region for the beams studied has been calculated from Equation (10.2.4) for different values of κ. The best agreement with the experimentally determined lengths was obtained for a value of κ approximately equal to 20.

If Equation (10.2.4) is studied with κ put equal to 20 in different extreme situations, it is found however that in certain cases the calculated length of the yield region is greater than λ. In order to avoid this, it has been decided here to put $\kappa = 10$. It must be pointed out that α_y, calculated from Equation (10.2.4), is only slightly dependent on the value of κ under normal circumstances.

The yield lengths $\alpha_{y,calc}$ calculated from Equation (10.2.4) with $\kappa = 10$, and the ratio $\alpha_{y,obs}/\alpha_{y,calc}$, are set out in the table. The mean value of the ratio is 1.14, with the coefficient of variation equal to 0.38. For large values of λ the effect of shear force on the rotation capacity is small - see Section 10.3 below. It is therefore interesting to compare the experimentally determined yield lengths with the calculated ones, particularly for small values of λ. Of the 22 beams studied here, 11 have a value of λ less than 8. For these 11 beams the mean value of the ratio $\alpha_{y,obs}/\alpha_{y,calc}$ is equal to 1.10, with the coefficient of variation equal to 0.33. The agreement may be considered acceptable in view of the way in which the length of the yield region was determined in the experimental investigations.

The expression (10.2.2) can then be written as

$$\alpha = 10 \frac{\mu_u}{\lambda} \qquad (10.2.5)$$

This expression is used for calculation of the moment shift in Equations (10.1.5) - (10.1.8).

10.3 Calculation results

Using the computer program as augmented by the modified model developed in Section 10.1, the rotation capacity θ_{uv} is now calculated for some material combinations, for values of λ varying between 2 and 10. The first calculation relates to HR steel and concrete type B. The beam is assumed to have no compression reinforcement. The results are set out in FIG. 10.3a. FIG. 7.1a

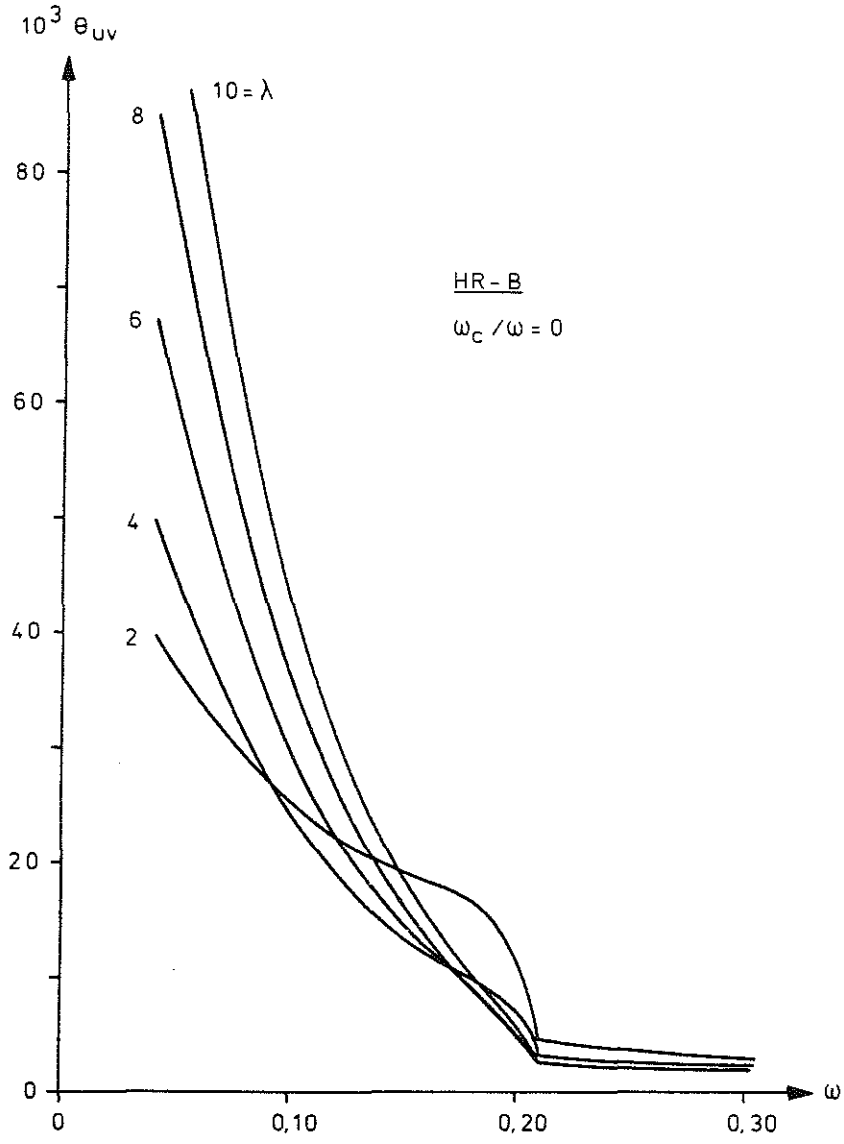

FIG 10.3a Rotation capacity θ_{uv} for a plastic hinge reinforced with HR steel calculated with the effect of shear force taken into consideration. The figure relates to a section without compression reinforcement.

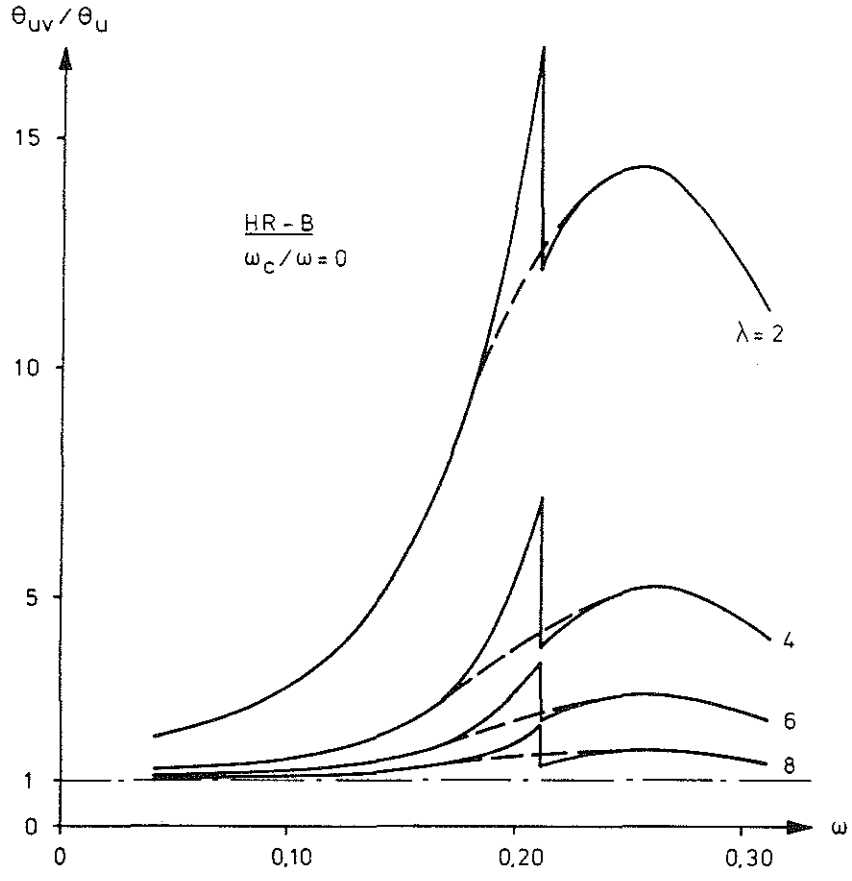

FIG 10.3b Comparison of the values of the rotation capacity for a plastic hinge with HR steel, obtained when the calculations consider (θ_{uv}) and do not consider (θ_u) the effect of shear force. The comparison relates to a section without compression reinforcement.

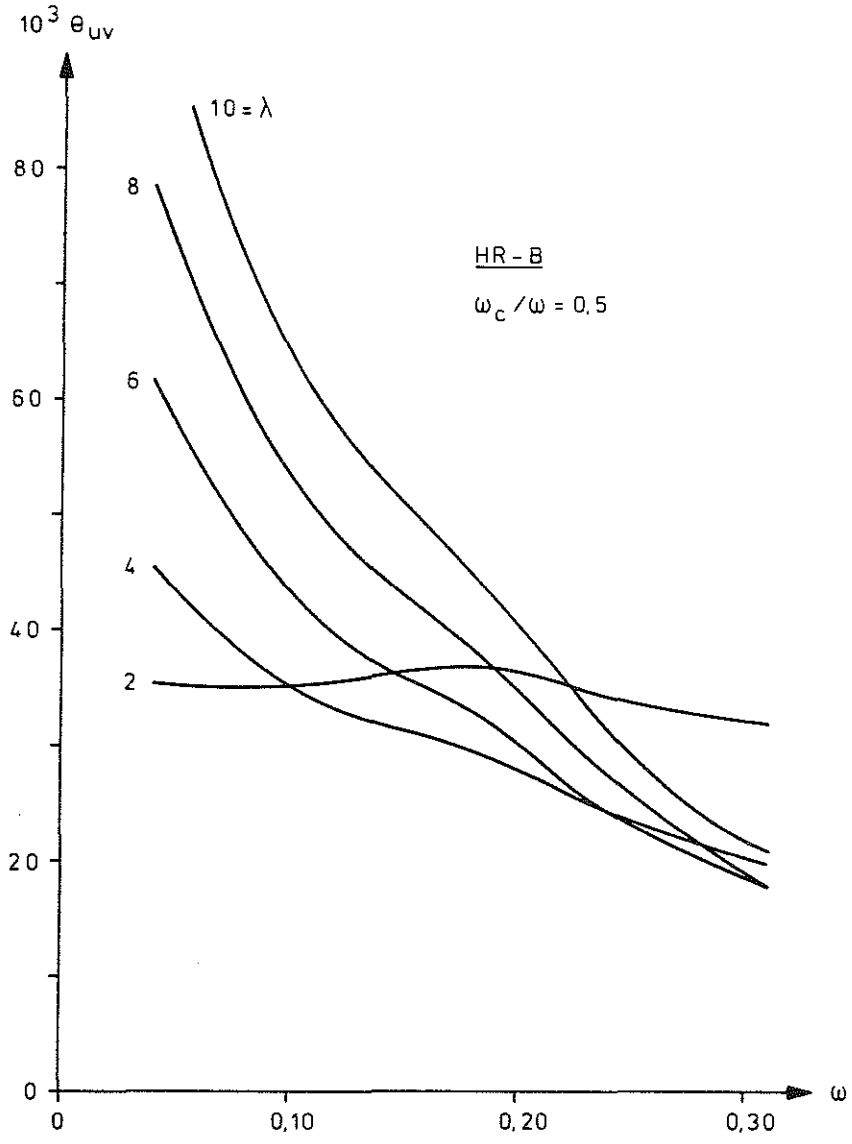

FIG 10.3c Rotation capacity θ_{uv} for a plastic hinge reinforced with HR steel calculated with the effect of shear force taken into consideration. The figure relates to a section with compression reinforcement characterised by $\omega_c/\omega = 0.5$.

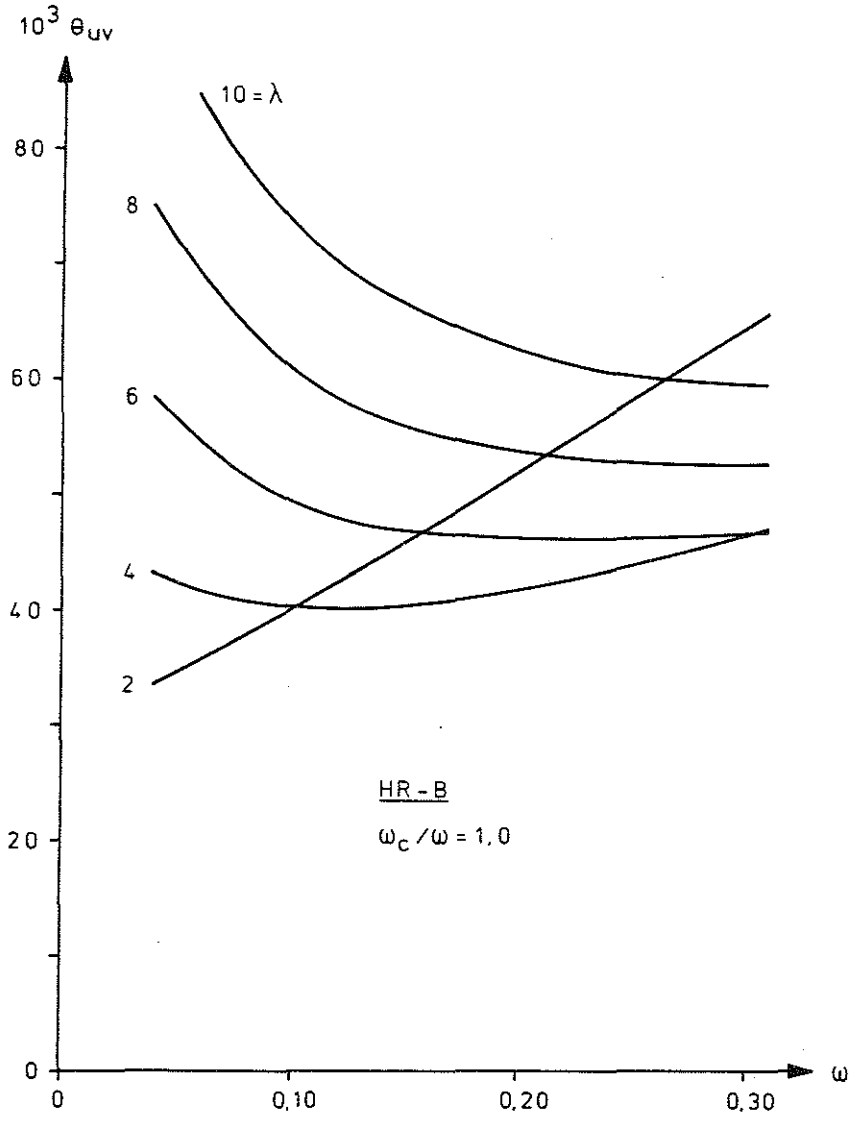

FIG 10.3d Rotation capacity θ_{uv} for a plastic hinge reinforced with HR steel calculated with the effect of shear force taken into consideration. The figure relates to a section with compression reinforcement characterised by ω_c/ω = 1.0.

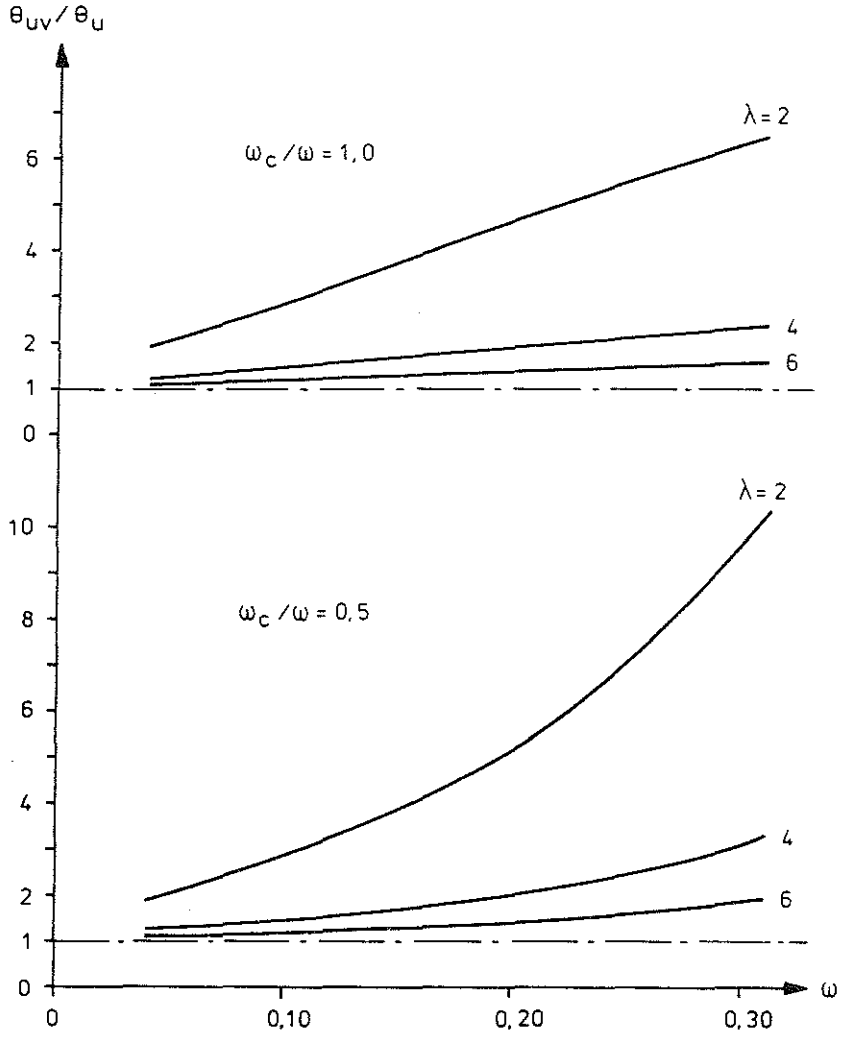

FIG 10.3e Comparison of the values of the rotation capacity for a plastic hinge with HR steel, obtained when the calculations consider (θ_{uv}) and do not consider (θ_u) the effect of shear force. The comparison relates to a section with compression reinforcement characterised by ω_c/ω = 0.5 and 1.0.

($\beta = 0$) shows the results of a corresponding calculation performed under the same conditions, but with the effect of shear force ignored. The two figures cannot be compared directly as one shows θ_{uv} and the other θ_u/λ. However, the curve for θ_u/λ can be multiplied by the fixed value of λ and the ratio θ_{uv}/θ_u can then be formed which gives an idea of the effect of shear force. For the example in question this yields the results set out in FIG. 10.3b. The peaks which the curves exhibit occur at ω_{cr} where the θ curves change direction. It is not very likely that, in actual fact, the peak is as pronounced as it appears in the figure. It is probable that some equalisation can be expected in the region around ω_{cr}, as indicated by the dashed lines in the figure. As will be seen, the effect of shear force is a function of ω. As ω increases, the effect increases up to $\omega = 0.26$, after which it again decreases.

In order to find an explanation for the fact that there is a maximum value for the effect of shear force, it is necessary to study the detailed calculations. The following can be seen from these. As ω increases, so does the ultimate moment μ_u, and this means, according to Equation (10.2.5), that α and thus, according to Equation (10.2.3), the extent α_y of the yield region also increase. On the other hand, at the same time the ratio μ_y/μ_u approaches the value 1.0 asymptotically. According to Equation (10.2.3) this means that α_y decreases as ω increases. For $\omega < 0.26$ one of these effects is dominant, and for $\omega > 0.26$ the other, and therefore a maximum can occur. It is also evident from FIG. 10.3b that the value of the ratio θ_{uv}/θ_u increases as λ decreases, i.e. as the shear force increases.

Corresponding calculations for the combination HR steel and concrete type B have also been performed for a section with compression reinforcemnt. For $\omega_c/\omega = 0.5$ and $\omega_c/\omega = 1.0$ the results are set out in FIG. 10.3c and 10.3d respectively. It is evident from these figures that the effect of shear force is considerable for short rotation spans. It is seen that, for $\lambda = 2$ and $\omega_c/\omega = 0.5$, the rotation capacity remains practically constant as ω increases, and that for $\lambda = 2$ and $\omega_c/\omega = 1.0$ it even increases as ω increases. A comparison of the rotation capacities calculated with and without shear force is made for these cases in FIG. 10.3e. It is seen in this figure also that the effect decreases as the value of λ increases, and increases as the value of ω increases.

Analogous calculations for CW steel in combination with concrete type B are shown in FIG. 10.3f for $\omega_c/\omega = 0$, $\omega_c/\omega = 0.5$ and $\omega_c/\omega = 1.0$. In this case the effect of shear force is relatively large, which is perhaps not directly evident from the figure, but will be seen if the associated ratio

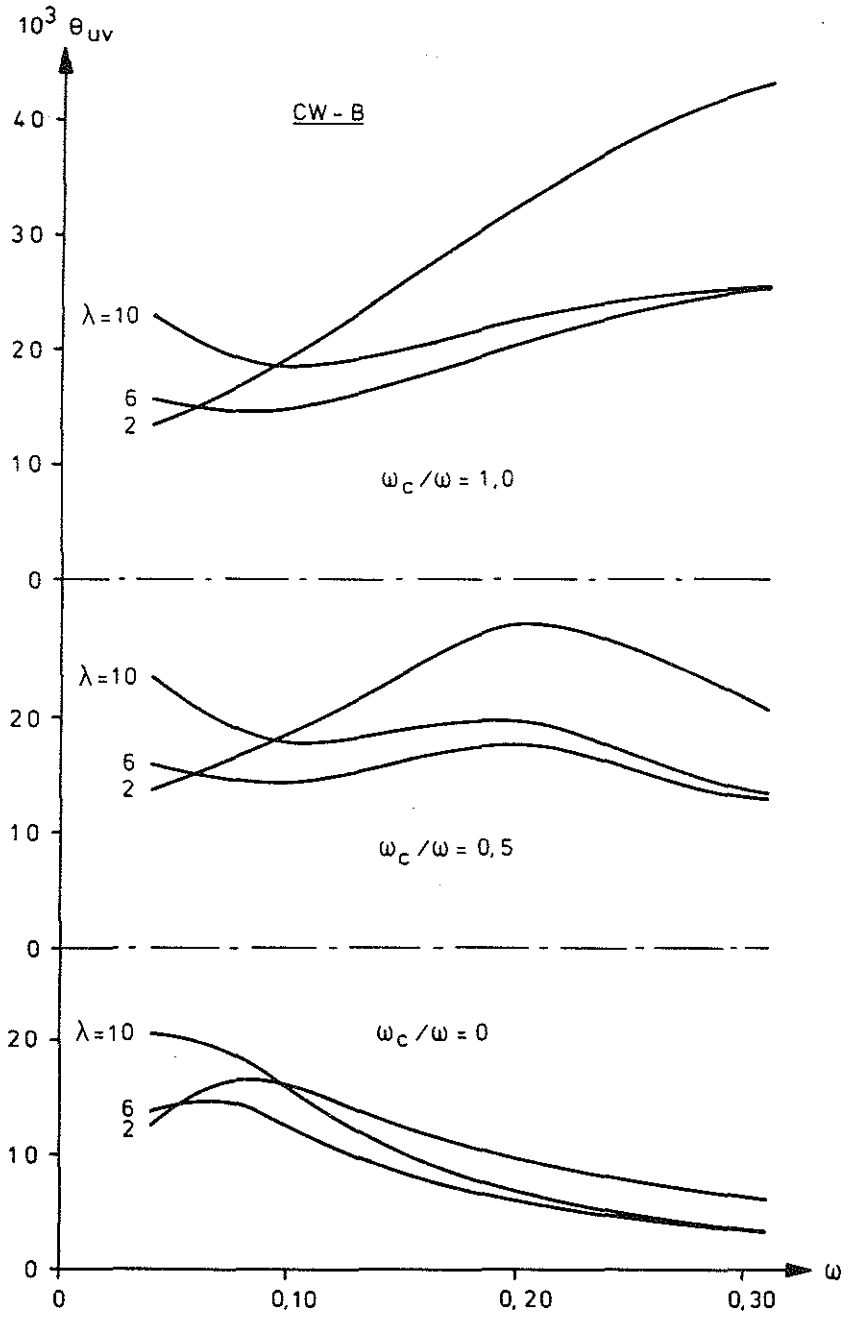

FIG 10.3f Rotation capacity θ_{uv} for a plastic hinge reinforced with CW steel calculated with the effect of shear force taken into consideration. The figure relates to a section with variable amounts of compression reinforcement.

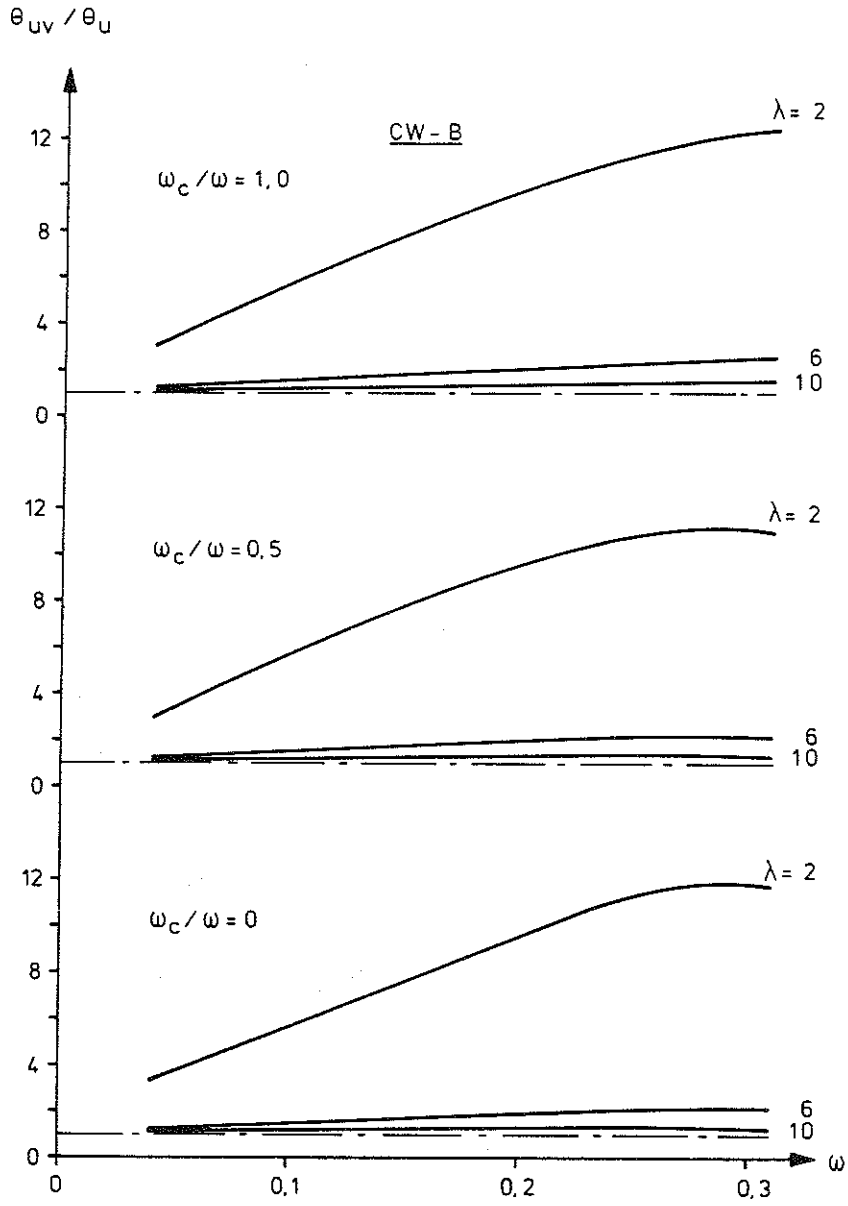

FIG 10.3g Comparison of the values of the rotation capacity for a plastic hinge with CW steel, obtained when the calculation consider (θ_{uv}) and do not consider (θ_u) the effect of shear force. The comparison relates to a section with variable amounts of compression reinforcement.

θ_{uv}/θ_u, which is plotted in FIG. 10.3g, is studied.

It is evident from the studied worked examples that the analytical model constructed yields results in good agreement with those to be expected in view of previous experimantal experiences.

11 THE EFFECT OF STIRRUPS

It is known from the literature that the presence of stirrups in the beam in the vicinity of a plastic hinge has the effect of raising the rotation capacity. This effect is primarily due to the fact that the stirrups hold together the concrete in the compression zone in the stress interval μ_y to μ_u. It is in consequence possible for compressive strains several times higher than the ultimate strain of the unreinforced concrete to occur without splitting of the concrete in the compression zone.

Tests on concrete surrounded by stirrups and subjected to compressive stresses show that the presence of stirrups affects the stress-strain diagram of the concrete in different respects. Both the ultimate compressive strain ε_{cu} and the limit strain ε_o corresponding to the maximum compressive stress are increased, the latter more moderately. The compressive strength f_{cc} of the concrete and the stress corresponding to the ultimate strain ε_{cu} are also raised. Taken together, the effect is that the area bounded by the stress-strain diagram increases owing to the application of stirrups, which in turn means that the ability of the compression zone to store deformation energy is enhanced. In particular, the fact that ε_{cu} increases also means that the tension reinforcement can develop a larger strain before crushing failure of the concrete occurs. The deformation energy of the tension reinforcement also increases in consequence. The use of stirrups thus results in a total increase in the capacity of the concrete to store deformation energy within the volume of the rotation span, which gives the plastic hinge a higher rotation capacity as most of the increment in energy consumption is of an irreversible nature.

In the following, a method whereby the previously constructed analytical model can be extended so as to take into account the effect of stirrups will be developed semi-empirically.

11.1 Phenomenological discussion

The magnitudes of the above parameters which determine the stress-strain curve of the concrete are functions of the extent of stirrup reinforcement, i.e. the dimension, strength and spacing of the stirrups and the strength of the surrounded concrete. The way one set of parameters is dependent on the other is unknown at present. It is therefore necessary to group together a number of parameters in a reasonable manner so as to constitute a single parameter which is then used as a measure of the extent of the effect due to the stirrups.

The effective reinforcement ratio of the stirrups, defined by the expression

$$\omega_v = \frac{A_{sv}}{bs} \frac{f_{sv}}{f_{ct}} \qquad (11.1.1)$$

is used as the governing parameter, where

A_{sv} = cross sectional area of one stirrup bar
f_{sv} = tensile strength of the steel in the stirrup
b = width of the compression zone
s = stirrup spacing
f_{ct} = tensile strength of concrete

That the selected parameter combination is a reasonable one will be evident from the following. The stirrups have the effect of holding together the concrete in the compression zone which, under the influence of large compressive stresses in the axial direction, expands in the transverse direction. When the stirrups are rectangular in shape, the counterbalancing forces can principally be developed at the corners of a stirrup. This effect should therefore decrease with increasing distance between the two interacting corner forces, i.e. for the usual stirrup shape with increasing width b. The maximum magnitude of the corner forces is directly proportional to both A_{sv} and f_{sv}, and the maximum corner force per unit length of beam is inversely proportional to the stirrup spacing s. Immediately prior to crushing failure of the concrete, this disintegrates while undegoing transverse expansion. This transverse expansion cannot take place without the formation of a large number of microcracks in the concrete in the compression zone. It is therefore probable that the tensile strength of concrete is a more significant parameter in this context than the compressive strength.

It is assumed in the following that the stirrup effect is a function only of the parameter ω_v.

In order to exemplify the above, let us first calculate the rotation capacity for a beam with $\omega_v = 0$, i.e. for a beam without stirrup reinforcement. The beam is assumed to be of concrete type B, see FIG. 11.1a, in combination with both CW steel and HR steel. The beam is then assumed to be provided with stirrup reinforcement corresponding to a value ω_{v1}, and as a result the stress-strain curve of the concrete in the compression zone is assumed to change to the curve marked B1 in FIG. 11.1a. The rotation capacity is calculated for this curve. Finally, it is assumed that stirrup reinforcement

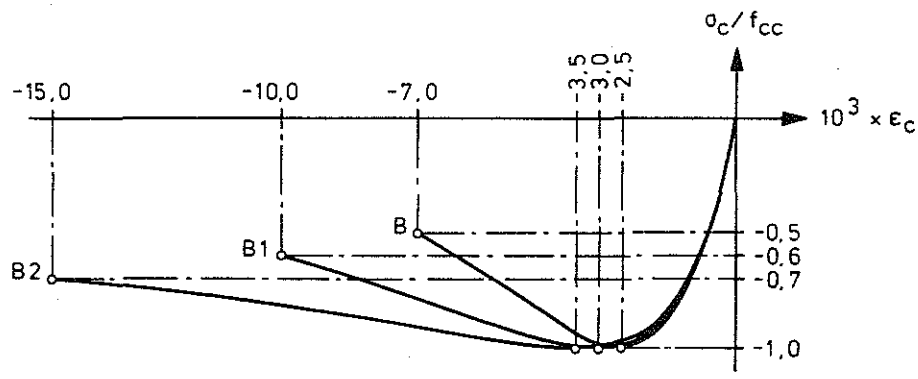

FIG 11.1a Stress-strain curve for concrete type B in compression, and two modified stress-strain curves B1 and B2.

with $\omega_{v2} > \omega_{v1}$ is applied, the stress-strain curve of the concrete being assumed to change to curve B2 in the figure, and the corresponding rotation capacity is calculated. Unfortunately, we do not know the relationship between the values ω_{v1} and ω_{v2} on the one hand, or between curves B1 and B2 on the other. We can thus assume only that the greater the value of ω_v, the larger also will be the area bounded by the stress-strain diagram. The results of calculation are set out in FIG. 11.1b. It is evident from the families of curves obtained that, within each such group, the curves B_1 and B_2 can be approximately obtained from curve B by changing the scale along the horizontal axis. This implies that both curves B1 and B2 can be changed back into curve B, i.e. the curve representing the beam with no stirrup reinforcement, by converting the actual value of ω for the beam with stirrups into a fictitious value ω_{fic} relating to curve B. This conversion is performed by division by some expression which is a function of ω_v. We can therefore write

$$\omega_{fic} = \frac{\omega}{f(\omega_v)} \qquad (11.1.2)$$

The requirement for the function $f(\omega_v)$ is that it must assume the value 1 for $\omega_v = 0$, and increase with increasing value of ω_v. In view of all the other factors of uncertainty, there is no point in selecting a very complicated expression for this function. The expressions

$$f(\omega_v) = 1+\kappa_1\omega_v \qquad (11.1.3)$$

$$f(\omega_v) = (1+\kappa_2\omega_v)^2 \qquad (11.1.4)$$

$$f(\omega_v) = 1+\kappa_3\omega_v^2 \qquad (11.1.5)$$

will be tested in the following, where κ_1, κ_2 and κ_3 are assumed to be non-dimensional constants which must be determined from the test results reported in the literature.

11.2 The tests of Mattock and Corley

A large number of tests concerning the rotation capacity of plastic hinges are described in the literature. From these, the reports published by Mattock (1965) and Corley (1966) have been selected. These test series are relatively comprehensive and supplement one another, and in addition the results are reported in such a way that all the information required for this investigation is clearly set out. All the tests performed by Mattock and Corley for which the measured rotation capacities are reported relate to simply supported beams over one span acted upon by a point load at the

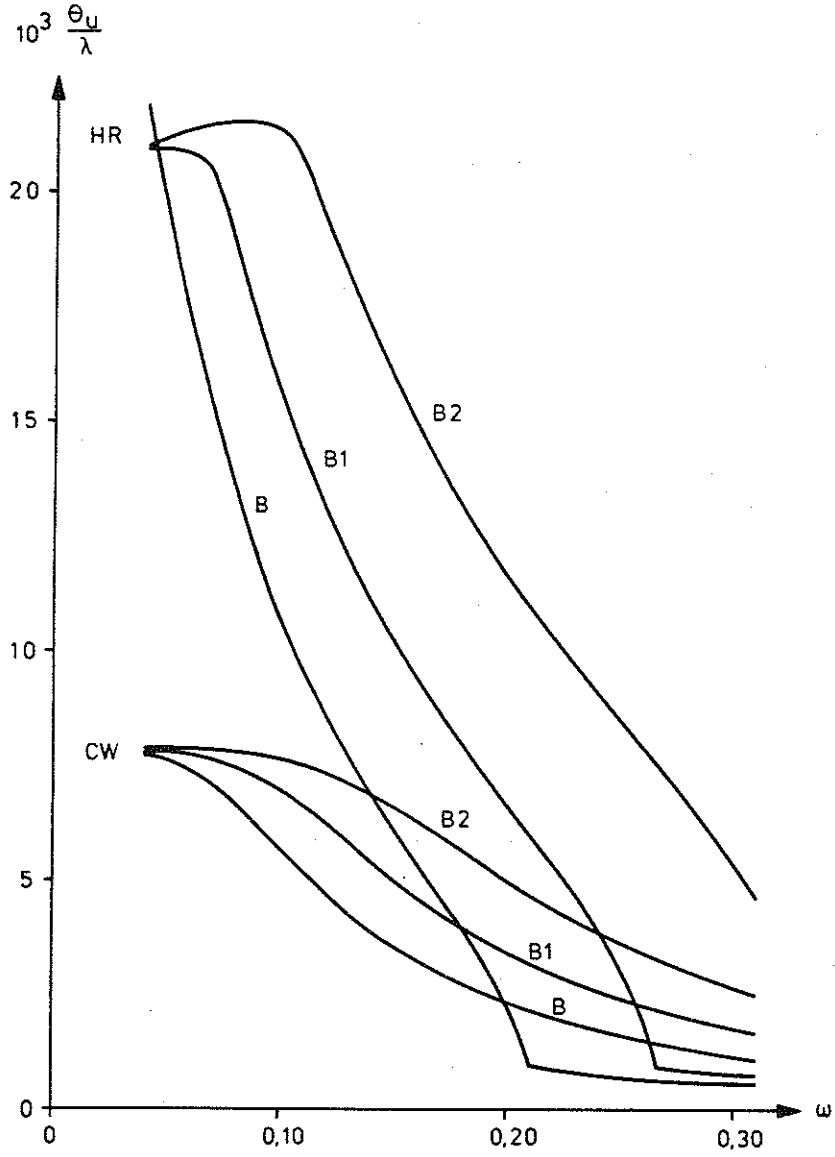

FIG 11.1b Rotation capacity calculated for a beam reinforced with CW steel and HR steel in combination with concrete types B, B1 and B2 according to FIG 11.1a.

midpoint of the beam. Mattock's series comprises 31 beams, and that of Corley 40. A total of 71 beams have therefore been studied, the parameters of interest being varied over wide limits. The effective depth d of the beam is thus varied between 5" and 30" (127-762 mm), the width b of the beam between 3" and 12" (76-305 mm), and the slenderness λ between 2.75 and 11 . The cylinder strength of the concrete is between 3400 and 6200 psi (23-43 MPa), and the yield stress of the tensile reinforcement varies between 45 and 80 ksi (310-550 MPa). The effective reinforcement ratio for the tension reinforcement covers the range $\omega = 0.11$ to $\omega = 0.57$, which is combined with compression reinforcement corresponding to the range $\omega_c = 0.01$ to $\omega_c = 0.33$.

What is of the greatest interest in this context is the large variation in stirrup reinforcement covered by these tests. Reinforcing steel of dimensions 1/4", 3/8" and 1/2" (6.4, 9.5 and 12.7 mm) and of grades indicated by yield stresses ranging from 49 to 80 ksi (340-550 MPa) has been used. The stirrup spacing varies between 1.25" and 15" (32-381 mm). The effective reinforcement ratio ω_v for the stirrups, calculated from Equation (11.1.1), thus varies from 0.14 to 2.32. In determining ω_v, the tensile strength of concrete has been calculated from the expression

$$f_{ct} = 4{,}52 \sqrt{f_{cc}} \qquad (11.2.1)$$

where both f_{cc} and f_{ct} are in psi.

For the beams in Mattock's and Corley's test series the rotation capacity has been calculated by means of the program developed here, account being taken of the extent and position of the compression reinforcement and of the effect of shear force, the latter according to the analytical model developed in Chapter 10. Concrete type B was assumed in the calculations, while for the tension and compression reinforcement the actual stress-strain diagrams applicable to the steels concerned were used. The calculated relation between ω and θ_{uv} has been plotted for all the beams. Two calculated curves, one relating to beams B1 and D1 and one relating to beams B2 and D2 according to the notation used by Mattock, are shown in FIG. 11.2a as examples. Using the rotation capacities measured in the tests as initial values, corresponding values of the fictitious effective reinforcement ratio ω_{fic} are obtained from the curves, see FIG. 11.2a. The ratio of the actual ω to the value of ω_{fic} obtained as above gives a value of the function $f(\omega_v)$ according to Equation (11.1.2). Once the value of ω_v is known for each beam, the coefficients κ_1, κ_2 and κ_3 can then be calculated for each beam by means oc Equations (11.1.3), (11.1.4) and (11.1.5). Since it is assumed that κ_1, κ_2 and κ_3

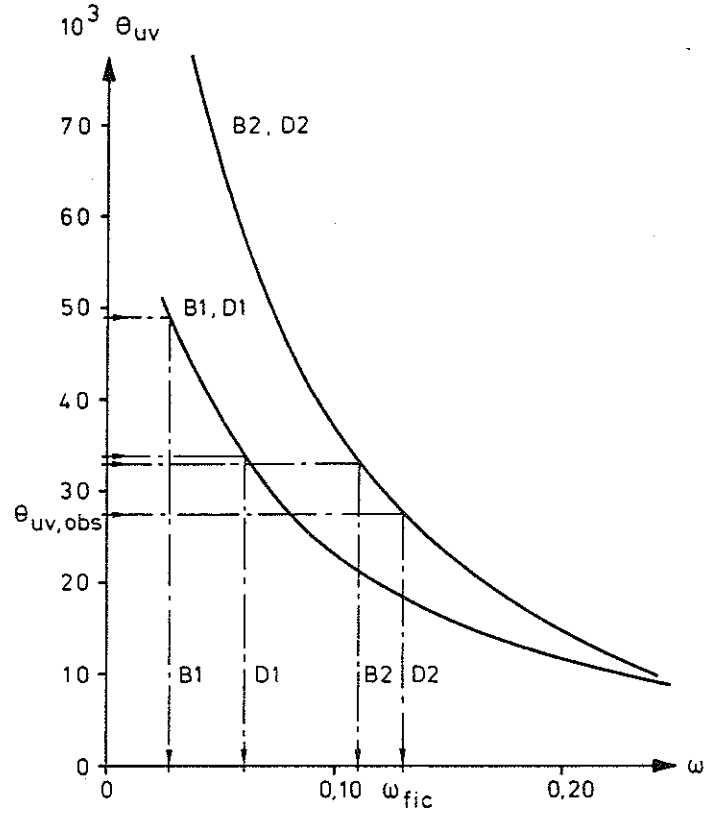

FIG 11.2a θ_{uv} - ω curves calculated for beams B1, D1, B2 and D2 in Mattock's test series. The experimentally determined value of the rotation capacity, $\theta_{uv,obs}$, gives the value of ω_{fic} by means of the curve relating to the test.

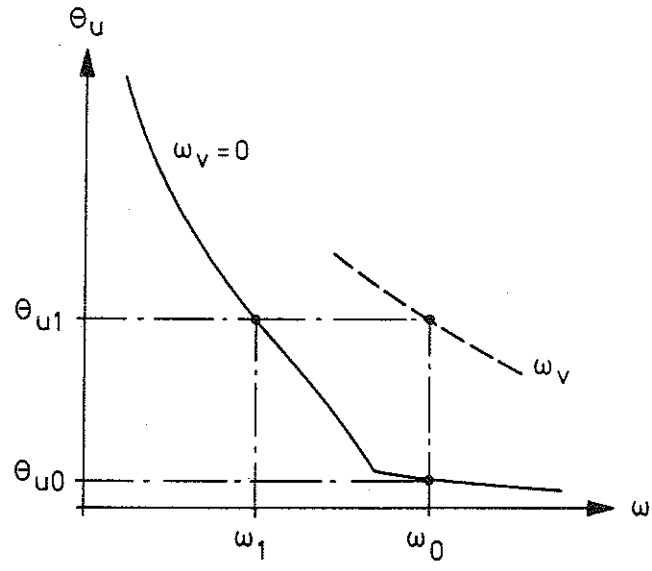

FIG 11.2b The appropriate value of the effective reinforcement ratio ω_o gives the rotation capacity θ_{uo} for a section without stirrup reinforcement. When the section is provided with stirrup reinforcement, ω_o is transformed into ω_1, and as a result the rotation capacity increases to θ_{u1}.

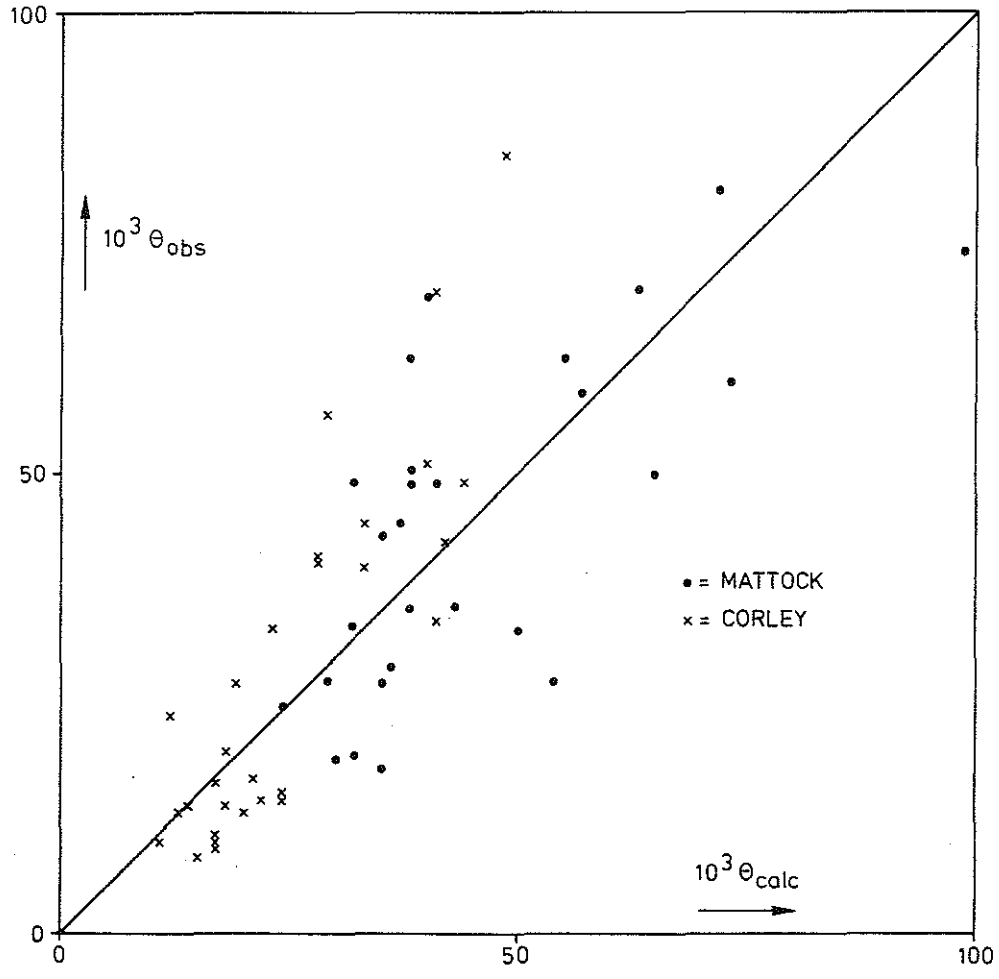

FIG 11.2c Comparison of the calculated rotation capacities and those determined by the tests of Mattock and Corley.

are constants, they can be determined as the means of the individual values calculated from the test material in the way described above. Of the suggested expressions (11.1.3), (11.1.4) and (11.1.5), the one which exhibits the least scatter with respect to the mean is then selected. Such an analysis performed on the present test material verifies expression (11.1.4) as the best. This expression yields the value $\kappa_2 = 1.31$ when all 71 tests are included. When seven extreme values are removed, the mean for the remaining 64 beams is $\kappa_2 = 0.97$. The approximation $\kappa_2 = 1.0$ is chosen. Equations (11.1.2) and (11.1.4) then yield the relation

$$\omega_{fic} = \frac{\omega}{(1+\omega_v)^2} \qquad (11.2.2)$$

Calculation of the rotation capacity with respect to the effect of the stirrup reinforcement can now be carried out as follows, see FIG. 11.2b. The plastic hinge is assumed to have the actual effective reinforcement ratio ω_0. Without stirrup reinforcement, the rotation capacity θ_{uo} is thus obtained by means of a curve for $\omega_v = 0$, calculated by means of the computer program. With stirrup reinforcement corresponding to ω_v, the rotation capacity θ_{u1} for ω_0 would be obtained by means of the dashed curve. The method adopted in practice is to convert ω_0 to $\omega_1 = \omega_{fic}$ by means of Equation (11.2.2), and to obtain the sought rotation capacity θ_{u1} from the curve relating to $\omega_v = 0$.

That it is functionally correct to adopt the above procedure is confirmed by the following. The way the stress-strain curve of the concrete increases in deformation capacity for increasing ω_v is indicated in FIG. 11.1a. What this figure, which is non-dimensional, does not show is that f_{cc} also increases for increasing ω_v. An increase in f_{cc} implies a reduction in ω, which corresponds to some of the shift in the curve shown in FIG. 11.2b.

The power 2 in expression (11.2.2) for the scale factor $f(\omega_v)$ can be explained by the dual effect of the stirrup reinforcement. Surrounding of the concrete increases not only f_{cc} but also ε_{cu}, and the latter increase also results in an increase in rotation capacity, which in calculations according to the proposed method is taken into account by further reduction of ω.

As mentioned above, the calculation procedure developed has been systematically applied to the tests of Mattock and Corley. The measured rotation capacities θ_{obs} were then compared with the calculated rotation capacities θ_{calc} by means of the ratio $\theta_{obs}/\theta_{calc}$. In the investigation a number of test results were rejected. These related to tests which exhibited such extreme discrepancies from the general trend that there was justification to suspect a measuring

error or some other procedural error. Mattock and Corley themselves report difficulties in measurement. Two tests from Mattock's series, and 11 tests from Corley's series, have been omitted. The remaining tests yield the following results.

For Mattock's tests, the mean value of 29 values of $\theta_{obs}/\theta_{calc}$ = 0.97, with the coefficient of variation = 0.35.

For Corley's tests, the mean value of 29 values of $\theta_{obs}/\theta_{calc}$ = 1.08, with the coefficient of variation = 0.40.

For all the 58 tests analysed, the mean value of $\theta_{obs}/\theta_{calc}$ = 1.03, with the coefficient of variation = 0.38.

The comparative calculation performed is shown in detail in FIG. 11.2c. The validity of the results obtained must be judged in view of the fact that in these test series the value of ω_v varies over very wide limits, viz. between 0.14 and 2.32.

12 DISCUSSION OF THE SAFETY ASPECT

The following discussion relates to the safety philosophy advocated by the CEB (1976). In principle, it is the same philosophy as that on which the Swedish "General regulations for loadbearing structures" (AK 77) and "Regulations for concrete structures" (BBK 77) are based.

According to the CEB, the ultimate limit state due to a bending moment is to be checked by comparing the ultimate moment with the bending moment capacity of the section concerned. Determination of the bending moment capacity is to be based on the design compressive strength f_{cc} of the concrete and the design tensile strength f_{st} of the reinforcement. In turn, these design strengths are to be obtained from the characteristic strengths f_{cck} and f_{stk} respectively of the materials, defined in a certain manner, by dividing these by partial coefficients. The following expressions apply

$$f_{cc} = \frac{f_{cck}}{\gamma_c} \tag{12.1}$$

where γ_c is the partial coefficient for concrete in compression, and

$$f_{st} = \frac{f_{stk}}{\gamma_s} \tag{12.2}$$

where γ_s is the partial coefficient for reinforcement in tension.

An analogous procedure should be applicable when a deformation characteristic is studied. The rotation capacity of a plastic hinge is essentially determined by the strain capacities of the steel and concrete, and it therefore appears reasonable to apply the factors of safety to these. We therefore assume that the characteristic ultimate strain ε_{suk} of the reinforcement and the characteristic ultimate compressive strain ε_{cuk} of the concrete are quantities defined in a certain manner, and determine the corresponding design values from these. We thus have

$$\varepsilon_{cu} = \frac{\varepsilon_{cuk}}{\gamma_c} \tag{12.3}$$

and

$$\varepsilon_{su} = \frac{\varepsilon_{suk}}{\gamma_s} \tag{12.4}$$

In principle, the partial coefficients relating to ultimate strains should be chosen in view of the appropriate scatter characteristics of these strains. For the sake of simplicity, however, in the following calculations the partial

coefficients relating to strains are given the same values as those relating to the corresponding strengths.

The deformation limit state considered here occurs when $\theta_r = \theta_u$, i.e. when the design value of the rotation requirement attains the design value of the rotation capacity. It is therefore of interest to see how the operations (12.3) and (12.4) affect the design value of the rotation capacity. The following comparative calculations are therefore made.

Since the CEB proposes that the ultimate compressive strain of concrete is to be taken as $\varepsilon_{cuk} = -0.0035$, the calculations are made using concrete type A. The value quoted is considered to be a characteristic value. If the partial coefficient $\gamma_c = 1.5$ is selected, the corresponding design value is $\varepsilon_{cu} = -0.0035/1.5 = -0.0023$.

For reinforcement of HR steel, the characteristic value of the ultimate strain is taken to be $\varepsilon_{suk} = 0.100$. If the partial coefficient $\gamma_s = 1.2$ is chosen for steel, then the design value of the ultimate strain is $\varepsilon_{su} = 0.100/1.2 = 0.083$. The characteristic value of the ultimate strain of CW steel is assumed to be $\varepsilon_{suk} = 0.065$, and the design value is therefore $\varepsilon_{su} = 0.065/1.2 = 0.054$.

Calculations made with HR and CW steels combined with concrete type A yield the results set out in FIG. 12a and b. The calculations are made using both the characteristic values and the design values of the ultimate strains of the steel and concrete. The results relate to moment distribution along the rotation span determined by $\beta = 0.25$, and to a cross section without compression reinforcement. For the sake of completeness, FIG. 12c and d give the results of corresponding calculations relating to cross section with compression reinforcement to an extent determined by $\omega_c/\omega = 0.5$.

The figures show the way in which the ratio θ_u/χ decreases from a characteristic to a design value when partial coefficients are applied to the strain capacities of the steel and concrete.

It is evident from the printouts that it is only the ultimate compressive strain of the concrete which determines the rotation capacity in the cases studied. In no case has the ultimate strain of the steel been reached. Application of the partial coefficient $\gamma_s = 1.2$ has therefore had no effect at all on the design value of the rotation capacity, and may just as well have been omitted in the cases studied.

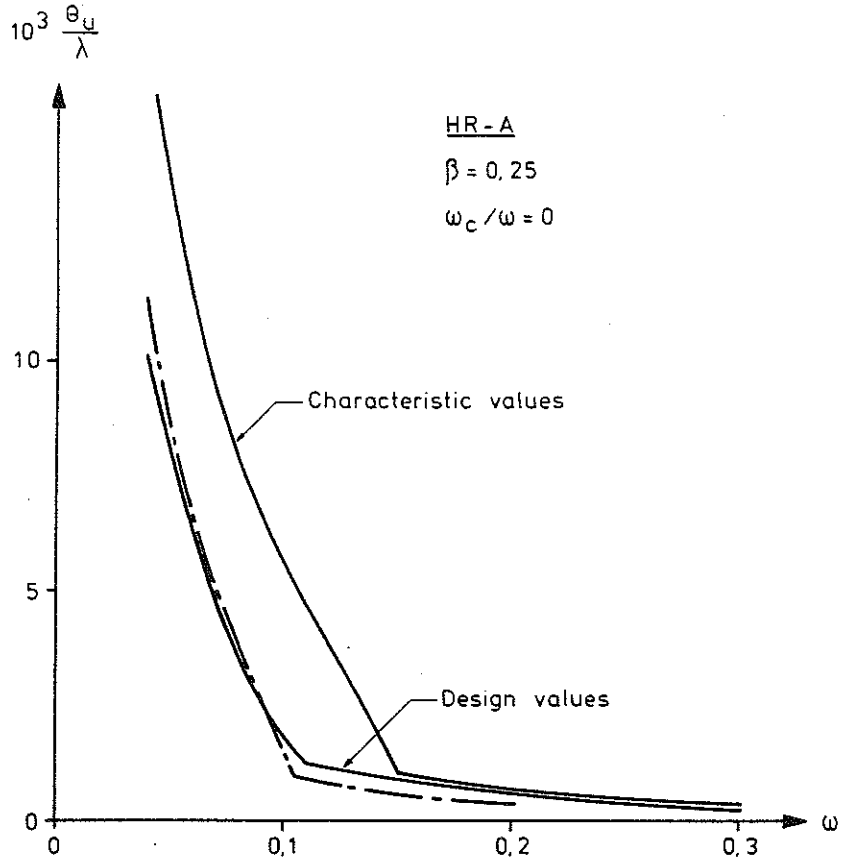

FIG 12a Values of the rotation capacity calculated on the basis of the characteristic and design values of the ultimate strains of the steel and concrete. The figure relates to a section with tension reinforcement of HR steel, and without compression reinforcement.

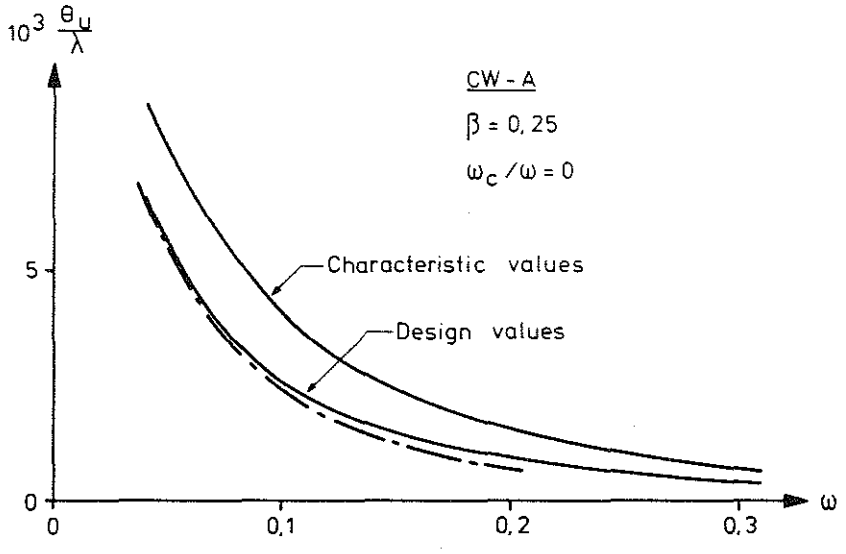

FIG 12b Values of the rotation capacity calculated on the basis of the characteristic and design values of the ultimate strains of the steel and concrete. The figure relates to a section with tension reinforcement of CW steel, and without compression reinforcement.

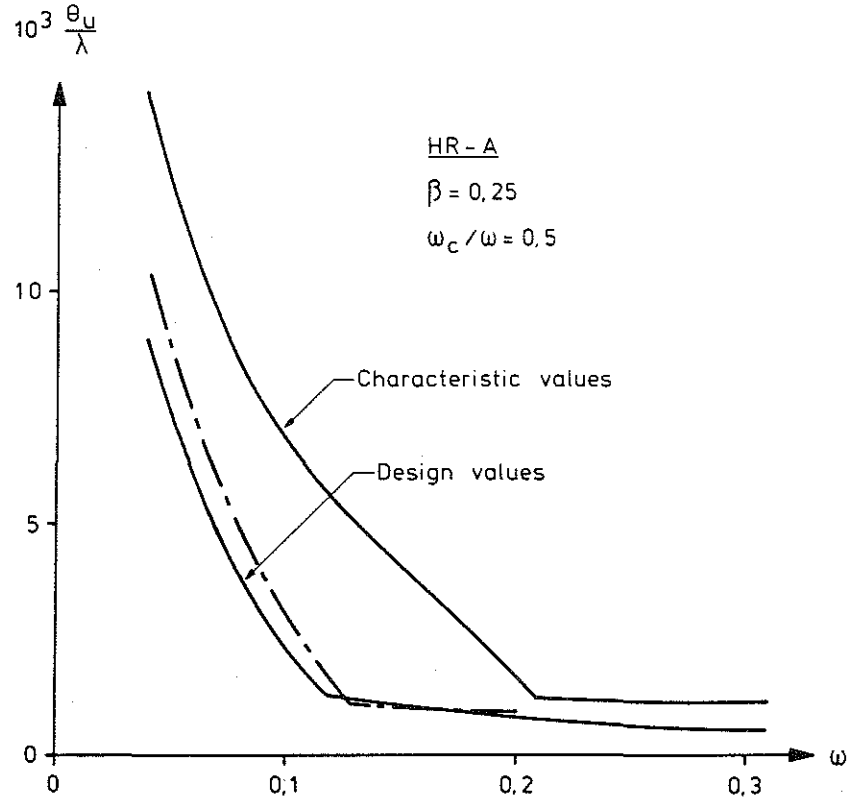

FIG 12c Values of the rotation capacity calculated on the basis of the characteristic and design values of the ultimate strains of the steel and concrete. The figure relates to a section reinforced with HR steel, and with compression reinforcement represented by $\omega_c/\omega = 0.5$.

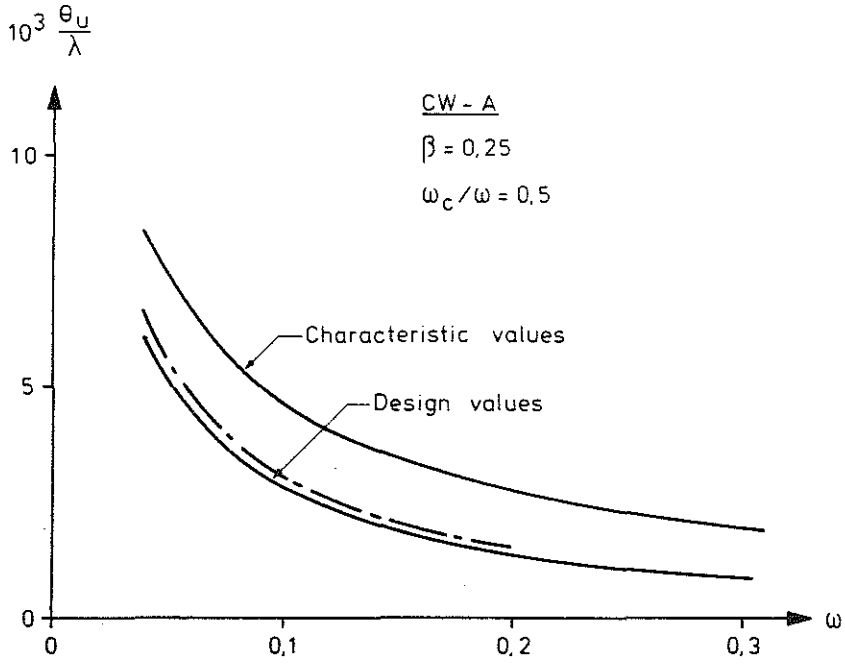

FIG 12d Values of the rotation capacity calculated on the basis of the characteristic and design values of the ultimate strains of the steel and concrete. The figure relates to a section reinforced with CW steel, and with compression reinforcement represented by ω_c/ω = 0.5.

In practice, it would be an advantage if the curves relating to the rotation capacity could be calculated from the characteristic ultimate strains and the factor of safety instead applied to ω, i.e. by replacing the characteristic strengths by the design strengths when ω is calculated. This would give rise to the expression

$$\omega_d = \rho \frac{f_{st}}{f_{cc}} = \rho \frac{f_{stk}}{f_{cck}} \frac{\gamma_c}{\gamma_s} = \omega_k \frac{\gamma_c}{\gamma_s} \qquad (12.5)$$

where ω_d is the design value of ω and ω_k the corresponding characteristic value.

In view of the fact that in the cases studied, and probably also in ordinary practical cases, γ_s has no effect on the design value of the rotation capacity, it should be possible to simplify Equation (12.5) to

$$\omega_d = \gamma_c \omega_k \qquad (12.6)$$

Expression (12.6) implies a change of scale in relation to the ω axis, with γ_c as the scale factor. This hypothesis is checked for $\omega_c/\omega = 0$ by changing the scale of the curves in FIG. 12a and b dividing ω by $\gamma_c = 1.5$. The curves shown by chain lines in the figures are obtained in this way. These are practically completely coincident with the full lines based on the design strains of the steel and concrete when $\omega_c/\omega = 0$.

For the sake of consistency, the characteristic value of the ratio $\omega_c/\omega_k = (\omega_c/\omega)_k$ for a section with compression reinforcement should be replaced by its design value

$$(\omega_c/\omega)_d = \omega_c/\omega_d = \omega_c/\gamma_c\omega_k = (\omega_c/\omega)_k/\gamma_c \qquad (12.7)$$

For the case studied, this implies that the curve relating to the design value of the rotation capacity is obtained by the above change in scale in relation to the curve calculated for $\omega_c/\omega = 0.5/1.5 = 0.33$. The curves plotted with chain lines in FIG. 12c and d, which are a good approximation to the curves calculated by means of the design values of the ultimate strains, are obtained in this way.

It is proposed on the basis of the above analysis that the curves which can be calculated with the computer program described in this report should in practice be applied by first determining ω for the characteristic strengths

of the steel and concrete and then introducing the factor of safety by multiplying the value of ω thus calculated by a partial coefficient γ_r relating to the rotation capacity. In ordinary cases, γ_r should be made equal to γ_c, and equal to unity when abnormal loads are studied.

13 OVERALL CONCLUSIONS

The author has earlier analysed the rotation capacity of plastic hinges - see Plem (1973a), the following expression being derived for approximate calculation of the rotation capacity θ_u

$$\theta_u = 2 \cdot 10^{-3} \frac{a_n}{x} (1+250\rho_v) \qquad (13.1)$$

x is the depth of the compression zone and a_n a fictitious yield length, which can generally be made the length of that section of the beam adjacent to the plastic hinge over which the ultimate moment exceeds n% of the ultimate moment M_u. The effect of stirrups is taken into account by means of the quantity ρ_v which is the geometrical reinforcement percentage of the stirrups, calculated in a certain way.

Expression (13.1) is discussed by Cederwall, Losberg & Palm (1974) who propose certain additional rules in order that this expression may have a greater degree of differentiation.

In some circumstances, a_{80}, i.e. the section over which the moment is greater than $0.8M_u$, can be selected for a_n. If at the same time we assume a linear moment distribution ($\beta = 0$) and ignore the effect of stirrups, Equation (13.1) can be written

$$\theta_u = 0{,}4 \cdot 10^{-3} \frac{l_o}{x} = 0{,}4 \cdot 10^{-3} \lambda \frac{d}{x} \qquad (13.2)$$

where $\lambda = l_o/d$ is the slenderness of the rotation span. If we apply the rectangular stress distribution proposed by the CEB to the compression zone of the beam cross section, we obtain the value $x/d = 1.25\omega$ by means of an equilibrium expression, which, substituted into Equation (13.2), yields the expression

$$\frac{\theta_u}{\lambda} = 0{,}32 \cdot 10^{-3} \frac{1}{\omega} \qquad (13.3)$$

This relation is plotted in FIG. 13a. As will be seen from the figure, the curve (part of a hyperbola) has the same general shape as the curves calculated in another way and presented in the previous publication.

However, Equation (13.1) is far too undifferentiated to permit closer study of the way in which different parameters affect the rotation capacity. This is particularly true with regard to those parameters which describe the

mechanical properties of the steel and concrete, but it is also difficult to take into account in a correct manner the other factors which affect the rotation capacity. For instance, there is a temptation to take into account the presence of compression reinforcement by replacing ω by $(\omega - \omega_c)$ in Equation (13.3). It is shown in Chapter 9 that such a procedure is erroneous.

The object of the work presented in this report has been to examine in greater detail the questions which can be posed concerning the yield characteristics of reinforced concrete beams, and to study in this connection the way in which the rotation capacity is affected by various factors. The analysis carried out is summarised and commented on briefly in the following.

The calculations are based on standardised, but realistic, stress-strain curves for the constituent materials concrete and steel. These are described in Chapter 2. The calculations are of such complexity that a computer must be employed. A program for the computation of the rotation capacity under the influence of various factors has been developed, and is presented in an appendix.

Mainly two types of reinforcement and two concrete types have been included in the investigation. One of the concretes, Type A, has an ultimate compressive strain $\varepsilon_{cu} = -0.0035$, while the other, Type B, has an ultimate compressive strain $\varepsilon_{cu} = -0.0070$. One of the typical steels, denoted HR (hot rolled), has a pronounced yield point, while the other, denoted CW (cold worked), has no pronounced yield point. The truncated stress-strain diagram for reinforcing steel at present recommended by the CEB is also mentioned in passing.

After derivation of the necessary formulae (Chapters 3 - 6), in which process expressions are constructed for determination of the rotation capacity by means of a study of the mechanical energy balance of the rotation span, the results of calculations relating to different combinations of typical steels and concrete types are given in Chapter 7. In this connection, the parameters describing the steel types are varied in different ways. Special mention must be made of one result from this investigation.

For plastic hinges reinforced with HR steel, there exists a critical value ω_{cr} of the effective reinforcement ratio ω. This critical value is characterised by the following. For beam cross sections with $\omega > \omega_{cr}$ the rotation capacity is low and almost constant irrespective of the value of ω. The cross section may be described as over-reinforced with respect to the

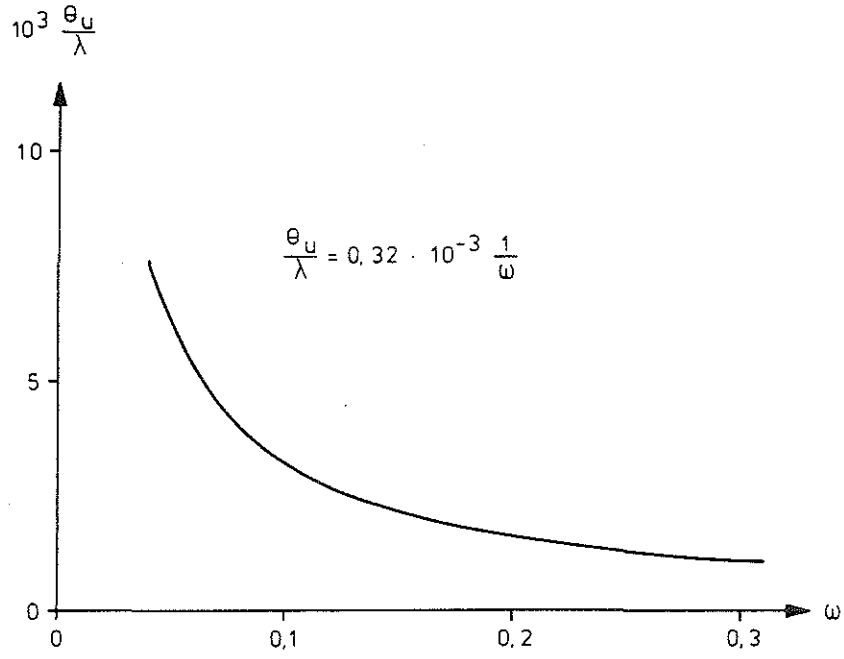

FIG 13a Rotation capacity expressed in terms of the ratio θ_u/λ as a function of the effective reinforcement ratio ω, the curve being calculated by means of the formula given in the figure.

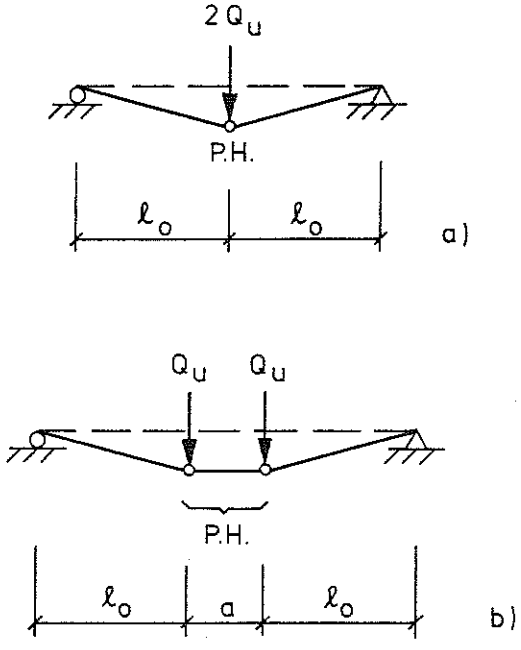

FIG 13b Plastic hinge underneath a single point load, figure a), and underneath a pair of point loads, figure b).

rotation capacity. For beam cross sections with $\omega < \omega$ the rotation capacity increases rapidly as the value of ω decreases. The cross section may be described as normally reinforced with respect to the rotation capacity. This phenomenon will be understood most easily by examination of FIG. 1.3a. The rotation capacity of a plastic hinge is represented by the hatched area B in the figure. This area has been obtained by transformation of the area A above the moment-curvature relation for the beam cross section by means of the moment diagram. For large values of ω failure of the beam occurs at small values of the curvature, with the result that area A and thus the rotation capacity are small. For small values of ω beam failure ensues at such large values of the curvature that the lower strain hardening limit of the steel has been passed, and the part of the moment-curvature relation which is again increasing has been entered. In this case, the area A and thus the rotation capacity will be large.

The value of ω_{cr}, i.e. the boundary between a cross section over-reinforced and normally reinforced with respect to the rotation capacity, is determined for a given concrete by the value of the lower strain hardening limit of the steel, i.e. the end of the yield region of the steel. This is quite analogous to the determination by the initial point of the yield region of a balanced reinforcement expressed in terms of ω_b, i.e. the boundary between a beam cross section over-reinforced and normally reinforced with respect to bending failure. It will be evident from this that a beam cross section may be under-reinforced with respect to bending failure ($\omega < \omega_b$) while at the same time it is over-reinforced with respect to the rotation capacity ($\omega > \omega_{cr}$). Generally, $\omega_b > \omega_{cr}$, and the rotation capacity is therefore at all times extremely small for a beam cross section over-reinforced with respect to bending moment. A beam which is over-reinforced with respect to bending moment should therefore never be used when reinforced concrete structures are designed purely by the plastic theory.

In Chapters 8 - 11, a study is made of the way in which factors other than the shape of the stress strain curves of the steel and concrete affect the rotation capacity of plastic hinges.

Creep of the concrete increases rotation capacity. However, inclusion of this effect in determining the rotation capacity is no guarantee that it will be easier to satisfy the condition in (1.1.7), since the rotation requirement of the plastic hinge also increases as a result of creep, as mentioned in Section 1.2. The overall effect is dependent on the design of the structure.

For values of ω in excess of 0.05 - 0.07. the presence of compression reinforcement increases the rotation capacity. The increase in relation to cross sections without compression reinforcement, for usual values of ω, is dependent on the value of this, a higher value of ω resulting in a greater increase. This is a favourable effect since the rotation capacity for the cross section without compression reinforcement decreases as the value of ω increases. In order that this effect may be utilised to the full, it is essential that the compression reinforcement should be fixed within the cross section by means of stirrups in order to prevent buckling of the reinforcing bars.

If the effect of shear force on the rotation capacity is not taken into account in calculating the rotation capacity, it is found for a given cross section that the rotation capacity is directly proportional to the slenderness λ of the rotation span. See Equation (13.3). If the effect of shear force is allowed for in calculations, it is found that the rotation capacity increases considerably and disproportionately for small values of λ, i.e. for λ = approx. 2. This increase diminishes for increasing values of λ, and vanishes for values of λ of about 8 - 10.

The effect of shear force is explained by the fact that the inclined shear cracks which occur in the part of the beam acted upon by shear force cause yield of the tension reinforcement to take place over a larger region of the rotation span. For a larger yield length, the capacity of the rotation span to store deformation energy increases, and the rotation capacity increases in consequence. It must be realised, however, that this favourable effect is never fully developed in practice, since intensive yield characterised by contraction of the cross section generally occurs only within a limited region of a reinforcing bar stressed up to the yield point. This is also taken into account in the computer program. The above fact must also be borne in mind in conjunction with determination of the rotation capacity of a plastic hinge which develops in a beam acted upon by a constant bending moment over a certain distance. The rotation capacity of the plastic hinge over the distance a in FIG. 13b, b), is thus hardly greater than that of tha plastic hinge shown in a), in spite of the fact that, computationally, yield in the tension reinforcement takes place over a longer distance in the former case than in the latter.

If the concrete in the compression zone is surrounded by stirrups, the deformation capacity of the compressed concrete is enhanced, and this means that the rotation capacity also increases. The report outlines the way in

which this effect can be approximately calculated. This method involves a downward correction of the value of ω, which generally results in an increase of the rotation capacity.

14 REFERENCES

Alemo, J, 1976, The Effects of Imposed Deformations on the Behaviour of Loaded Concrete Structures. (Lund Institute of Technology, Division of Structural Mechanics and Concrete Construction). Bulletin 53. Lund.

Baker, L L L, 1956, The Ultimate-Load Theory Applied to the Design of Reinforced and Prestressed Concrete Frames. (Concrete Publications Ltd). London.

Cederwall, K, Losberg, A, & Palm, G, 1974, Armerade betongbalkars rotationskapacitet. (The Rotation Capacity of Reinforced Concrete Beams). (Nordic Concrete Association). Nordisk betong, No 4, Volume 18. Malmö.

Code modele pour les structures en beton, 1976. (Comité Euro-international du Beton). Bulletin d'information no 117-F. Paris.

Corley, W G, 1966, Rotational Capacity of Reinforced Concrete Beams. (Portland Cement Association, Development Department). Bulletin D108. Skokie.

Larsen, P K & Vigerust, G, 1966, Praktisk beregning av stivhet og nedbøyning for revnet, armert betong. (Practical Calculation of the Stiffness and Deflection of Cracked Reinforced Concrete). (Nordic Concrete Association). Nordisk betong, No 3, Volume 10. Stockholm.

Mattock, A H, 1965, Rotational Capacity of Hinging Regions in Reinforced Concrete Beams. (Portland Cement Association, Development Department). Bulletin D101. Skokie.

Plem, E, 1973, Plasticeringsförmåga hos tvåsidigt inspänd betongbalk. (Nordiska betongförbundet). Nordisk betong, 2, årg. 17. Malmö.

Plem, E, 1973a, The Plastic Flow Capacity of Concrete Beams Fixed at Both Ends. (Nordic Concrete Association). Nordisk betong, No 1, Volume 17. Malmö.

Rechardt, T, 1968, Flexural Behaviour of Reinforced Concrete Beams at Working Loads. (National Technical Research Institute). Publication 126. Helsinki.

Sargin, M & Handa, V K, 1969, A General Formulation for the Stress-Strain Properties of Concrete. (Solid Mechanics Division, University of Waterloo). Report No 3. Ontario.

APPENDIX

The computer program developed for calculation of the rotation capacity of a plastic hinge in a reinforced concrete beam is presented and commented on in this appendix. The program has been written in ALGOL 60, with notation according to the conventions applied in conjunction with the computer system UNIVAC 1108.

The computational potential of the program is outlined in the introduction. The program is then described and reproduced, and finally examples of the printout are given.

A.1 Calculation alternatives

Three alternative calculation methods are possible. All begin with a computation of the following quantities which relate to the cross section under consideration. The non-dimensional curvature $1/\rho$ is employed as the governing parameter. The curvature is increased in discrete steps from zero to the value which results in material failure. The length of the increment prior to the yield moment is $\Delta(1/\rho) = 0.5 \cdot 10^{-3}$, and after the yield moment $\Delta(1/\rho) = 2.0 \cdot 10^{-3}$.

The calculated quantities, all of which are given in non-dimensional form, are as follows:

μ bending moment
ξ depth of compression zone
ε_c maximum compressive strain in the concrete
ε_{sc} compressive strain in compression reinforcement, if any
ε_s strain in tension reinforcement
ψ_c contribution of compressed concrete to ψ
ψ_t contribution of compression zone to ψ
ψ total deformation energy stored in the cross section per unit length of the beam

The values obtained in this introductory section are printed out in tabular form by means of the procedure SKRIV(K).

Computation can then proceed in two ways.

Alternative 1 relates to calculation without consideration of the effect of shear force on the rotation capacity. This yields the ratio θ_u/λ according to Equation (6.3.2) for the required moment variations expressed in terms of the coefficient β. The results of calculations according to this alternative are printed out by means of the procedure SKRIW 1.

Alternative 2 relates to calculation with regard to the effect of shear force according to the analytical model described in Chapter 10. In this alternative the value of β is at all times zero, i.e. variation of moment over the length of the rotation span is assumed to be linear. The calculation yields the rotation capacity θ_u corresponding to read-in values of the slenderness λ of the rotation span. Results according to this alternative are printed out by means of the procedure SKRIW 2.

Alternative 3 is a combination of Alternatives 1 and 2. It is used when it is desired to calculate the rotation capacity in the same run both with and without consideration of the effect of shear force. When this alternative is selected, values of both β and λ must be read.

A.2 Procedure declarations associated with the main program

Before the main program there are a number of procedure declarations which are commented on in the following. The numbers in brackets refer to the statement number in the program reproduced in Section A.4.

INDATA (12 - 26)

This procedure comprises reading of data cards. The following input data cards may be used.

TYP card. Contains an integer which specifies the desired calculation alternative. This integer may be 1, 2, 3 or a negative number. A negative number indicates the end of the input list.

STEEL card. Contains a description of the stress-strain curve of the reinforcing steel. The following data are punched consecutively.
Steel type, 1 for HR steel, 2 for CW steel.
Non-dimensional modulus of elasticity e_s of the steel.

The ratio $\eta = f_{stu}/f_{st}$.
The lower strain hardening limit ε_1. For CW steel $\varepsilon_1 = 0$ is put.
Limit strain ε_0.
Ultimate strain ε_{su}.

CONCRETE card. Contains a description of the stress-strain curve of the concrete. The following data are punched consecutively.

Non-dimensional modulus of elasticity e_c of the concrete.
The coefficient κ_2 in Equation (2.1.2)
Limit strain ε_0, with a negative sign.
Ultimate strain ε_{cu}, with a negative sign.
Creep factor φ. If creep is not taken into account, $\varphi = 0$ is put.

FC card. This card contains the ratio of the strength of the compression reinforcement to that of the tension reinforcement, i.e. $\upsilon = f_{sc}/f_{st}$, and the non-dimensional distance $\gamma = c/d$ of the compression reinforcement from the extreme fibre in compression. This card must be included even when there is no compression reinforcement, in which case 1.0 0.1 is punched.

OMEGA card. This card must begin with an integer which specifies the number of the values of ω which follow. The values of ω for which the calculation is to be performed are then given consecutively. If required, the values of ω may extend over several cards.

OMEGAC card. This card must begin with an integer which specifies the number of the values of ω_c/ω which follow. The values of ω_c/ω for which the calculation is to be performed are then punched consecutively. If required, these may extent over several cards. When there is no compression reinforcement, 1 0.0 is punched on this card.

BETA card. This card must begin with an integer which specifies the number of the values of β which follow. The values of β for which the calculation is to be performed are then punched consecutively. The following values of β may occur: - 0.06, 0 and 0.25. This card is to be omitted in Alternative 2.

LAMBDA card. This card must begin with an integer which specifies the number of the values λ which follow. The values of λ for which the calculation is to be performed are then given consecutively. This card is to be omitted in Alternative 1.

N card. This card contains an integer which specifies the number of strips in the fictitious compression zone. The length of the rotation span is divided into the same number of parts.

The cards must be read in the order specified.

A run may comprise a series of computations where each computation is described by a complete series of input data cards as above. The last data card in a run must be a TYP card containing a negative integer.

RUBRIC (28 - 38)

Call of this procedure causes shifting of the paper in the line printer to a new side and the printout of a heading which includes input data. The extent of the heading is shown in the example in Section A.5.

SKRIV(K) (40 - 46)

This procedure causes printout of one row in the table of results referred to in Section A.1.

SKRIW 1 (48 - 51)

Call of this procedure causes printout of a read value of β and the value of θ_u/λ calculated for this.

SKRIW 2 (53 - 56)

Call of this procedure causes printout of a read value of λ and the value of θ_{uv} calculated for this.

TRYCK (58 - 71)

Call of this procedure causes printout of the appropriate distribution of compressive stresses in the compression zone of the beam. Ordinarily, this procedure is not called in the main program, but the program thus incorporates a provision for the study of the stress distribution which can be made use of if required.

CONCRETE (E,DE,SI,EM,FI,EO,CR,I) (73 - 97)

This procedure gives the non-dimensional compressive stress σ_c/f_{cc} in the concrete as a function of the strain ε_c in strip No i in the compression zone. During application of load the stress is computed from Equation (2.1.2), and during removal of load from the expression for line AB in FIG 2.1a. This procedure requires two globally declared quantities, namely array EA, EB (1:N). Initially, these are zeroed, but when a strip is relieved of load, data which determines the position of the unloading line in the stress-strain diagram of the concrete is inserted into the corresponding positions in EA and EB. This procedure yields the value of σ_c/f_{cc} with a negative sign.

The parameters listed are as follows:

E the appropriate value ε_{ci} of the concrete strain in strip No i
DE the increment in ε_{ci} during a calculation step. Whether the concrete is being loaded or unloaded is determined by the sign
SI the value of σ_c/f_{cc} computed by the procedure
EM the instantaneous modulus of elasticity of concrete in a non-dimensional form
FI the coefficient κ_2 in Equation (2.1.2)
EO limit strain ε_0 of the concrete
CR the creep factor φ
I the number of the strip concerned.

STEEL (Z,E,DE,SI,EM,Y,E1,EO) (99 - 146)

This procedure gives the non-dimensional stress σ_s/f_{st} in the reinforcement as a function of the strain ε_s in the tension reinforcement, or the stress σ_{sc}/f_{sc} as a function of the strain ε_{sc} in the compression reinforcement. During application of load the stress is computed from the stress-strain diagram applicable to the steel type in question, see Section 2.2, and during removal of load from the expression for an unloading line, in principle in conformity with FIG 2.2a. The procedure requires two globally declared quantities, namely real TA,TB. Initially, these are zeroed, but when there is removal of load they are assigned values which determine the position of the unloading line in the stress-strain diagram of the steel. This procedure yields the non-dimensional stress with a positive sign. The main program must therefore perform a correction of sign when the procedure is applied to compression reinforcement.

The parameters listed are as follows:

Z indication of steel type, 1 for HR steel, 2 for CW steel
E the appropriate value of the steel strain ε_s
DE the increment in ε_s during the calculation step in question. Whether the steel is being loaded or unloaded is determined by the sign
SI the value of σ_s/f_{st} or σ_{sc}/f_{sc} computed by the procedure
EM the non-dimensional modulus of elasticity e_s of the steel
Y the coefficient $\eta = f_{stu}/f_{st}$
E1 the lower strain hardening limit ε_1 of the steel (= 0 for CW steel)
EO the limit strain ε_0 of the steel

INTERPOL (A,E,X,AE) (148 - 160)

This procedure is used for linear interpolation in the tables computed by the program. Application will be evident from the following parameter list.

A the name of the column in the table, declared as an array, in which interpolation is to be effected
E the name of the argument column declared as an array
X the argument value in question
AE the highest row number in columns A and E. It is stipulated that numbering of rows begins with 1.

This procedure is a real procedure. The procedure name INTERPOL therefore assumes the computed value when called.

A.3 The main program

The main program begins on line 162 by reading the actual data. The program structure is characterised by two loops, the outer one of which relates to successive values of ω_c/ω and the inner one to successive values of ω. Inside these loops the program can be divided into a number of sections. The first of these, which extends to statement 221, determines by iteration the internal equilibrium according to Equation (3.3.1) for each new increase in the curvature $1/\rho$. This section thus yields at the same time the distribution of strain over the depth of the cross section, and therefore the depth ξ of the compression zone also.

The iteration proceeds by variation of the strain ε_s in the tension reinforcement until Equation (3.3.1) has been satisfied with a certain tolerance. In order to save computation time, this tolerance has been made variable as follows. For a start, it is 0.2% of the force in the tension reinforcement. If equilibrium is not achieved within five iterations, the tolerance is increased by another 0.2%. This procedure is repeated, but the maximum tolerance is 1%. Control printouts have shown that the tolerance is normally 0.2 - 0.4%.

A subsequent section of the program, statement 222 to statement 238, calculates the non-dimensional bending moment μ according to Equation (4.10) which corresponds to the equilibrium postion found. In conjunction which this a check is made to see if the ultimate moment μ_u has been reached, the value of μ_u being determined according to one of the definitions given in Chapter 4. If the increase in moment in any one computation step is less than 1/10 of the increase in moment in the first computation step, then the yield moment μ_y is considered to have been reached. The step length of the governing parameter $\Delta(1/\rho)$ is then quadrupled.

The program section which extends from statement 239 to statement 267 determines, by means of Equation (5.5), the increase in deformation energy ψ per unit length of the beam which occurred during the calculation step. The contributions of the concrete, compression reinforcement and tension reinforcement are calculated separately. The calculated energy is summated according to Equation (5.9). This program section is concluded by printout of the tabulated values listed in Section A.1.

The next program section extends from statement 268 to statement 294. A check is now made to see if material failure has occurred during the computational step, i.e. whether $|\varepsilon_c| \geq |\varepsilon_{cu}$ or whether $\varepsilon_s \geq \varepsilon_{su}$. If this is not the case, the curvature is increased by yet another increment and the above calculations are repeated. If material failure is found then either ε_c or ε_s is a little too large. The quantities listed in Section A.1, which were determined during the last computational step, are therefore adjusted by interpolation so that they just correspond to ε_{cu} or to ε_{su}, depending on whether material failure occurs in the concrete or in the steel. After this correction, the new values relating to the last computational step are again printed out. This correction is made only when the ultimate moment is determined by material failure.

The next program section, statement 298 to statement 316, is employed for calculation alternatives 1 and 3. It calculates the rotation capacity without consideration of the effect of shear force for the desired moment distributions described by the coefficient β. See FIG 6.1b. The calculation is carried out using Equation (6.3.2). The appropriate values of β and the calculated values of the ratio θ_u/λ are printed out.

The last program section, statement 317 to statement 340, relates to calculation alternatives 2 and 3. It calculates the rotation capacity with the effect of shear force taken into consideration by means of Equation (10.1.9) for desired values of λ for the non-dimensional length of the rotation span. The appropriate values of λ and the calculated values of the rotation capacity θ_{uv} are printed out.

A.4 The complete program in ALGOL 60

```
BEGIN COMMENT ROTATIONSKAPACITET VERSION 10;
   INTEGER I,I1,I2,I3,M,N,NBE,NLA,NOM,NOMC,RV,RW,ST,TYP;
   REAL AL,BE,C,CU,DCU,DEC,DES,DS1,DS2,EC,ECAUX,ECU,ECO,EMC,EMS,ES,
        ESAUX,ESC,ESU,ESU,ES1,ETAUX,F,FS,KA1,KA2,KA3,MI,MU,MY,MYP,MY1,
        NY,OM,OMC,PHI,PSI,PSIC,PSIS,PSIT,RE,RIG,RIGO,SIC,SIS,SISC,SOM,
        SUM,T,TA,TAC,TAT,TB,TBC,TBT,TET,VI,X,XM,XO,Y,Z,ZU,A,LA,M1,M2,
        SMY,DESC,MF;
   BOOLEAN CONT,FIRST,ITER,VAL;
   ARRAY ABE,ALA,UMC(1:10),UM(1:20),EA,EB(1:50),
         ACU,AEC,AES,AESC,AMY,APSI,APSIC,APSIS,APSIZ,AX,SL(1:100);

   PROCEDURE INDATA;
   BEGIN INTEGER K;
      READ(TYP);
      IF TYP LSS 0 THEN GO TO FIN;
      READ(ST,EMS,Y,ES1,ESU,ESU);
      READ(EMC,PHI,ECU,ECU,VI);
      READ(F,C);
      READ(NOM,FOR K=(1,1,NOM) DO UM(K));
      READ(NOMC,FOR K=(1,1,NOMC) DO UMC(K));
      IF TYP EQL 1 OR TYP EQL 3 THEN
      READ(NBE,FOR K=(1,1,NBE) DO ABE(K));
      IF TYP EQL 2 OR TYP EQL 3 THEN
      READ(NLA,FOR K=(1,1,NLA) DO ALA(K));
      READ(N)
   END INDATA;

   PROCEDURE RUBRIC;
   BEGIN FORMAT RU(E4,X8,'CONCRETE:  EMC =',D7.1,X6,'STEEL:  EMS =',
      D6.1,X6,'OMEGA =',D5.2,A2,X19,'PHI =',D7.3,X14,'ETA =',D6.3,X6,
      'OMC/OM=',D5.2,A1,X19,'EPCO=',D7.4,X14,'EPS1=',D6.3,A1,X19,
      'EPCU=',D7.4,X14,'EPSO=',D6.3,A1,X45,'EPSU=',D6.3,A1,2,X8,
      'FSC/FST=',D5.2,X15,'C/D=',D6.3,X15,'CREEP=',D4.1,X15,'N=',I3,
      A1,2,X10,'1/RO',X8,
      'MY',X9,'KSI',X8,'EPSC',X7,'EPSSC',X8,'EPSS',X8,'PSIC',X8,
      'PSIT',X8,'PSI',A1,1);
      WRITE(RU,EMC,EMS,OM,PHI,Y,OMC,ECU,ES1,ECU,ESU,ESU,F,C,VI,N)
   END RUBRIC;

   PROCEDURE SKRIV(K);
   VALUE K;
   INTEGER K;
   BEGIN FORMAT TA(X8,D7.5,2D11.4,3D12.5,D14.7,2D12.7,A1);
      WRITE(TA,ACU(K),AMY(K),AX(K),AEC(K),AESC(K),AES(K),
            APSIC(K),APSIZ(K),APSI(K))
   END SKRIV;

   PROCEDURE SKRIW1;
   BEGIN FORMAT F(X8,'BETA=',D5.2,X4,'TETA/LAMBDA=',D8.6,A2);
      WRITE(F,BE,TET)
   END SKRIW1;

   PROCEDURE SKRIW2;
   BEGIN FORMAT F(X8,'LAMBDA=',D6.2,X8,'TETA=',D8.6,A2);
      WRITE(F,LA,TET)
   END SKRIW2;
```

```
 58     PROCEDURE TRYCK;
 59     BEGIN INTEGER K;
 60        REAL E,DE,S;
 61        FORMAT AA(E4,X10,'DISTRIBUTION OF CONCRETE STRESSES',A1,1,
 62                  X10,'STRIP NO',X6,'SIGMA/FCC',X9,'EA',X14,'EB',A1,1),
 63               BB(I15,D16.5,2D16.6,A1);
 64        WRITE(AA);
 65        FOR K=1 STEP 1 UNTIL N DO
 66        BEGIN E=ES+CU*(XM-1+AL*(0.5-K));
 67           DE=DES+DCU*(XM-1+AL*(0.5-K));
 68           CONCRETE(E,DE,S,EMC,PHI,ECU,VI,K);
 69           WRITE(BB,K,S,EA(K),EB(K))
 70        END
 71     END TRYCK;
 72
 73     PROCEDURE CONCRETE(E,DE,SI,EM,FI,EU,CR,I);
 74     VALUE E,DE,EM,FI,EU,CR,I;
 75     INTEGER I;
 76     REAL E,DE,SI,EM,FI,EU,CR;
 77     BEGIN REAL F,H,K,S;
 78        REAL PROCEDURE SIGMA(T);
 79        VALUE T;
 80        REAL T;
 81        BEGIN
 82           SIGMA=(K*T+(FI-1)*T*T)/(1+(K-2)*T+FI*T*T);
 83        END SIGMA;
 84        K=-EM*EU;
 85        S=E/EU/(1+CR);
           IF S LSS EB(I) THEN BEGIN SI=0; GO TO B END;
 87     A: IF EB(I) EQL 0 AND -DE GEQ 0 THEN
           BEGIN SI=-SIGMA(S); GO TO B END;
 89        IF EB(I) EQL 0 AND -DE LSS 0 THEN
 90        BEGIN EA(I)=F=S-DE/EU/(1+CR);
 91           H=SIGMA(F);
 92           EB(I)=F-H/K
 93        END;
           IF S GTR EA(I) THEN BEGIN EA(I)=EB(I)=0; GO TO A END;
 95        SI=-K*(S-EB(I));
 96     B:
 97     END CONCRETE;
 98
 99     PROCEDURE STEEL(Z,E,DE,SI,EM,Y,E1,EU);
100     VALUE Z,E,DE,EM,Y,E1,EU;
101     INTEGER Z;
102     REAL E,DE,SI,EM,Y,E1,EU;
103     BEGIN REAL H;
104        REAL PROCEDURE SIGMA(T);
105        VALUE T;
106        REAL T;
107        BEGIN REAL AL2,BE,D1,D2,D3,E2,G1,G2,G3,K,S,S1,S2;
108           IF Z EQL 2 THEN GO TO LL;
109           E2=1/EM;
              IF T LSS E2 THEN BEGIN SIGMA=T*EM; GO TO L END;
              IF T LSS E1 THEN BEGIN SIGMA=1.0; GO TO L END;
```

```
112           IF T LSS EO THEN
113           BEGIN S=(EO-T)/(EO-E1);
114              SIGMA=Y-(Y-1)*S*S;
115              GO TO L
116           END;
117           SIGMA=Y;
118           GO TO L;
119        LL:D1=EO-0,002-1/EM;
120           D2=EM*EO-Y;
121           D3=Y-1;
122           S1=EM*D1;
123           S2=D2*D3;
124           G1=S1*S1-4*S2;
125           G2=S2*(D2-D3);
126           G3=S2*S2;
127           BE=(G2+SQRT(G2*G2-G1*G3))/G1;
128           K=D1*D1/D3/(2*BE-D3);
129           E2=(EO+K*EM*(Y-BE))/(1+K*EM*EM);
130           AL2=K*BE*BE;
131           SIGMA=IF T LSS E2 THEN T*EM ELSE
132                 Y-BE*(1-SQRT(1-(EO-T)*(EO-T)/AL2));
133        L:
134        END SIGMA;
135     A: IF TB EQL 0 AND DE GEQ 0 THEN
           BEGIN SI=SIGMA(E); GO TO B END;
137        IF TB EQL 0 AND DE LSS 0 THEN
138        BEGIN TA=E-DE;
139           H=SIGMA(TA);
140           TB=TA-H/EM
141        END;
142        IF E GTR TA THEN
           BEGIN TA=TB=0; GO TO A END
144        ELSE SI=EM*(E-TB);
145     B:
146     END STEEL;
147
148     REAL PROCEDURE INTERPOL(A,E,X,AE);
149     VALUE X,AE;
150     INTEGER AE; REAL X; ARRAY A,E;
151     BEGIN INTEGER I,K;
152        REAL D,S;
153        FOR I=1 STEP 1 UNTIL AE DO
           IF ABS(X) LSS ABS(E(I)) THEN BEGIN K=I-1; GO TO Z END;
155     Z: IF K EQL 0 THEN K=1;
156        D=(E(K+1)-E(K))/E(K);
           IF ABS(D) LSS 1&-6 THEN BEGIN S=(A(K+1)+A(K))/2; GO TO Y END;
158        S=A(K)+(A(K+1)-A(K))*(X/E(K)-1)/D;
159     Y: INTERPOL=S
160     END INTERPOL;
```

```
162 LL:INDATA;
163    FOR I1=1 STEP 1 UNTIL NOMC DO
164    BEGIN OMC=UMC(I1);
165       FOR I2=1 STEP 1 UNTIL NOM DO
166       BEGIN OM=UM(I2);
167          RUBRIC;
168          CU=ES=MYP=PSIC=PSIT=PSIS=SMY=0;
169          DCU=5&-4;
170          FIRST=CONT=TRUE;
171          VAL=FALSE;
172          NY=OM*EMS*(1+VI)/EMC;
173          XO=NY*(SQRT((1+OMC/F)*(1+OMC/F)+2*(1+C*OMC/F)/NY)-(1+OMC/F));
174          XM=1,25*XO;
175          AL=XM/N;
176          RV=0;
177          FOR I=1 STEP 1 UNTIL N DO EA(I)=EB(I)=0;
178          TAT=TBT=TAC=TBC=0;
179 LO:      ITER=FALSE;
180          CU=CU+DCU;
181          IF FIRST THEN DES=(1-XO)*DCU;
182          DS1=DS2=0;
183          RW=0;
184          T=0,002;
185 L1:      IF RW EQL 5 THEN
186          BEGIN RW=0;
187             IF T LSS 0,010 THEN T=T+0,002
188          END;
189          IF ITER THEN RW=RW+1;
190          ES=ES+DES;
191          TA=TAT; TB=TBT;
192          STEEL(ST,ES,DES,SIS,EMS,Y,ES1,ESO);
193          TAT=TA; TBT=TB; TA=TAC; TB=TBC;
194          ESC=ES-(1-C)*CU;
195          DESC=SIGN(ESC)*(DES-(1-C)*DCU);
196          STEEL(ST,ABS(ESC),DESC,SISC,EMS,Y,ES1,ESO);
197          SISC=SIGN(ESC)*SISC;
198          TAC=TA; TBC=TB;
199          X=1-ES/CU;
200          IF FIRST THEN GO TO L3;
201          SUM=0;
202          FOR I=1 STEP 1 UNTIL N DO
203          BEGIN EC=ES+CU*(XM-1+AL*(0,5-I));
204             DEC=DES+DCU*(XM-1+AL*(0,5-I));
205             CONCRETE(EC,DEC,SIC,EMC,PHI,ECO,VI,I);
206             SUM=SUM+SIC
207          END;
208          FS=OM*SIS;
209          RE=AL*SUM+OM*OMC*SISC+FS;
210          IF ABS(RE) LSS T*FS THEN GO TO L3;
211          ES=ES-DES;
212          IF ITER THEN GO TO L2;
213          IF RE LSS 0 THEN
             BEGIN DS1=DES; DES=DES+0,0001 END ELSE
             BEGIN DS2=DES; DES=DES-0,0001 END;
216          IF DS1 NEQ 0 AND DS2 NEQ 0 THEN
             BEGIN DES=(DS1+DS2)/2; ITER=TRUE END;
218          GO TO L1;
```

```
219 L2:     IF RF LSS 0 THEN DS1=DES ELSE DS2=DES;
220         DES=(DS1+DS2)/2;
221         GO TO L1;
222 L3:     SUM=0;
223         FOR I=1 STEP 1 UNTIL N DO
224         BEGIN EC=ES+CU*(XM-1+AL*(0.5-I));
225            DEC=DES+DCU*(XM-1+AL*(0.5-I));
226            CONCRETE(EC,DEC,SIC,EMC,PHI,ECU,VI,I);
227            SUM=SUM+SIC*(0.5-I)
228         END;
229         MY=AL*AL*SUM+OM*(SIS*(1-XM)+OMC*SISC*(C-XM));
230         IF MY LSS MYP AND NOT VAL THEN
            BEGIN M=RV; SMY=MYP; VAL=TRUE END;
232         IF MY GTR SMY AND VAL THEN VAL=FALSE;
            IF FIRST THEN BEGIN MY1=MY/10; FIRST=FALSE END;
234         ESAUX=ES-DES/2;
235         ETAUX=ESC+(1-C)*DCU/2-DES/2;
236         IF MY-MYP LSS MY1 AND CONT THEN
            BEGIN DCU=4*DCU; DES=4*DES; CONT=FALSE; MF=MY END;
238         MYP=MY;
239         TA=TAT; TB=TBT;
240         STEEL(ST,ESAUX,DES,SIS,EMS,Y,ES1,ESU);
241         TAT=TA; TBT=TB; TA=TAC; TB=TBC;
242         STEEL(ST,ABS(ETAUX),DESC,SISC,EMS,Y,ES1,ESU);
243         SISC=SIGN(ETAUX)*SISC;
244         TAC=TA; TBC=TB;
245         SUM=0;
246         FOR I=1 STEP 1 UNTIL N DO
247         BEGIN EC=ES+CU*(XM-1+AL*(0.5-I));
248            DEC=DES+DCU*(XM-1+AL*(0.5-I));
249            ECAUX=EC-DEC/2;
250            CONCRETE(ECAUX,DEC,SIC,EMC,PHI,ECU,VI,I);
251            SUM=SUM+SIC*DEC
252         END;
253         PSIC=PSIC+AL*SUM;
254         PSIT=PSIT+OM*OMC*SISC*(DCU*(C-1)+DES);
255         PSIS=PSIS+OM*SIS*DES;
256         RV=1+RV;
257         ACU(RV)=CU;
258         AES(RV)=ES;
259         AX(RV)=X;
260         AMY(RV)=MY;
261         AESC(RV)=ESC;
262         AEC(RV)=EC=ES-CU;
263         APSIC(RV)=PSIC;
264         APSIS(RV)=PSIS;
265         APSIZ(RV)=PSIC+PSIT;
266         APSI(RV)=PSIC+PSIT+PSIS;
267         SKRIV(RV);
268         IF EC GTR ECU*(1+VI) AND ES LSS ESU THEN GO TO L0;
269         IF VAL THEN GO TO L4;
270         M=RV;
271         FOR I=1 STEP 1 UNTIL M DO SL(I)=0;
```

```
272             IF ESU LSS AES(M) THEN
273             BEGIN Z=ESU;
274                SL(M-1)=AES(M-1); SL(M)=AES(M)
275             END ELSE
276             BEGIN Z=ECU*(1+VI);
277                SL(M-1)=AEC(M-1); SL(M)=AEC(M)
278             END;
279             ACU(M)=INTERPOL(ACU,SL,Z,M);
280             AMY(M)=INTERPOL(AMY,SL,Z,M);
281             AX(M)=INTERPOL(AX,SL,Z,M);
282             AESC(M)=INTERPOL(AESC,SL,Z,M);
283             APSIC(M)=INTERPOL(APSIC,SL,Z,M);
284             APSIS(M)=INTERPOL(APSIS,SL,Z,M);
285             APSIZ(M)=INTERPOL(APSIZ,SL,Z,M);
286             APSI(M)=INTERPOL(APSI,SL,Z,M);
287             IF ESU LSS AES(M) THEN
288             BEGIN AEC(M)=INTERPOL(AEC,SL,Z,M);
289                AES(M)=ESU
290             END ELSE
291             BEGIN AES(M)=INTERPOL(AES,SL,Z,M);
292                AEC(M)=ECU*(1+VI)
293             END;
294             SKRIV(M);
295 L4:         MU=AMY(M);
296             XO=AX(M);
297             RIGO=OM*EMS*((1-XO/3)*(1-XO)+OMC*(C-XO/3)*(C-XO)/F);
298             IF TYP EQL 1 OR TYP EQL 3 THEN
299             FOR I3=1 STEP 1 UNTIL NRE DO
300             BEGIN RE=ARE(I3);
301                SUM=KA2=MU/RIGO/2;
302                SOM=APSI(M)/2;
303                KA3=0;
304                FOR I=1 STEP 1 UNTIL N-1 DO
305                BEGIN MI=MU*(N-I)*(N+4*RE*I)/N/N;
306                   X=INTERPOL(AX,AMY,MI,M);
307                   RIG=OM*EMS*((1-X/3)*(1-X)+OMC*(C-X/3)*(C-X)/F);
308                   ZU=MI/RIG;
309                   KA1=2*KA2-KA3+ZU;
310                   SUM=SUM+KA1;
311                   KA3=KA2; KA2=KA1;
312                   SOM=SOM+INTERPOL(APSI,AMY,MI,M)
313                END I;
314                TET=(2*SOM/N/MU+(8*RE*SUM/N-(1+4*RE)*KA1)/N/N)/(1+MF/MU);
315                SKRIW1
316             END BETA;
317             IF TYP EQL 2 OR TYP EQL 3 THEN
318             FOR I3=1 STEP 1 UNTIL NLA DO
319             BEGIN LA=ALA(I3);
320                A=10*KU/LA;
321                KA2=MU/RIGO/2;
322                SUM=APSIS(M)/2+APSIZ(M)/2;
323                KA3=0;
```

```
324                FOR I=1 STEP 1 UNTIL N-1 DO
325                BEGIN MI=MU*(N-I)/N;
326                   IF I LSS N*A/LA THEN M1=(1-0,U2*LA*I/N)*MU
327                   ELSE M1=(1-I/N)*(1-0,U2*A)*MU/(1-A/LA);
328                   IF I LSS N*A/LA/2 THEN M2=(1-3*I/N/(1+A/LA))*MU ELSE
329                   M2=(1-I/N)*MU/(1+A/LA);
330                   X=INTERPOL(AX,AMY,MI,M);
331                   RIG=OM*EPS*((1-X/3)*(1-X)+OMC*(C-X/3)*(C-X)/F);
332                   ZU=MI/RIG;
333                   KA1=2*KA2-KA3+ZU;
334                   KA3=KA2; KA2=KA1;
335                   SUM=SUM+INTERPOL(APSIS,AMY,M1,M)
336                           +INTERPOL(APSIZ,AMY,M2,M);
337                END I;
338                TET=LA*(2*SUM/N/MU-KA1/N/N)/(1+MF/MU);
339                SKRIV2
340             END LAMBDA;
341          END OMEGA
342       END OMC;
343       GO TO LL;
344    FIN:
345    END PROGRAM
```

A.5 Examples of printouts

Two examples of the printout of the results are shown. The first relates to calculation alternative 1. The conditions are as follows.

Concrete Type A, see Section 2.1.
Tension reinforcement of HR steel, see Section 2.2, with the effective reinforcement ration $\omega = 0.07$.
No compression reinforcement.
Creep of the concrete is not taken into consideration.

The printout of the results is reproduced in FIG A.5a. The procedure RUBRIC results in printout ot the input values and table heading. The procedure SKRIV (K) causes printout of the table in which the different quantities are functions of the parameter $1/\rho$ (1/RO in the printout). As will be seen, the ultimate moment μ_u is determined by material failure in the concrete. In the penultimate line $\varepsilon_c = -0.00356$. All the values in this line have therefore been converted so as to correspond to $\varepsilon_c = -0.0035$. The modified values are given in the last line of the table. The example studied does not include compression reinforcement, and the strains given in the column for ε_{sc} are therefore fictitious - they relate to strains at a level within the cross section determined by $\gamma = c/d = 0.1$. Since there is no compression reinforcement, the contents of the columns for ψ_c and ψ_t are equal.

Three values of β and the values of the ratio θ_u/λ calculated for these values are printed out underneath the table. This printout is controlled by the procedure SKRIW 1.

The second example relates to calculation alternative 2. The conditions are as follows.

Concrete Type B.
Tension and compression reinforcement of CW steel, with $\omega = 0.20$ and $\omega_c = 0.05$, $\upsilon = f_{sc}/f_{st} = 1.0$, and $\gamma = c/d = 0.1$.
Creep of the concrete is not taken into consideration.

CONCRETE: EMC = 1200.0 STEEL: EMS = 350.0 OMEGA = 0.07
PHI = 0.363 ETA = 1.400 OMC/OM= 0.00
EPC0=-0.0020 EPS1= 0.015
EPCU=-0.0035 EPS0= 0.080
EPSU= 0.100

FSC/FST= 1.00 C/D= 0.100 CREEP= 0.0 N= 50

1/RO	MY	KSI	EPSC	EPSSC	EPSS	PSIC	PSIT	PSI
0.00050	0.0094	0.1827	-0.00009	-0.00004	0.00041	0.0000003	0.0000003	0.0000023
0.00100	0.0187	0.1862	-0.00019	-0.00009	0.00081	0.0000013	0.0000013	0.0000094
0.00150	0.0279	0.1884	-0.00028	-0.00013	0.00122	0.0000029	0.0000029	0.0000210
0.00200	0.0371	0.1903	-0.00038	-0.00018	0.00162	0.0000052	0.0000052	0.0000373
0.00250	0.0462	0.1921	-0.00048	-0.00023	0.00202	0.0000081	0.0000081	0.0000581
0.00300	0.0552	0.1948	-0.00058	-0.00028	0.00242	0.0000120	0.0000120	0.0000835
0.00350	0.0641	0.1967	-0.00069	-0.00034	0.00281	0.0000165	0.0000165	0.0001133
0.00400	0.0654	0.1873	-0.00075	-0.00035	0.00325	0.0000184	0.0000184	0.0001460
0.00450	0.0656	0.1778	-0.00080	-0.00035	0.00370	0.0000231	0.0000231	0.0002764
0.00650	0.0663	0.1529	-0.00099	-0.00034	0.00551	0.0000287	0.0000287	0.0004085
0.00850	0.0666	0.1367	-0.00116	-0.00031	0.00734	0.0000334	0.0000334	0.0005414
0.01050	0.0668	0.1258	-0.00132	-0.00027	0.00918	0.0000380	0.0000380	0.0006748
0.01250	0.0670	0.1177	-0.00147	-0.00022	0.01103	0.0000424	0.0000424	0.0008087
0.01450	0.0671	0.1118	-0.00162	-0.00017	0.01288	0.0000470	0.0000470	0.0009428
0.01650	0.0672	0.1069	-0.00176	-0.00011	0.01474	0.0000514	0.0000514	0.0010772
0.01850	0.0685	0.1041	-0.00193	-0.00008	0.01657	0.0000573	0.0000573	0.0012127
0.02050	0.0700	0.1025	-0.00210	-0.00005	0.01840	0.0000642	0.0000642	0.0013512
0.02250	0.0714	0.1014	-0.00228	-0.00003	0.02022	0.0000717	0.0000717	0.0014926
0.02450	0.0727	0.1008	-0.00247	-0.00002	0.02203	0.0000798	0.0000798	0.0016367
0.02650	0.0740	0.1005	-0.00266	-0.00001	0.02384	0.0000884	0.0000884	0.0017834
0.02850	0.0752	0.1004	-0.00286	-0.00001	0.02564	0.0000975	0.0000975	0.0019325
0.03050	0.0763	0.1010	-0.00308	-0.00003	0.02742	0.0001082	0.0001082	0.0020840
0.03250	0.0774	0.1019	-0.00331	-0.00006	0.02919	0.0001198	0.0001198	0.0022377
0.03450	0.0783	0.1031	-0.00356	-0.00011	0.03094	0.0001324	0.0001324	0.0023934
0.03404	0.0781	0.1028	-0.00350	-0.00010	0.03054	0.0001295	0.0001295	0.0023577

BETA=-0.06 TETA/LAMBDA=0.002545

BETA= 0.00 TETA/LAMBDA=0.003159

BETA= 0.25 TETA/LAMBDA=0.009290

FIG A.5a Example of the printout of the results calculated according to Alternative 1

```
CONCRETE:  EMC = 1200.0        STEEL:  EMS = 350.0        OMEGA = 0.20
           PHI =  0.342                ETA = 1.100        OMC/OM= 0.25
           EPC0=-0.0025                EPS1= 0.000
           EPCU=-0.0070                EPS0= 0.050
                                       EPSU= 0.065

FSC/FST= 1.00                C/D= 0.100                 COEFP= 0.0                N= 50

   1/RO          MY          KSI          EPSC         EPSSC         EPSS          PSIC          PSIT          PSI
0.00050       0.0225       0.2805      -0.00014      -0.00009      0.00036     0.0000011     0.0000011     0.0000057
0.00100       0.0447       0.2914      -0.00029      -0.00019      0.00071     0.0000046     0.0000050     0.0000225
0.00150       0.0663       0.2961      -0.00044      -0.00029      0.00106     0.0000105     0.0000113     0.0000503
0.00200       0.0874       0.3024      -0.00060      -0.00040      0.00140     0.0000192     0.0000206     0.0000888
0.00250       0.1080       0.3080      -0.00077      -0.00052      0.00173     0.0000305     0.0000329     0.0001377
0.00300       0.1279       0.3143      -0.00094      -0.00064      0.00206     0.0000450     0.0000486     0.0001967
0.00350       0.1473       0.3207      -0.00112      -0.00077      0.00238     0.0000624     0.0000677     0.0002655
0.00400       0.1661       0.3270      -0.00131      -0.00091      0.00269     0.0000830     0.0000903     0.0003439
0.00450       0.1722       0.3187      -0.00143      -0.00098      0.00307     0.0000947     0.0001032     0.0004293
0.00500       0.1743       0.3077      -0.00154      -0.00104      0.00346     0.0001058     0.0001381     0.0007741
0.00700       0.1797       0.2771      -0.00194      -0.00124      0.00506     0.0001591     0.0001754     0.0011291
0.00900       0.1830       0.2560      -0.00230      -0.00140      0.00670     0.0001882     0.0002083     0.0014921
0.01100       0.1855       0.2420      -0.00266      -0.00156      0.00834     0.0002177     0.0002419     0.0018607
0.01300       0.1873       0.2313      -0.00301      -0.00171      0.00999     0.0002457     0.0002741     0.0022336
0.01500       0.1888       0.2239      -0.00336      -0.00186      0.01164     0.0002752     0.0003083     0.0026098
0.01700       0.1901       0.2183      -0.00371      -0.00201      0.01329     0.0003047     0.0003430     0.0029888
0.01900       0.1910       0.2138      -0.00406      -0.00216      0.01494     0.0003341     0.0003779     0.0033699
0.02100       0.1919       0.2105      -0.00442      -0.00232      0.01658     0.0003642     0.0004142     0.0037530
0.02300       0.1926       0.2077      -0.00478      -0.00248      0.01822     0.0003937     0.0004503     0.0041376
0.02500       0.1932       0.2059      -0.00515      -0.00265      0.01985     0.0004247     0.0004890     0.0045234
0.02700       0.1935       0.2062      -0.00557      -0.00287      0.02143     0.0004633     0.0005381     0.0049103
0.02900       0.1934       0.2100      -0.00609      -0.00319      0.02291     0.0005172     0.0006076     0.0052973
0.03100       0.1931       0.2148      -0.00666      -0.00356      0.02434     0.0005780     0.0006866     0.0056839
0.03300       0.1923       0.2206      -0.00728      -0.00398      0.02572     0.0006450     0.0007744     0.0060693

LAMBDA=  2.00        TETA=0.027428

LAMBDA=  3.00        TETA=0.021413

LAMBDA=  4.00        TETA=0.018280

LAMBDA=  5.00        TETA=0.016373
```

FIG A. 5b Example of the printout of the results calculated according to Alternative 2

In this case the printout is reproduced in FIG A.5b. The ultimate moment here has been determined by the highest point in the moment-curvature curve. The table shows that $\mu_u = 0.1935$ for $1/\rho = 0.027$. As $1/\rho$ increases, the moment decreases. The table continues right up to material failure, in this case crushing failure of the concrete.

Four values of λ and the rotation capacities θ_{uv} calculated for these values are printed out underneath the table. This printout is controlled by the procedure SKRIW 2.

Lunds universitet
Reprocentralen 1981